Analysis of the Spatiotemporal Organization of Immune Receptors in Plant Plasma Membrane by sptPALM and the Impact of HIR2 as Putative Organizing Factor

Dissertation

der Mathematisch-Naturwissenschaftlichen Fakultät
der Eberhard Karls Universität Tübingen
zur Erlangung des Grades eines
Doktors der Naturwissenschaften
(Dr. rer. nat.)

vorgelegt von
M. Sc. Alexandra Susanne Ehinger
aus Achern

Tübingen
2022

Gedruckt mit Genehmigung der Mathematisch-Naturwissenschaftlichen Fakultät der Eberhard Karls Universität Tübingen.

Tag der mündlichen Qualifikation:	01.12.2022
Dekan:	Prof. Dr. Thilo Stehle
1. Berichterstatter:	Prof. Dr. Klaus Harter
2. Berichterstatter:	Prof. Dr. Thorsten Nürnberger

TABLE OF CONTENT

1 INTRODUCTION

Plants are constantly exposed to variable environmental conditions. In order to survive, plants need to ensure a balance between stress adaption and modulation of growth and development. Thus, plants rely on sensing and adaption to developmental and environmental cues (Escocard de Azevedo Manhães et al., 2021). A multitude of signaling pathways depend on plasma membrane localized receptors. One major group is represented by Leucine-Rich Repeat Receptor-Like Kinases (LRR-RLKs), with an extracellular domain perceiving the cognate ligand and a cytoplasmatic kinase domain, which activates downstream signaling (Couto & Zipfel, 2016; Albert et al., 2019). LRR-RLKs are involved in the response to various endogenous signals, such as the plant growth hormones brassinosteroids, but they also sense exogenous cues as LRR-RLKs are part of the innate immune system of plants (Tang et al., 2017). Although the activation of the different LRR-RLKs results in diverse responses, they still share many components in their signaling pathways. Until now, it is still not conclusively clarified how signaling specificity between immune and growth signaling is mediated (DeFalco & Zipfel, 2021).

1.1 Cell surface receptors regulate immunity and development

1.1.1 Environmental threats are perceived by cell-surface receptors

Plants are protected against the majority of pathogens by the establishment of the cell wall and the cuticle, which together form a physical barrier (Bigeard et al., 2015). Additionally, plants employ an innate immune system. On the one hand, this relies on the recognition of conserved pathogen- or microbe-associated pattern (PAMPs/ MAMPs), which elicit the pattern-triggered Immunity (PTI) (Boller & Felix, 2009). On the other hand, the perception of microbe specific effectors by intracellular nucleotide-binding leucine-rich repeat receptors (NLR) induces the effector-triggered immunity (ETI) (Jones et al., 2016). Moreover, plants detect host-derived damage-associated molecular pattern (DAMPs) and phytocytokines, which contribute to PTI responses (Gust et al., 2017). It is important to note that the boundaries between PTI and ETI often cannot be clearly defined and it is suggested to understand the plant immune system more uniformly as system to perceive danger (Thomma et al., 2011; Gust et al., 2017; Albert et al., 2019; Pruitt et al., 2021).

In order to activate the immune response, plants are able to sense M/PAMPs, which can originate from organisms of all kingdoms such as bacteria, fungi, animals or even from plants (Pieterse et al., 2009; Bigeard et al., 2015; Couto & Zipfel, 2016; Hegenauer et al., 2016; Yu et al., 2017b). The recognition is mediated by plasma membrane localized pattern recognition receptors (PRRs). PRRs are classified into Receptor-Like Kinases (RLK) or Receptor-Like Proteins (RLP), depending on the presence or absence of an intracellular kinase domain, respectively (Böhm et al., 2014). The extracellular domain of PRRs is decisive for the binding of ligands and based on the composition, they can be subdivided into different groups, including Leucine-rich repeat (LRR), Lysin motif (LysM) and Malectin-like RKs. One of the first described and best-characterized LRR-RK is the immune receptor FLAGELLIN SENSING 2 (FLS2). FLS2 recognizes a 22-amino acid minimal epitope flg22, the most conserved motif domain of bacterial flagellin (Felix et al., 1999; Gómez-Gómez & Boller, 2000). Another abundant and conserved protein in bacteria is the elongation factor-Tu, whose epitope elf18 is perceived by the LRR-RLK ELONGATION FACTOR-TU RECEPTOR (EFR). Apart from the detection of MAMPs/PAMPs, LRR-RLKs sense endogenous DAMP signals, which also activates immune responses. DAMPs can be released as a response to physical damage by, e.g., disruption of the cell wall after herbivore attack or they can be generated by processing of precursor molecules, which were induced by wounding. Exemplary for DAMP signals are the peptides *At*Pep1 and 2, which are derived from their respective precursor PROPEP1 or 2. Through the perception of the peptides by the LRR-RLK PEPR1/2, the transcription of defense related genes is induced (Huffaker et al., 2006; Yamaguchi et al., 2006; Yamaguchi et al., 2010). Small secreted peptides like the Peps act as secondary danger signals and are termed as phytocytokines due to their similarities to metazoan cytokines (Gust et al., 2017). Although LRRs represent the most common extracellular domain of PRRs, the perception of chitin, which is the main component of fungal cell wall, is perceived by a complex of LysM-RLKs (Shiu & Bleecker, 2001; Miya et al., 2007). LYSIN MOTIF RECEPTOR KINASE 5 (LYK5) is the primary receptor for chitin (Cao et al., 2014). It interacts constitutively with LYK4, which acts as scaffold protein to increase the chitin-induced signaling (Xue et al., 2019). The heteromerization of LYK5 with CHITIN ELICITOR RECEPTOR 1 (CERK1) in a ligand-dependent manner is required for the signal transduction (Cao et al., 2014).

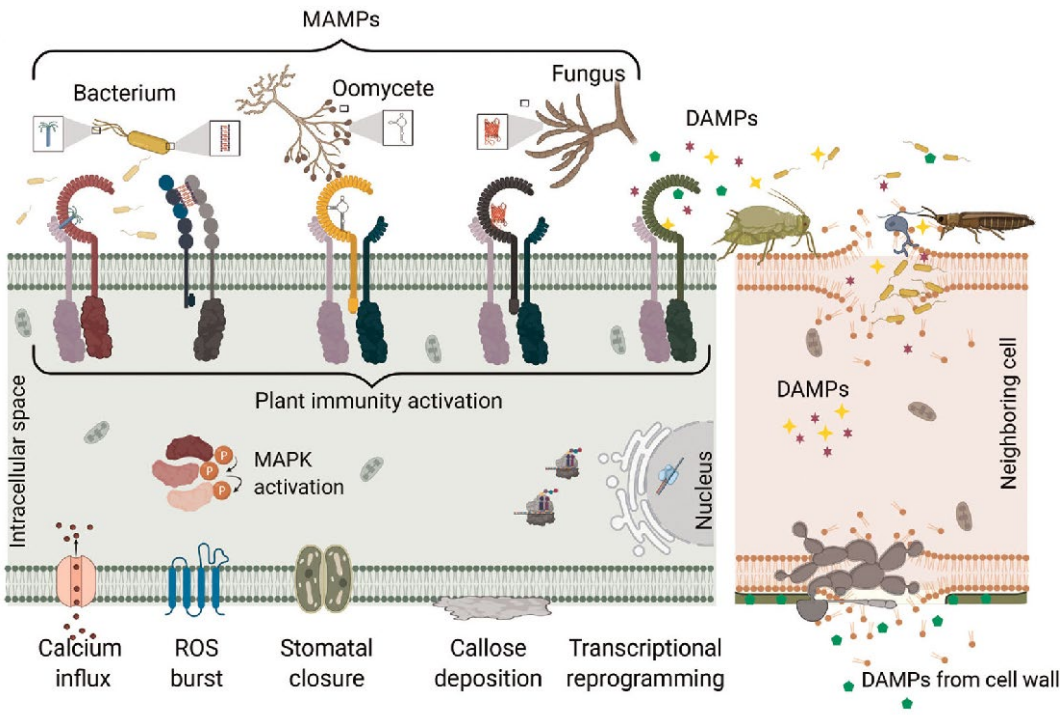

Figure 1-1: Pattern-triggered immunity. Cell-surface located receptors recognize MAMPs or DAMPs. Plant immunity is activated by RLKs and RLPs, which recruit co-receptors to amplify and transduce the signal. MAPK cascade activation leads to transcriptional reprogramming and resulting output responses include Ca^{2+} influx, ROS burst, stomatal closure and callose deposition (Escocard de Azevedo Manhães et al., 2021).

Upon pattern recognition, several cellular and physiological responses take place in order to gain resistance against pathogens (Yu et al., 2017b). The PRRs form heteromeric complexes with co-receptors, which subsequently induce transphosphorylation events within their kinase domains and the initiation of downstream signaling, including the phosphorylation of cytosolic Receptor-Like Cytoplasmatic Kinases (RLCKs). Further, the activation of MITOGEN-ACTIVATED PROTEIN KINASE (MAPK) cascades leads to the transduction of the signaling to the nucleus, where it triggers a transcriptional reprogramming (Yu et al., 2017b; Escocard de Azevedo Manhães et al., 2021). Moreover, acute PRR signaling results in an extracellular alkalization due to ion fluxes, which includes increased influxes of Ca^{2+} and H^{+} and furthermore an accumulation of reactive oxygen species (ROS) (Boller & Felix, 2009; Belkhadir et al., 2014; Yu et al., 2017b). These are hallmarks of early MAMP responses, which happen with a lag phase of less than one minute to 10 minutes (Boller & Felix, 2009; Yu et al., 2017b). Additionally, the accumulation of phytohormones, such as Salicylic Acid (SA), Jasmonic Acid (JA) and Ethylene (ET), contribute to the immune responses (Bigeard et al., 2015; Yu et al., 2017b). SA signaling mediates resistance to biotrophic pathogens, while JA and ET signaling is important to fight necrotrophic pathogens (Loake & Grant, 2007;

Bigeard et al., 2015). The biosynthesis of the stress hormone ethylene was observed to start an hour after flg22 treatment and contributes together with pattern-triggered ROS to the deposition of callose and the closure of stomata (Tang et al., 2017; Yu et al., 2017b). Both mechanisms hamper the entry of pathogens into the inside of the cell: while callose deposition strengthens the cell wall and forms a physical barrier for pathogen attack, the closure of the stomata prevent pathogens to penetrate the cell through these pores (Yu et al., 2017b).

Together these cellular and physiological responses contribute to the recognition and defense mechanisms to mediate basal resistance of plants.

1.1.2 Small RLKs control cell-surface receptors

1.1.2.1 The co-receptor family SERKs ensure downstream signaling

A successful signaling transduction requires the complex formation of the PRRs with a co-receptor, which mainly belong to the family of SOMATIC EMBRYOGENESIS RECEPTOR KINASE (SERK). (Brandt & Hothorn, 2016). The SERKs are LRR-RLKs, containing a small extracellular domain of five LRRs (Chinchilla et al., 2009). The genome of *Arabidopsis* contains five members of the SERKs, of which BRI1-ASSOCIATED KINASE (BAK1/ SERK3) is the best characterized relative. Originally, BAK1 was identified as signaling partner of the receptor BRASSINOSTEROID INSENSITIVE 1 (BRI1) and its involvement in the plant developmental pathways (Li et al., 2002; Nam & Li, 2002; Wang et al., 2005). Later on, it was shown that BAK1 is a multifunctional co-receptor (Postel et al., 2010). It is essential for the proper functionality of numerous LRR-RLKs of immunity-related pathways such as FLS2, EFR as well as for PEPR1/2 (Chinchilla et al., 2007; Postel et al., 2010; Roux et al., 2011). Heteromerization of BAK1 and FLS2 occurs almost instantaneously after flg22 elicitation (Chinchilla et al., 2007; Schulze et al., 2010). Structural studies revealed that flg22 does not only bind to the extracellular domain of FLS2 but also to the LRR domain of BAK1 and thereby stabilizing the complex by acting as “molecular glue” (Sun et al., 2013; Couto & Zipfel, 2016; He et al., 2018). However, there is no evidence that the complex is formed in a ligand-independent manner. Analogous to the interaction with FLS2, BAK1 interacts with EFR, PEPR1, BRI1 and their respective ligands in an identical manner (Couto & Zipfel, 2016; Ma et al., 2016; He et al., 2018). Although BAK1 is the most prominent member of the SERK family, its relatives can act partially redundantly, whereas individual members function differently in distinct physiological responses (Ma et al., 2016; He et al., 2018). For example, BAK1 and SERK4, but not SERK1 and SERK2 are required for immune responses (Roux et al., 2011; He et al., 2018). Single *bak1* mutants are strongly impaired in flg22 signaling, but only *bak1 serk4*

double mutants are fully insensitive (Chinchilla et al., 2007; Roux et al., 2011). The involvement of the SERKs in developmental pathways can be demonstrated by the phenotypic similarity of *serk1 bak1 serk4* triple mutants and *bri1* null mutants. Both display de-etiolation in dark-grown seedlings, a strong dwarfism and a complete insensitivity to BR treatment (Gou et al., 2012). The growth defects observed in *bak1* mutants are related to the insensitivity to the growth hormone brassinolide (BL) and can be restored by exogenous BL treatment (Nam & Li, 2002; Kemmerling et al., 2007). Moreover, *Arabidopsis* plants with enhanced BAK1 levels show a stunted phenotype, which can be rescued by simultaneous overexpression of BRI1 (Belkhadir et al., 2012). Thereby it has to be noticed that BAK1 also plays an important role in cell death control. The overexpression and the absence of BAK1 leads to spontaneous cell death (He et al., 2007; Kemmerling et al., 2007; Belkhadir et al., 2012; Domínguez-Ferreras et al., 2015). This autoimmune phenotype is caused by the loss of cell death control, which is linked to ETI signaling and the involvement of NLRs (Wu et al., 2020; Schulze et al., 2021). This indicates that keeping the cellular homeostasis of BAK1-levels in a physiological dose is crucial to control cell death and to facilitate the proper development of a plant.

1.1.2.2 The BIR protein family control ligand binding receptors and co-receptors

BAK1 is a multifunctional co-receptor of immunity and developmental pathways. Additionally, it is involved in the control of cell death (He et al., 2007; Kemmerling et al., 2007; Domínguez-Ferreras et al., 2015; Gao et al., 2019). The regulation of proper receptor levels is decisive to control an adequate signaling. LC/ESI-MS/MS analysis identified BAK1-INTERACTING RECEPTOR KINASE (BIR) proteins as negative regulators of BAK1 (Halter et al., 2014; Imkampe et al., 2017). The BIR protein family contains four members and forms the subgroup Xa of RLKs. They contain an extracellular domain with five leucine-rich repeats, a single-pass transmembrane domain and an intracellular kinase domain. BIR1 is the most ancient member and only shows a week interaction with BAK1 (Halter et al., 2014). It is described to be involved in cell death control as *bri1* mutants exhibit extensive cell death and constitutive activation of defense responses (Gao et al., 2009). BIR1 contains a functional kinase domain, whereas BIR2 and BIR3, are described to be pseudokinases (Blaum et al., 2014; Halter et al., 2014; Imkampe et al., 2017). The crystal structure of BIR2 revealed that the ATP-binding pocked within the kinase domain is occluded and thus unable to phosphorylate substrates (Blaum et al., 2014). However, BIR2 and BIR3 bind directly to BAK1, but only BIR2 gets phosphorylated by BAK1 (Halter et al., 2014; Imkampe et al., 2017). In the absence of a ligand, BIR2 and BIR3 constitutively interact with BAK1 and thereby preventing its interaction

with the ligand-binding receptors. Accordingly, they act as negative regulators of BAK1-dependent pathways. Beyond sharing this regulatory function, BIR2 and BIR3 feature distinct differences. BIR2 negatively regulates MAMP responses by preventing BAK1 from heteromerization with FLS2. After flg22 treatment, BAK1 gets released from BIR2, allowing BAK1 to interact with FLS2, accordingly *bir2* mutants show hypersensitive responses to flg22 (Böhm et al., 2014; Halter et al., 2014). Moreover, *bir2* knockout mutants are impaired in cell death control but show no defects in BRI1-dependent signaling pathways (Halter et al., 2014). Contrary, BIR3 has a strong impact on BRI1 signaling by forming complexes with both, BRI1 and BAK1 (Imkampe et al., 2017; Großeholz et al., 2020). *In-silico* modeling revealed that BIR3 interact with BAK1 on its catalytic site and so blocking the signaling between BAK1 and BRI1 in absence of brassinosteroids. Additionally, the modeling indicated that BAK1 provides a second binding site for BRI1, allowing complex formation without activating the BL-pathway (Großeholz et al., 2020). The function of BIR3 is dose dependent as overexpression of BIR3 causes a dwarf phenotype, which resembles the *bri1* null mutants. These overexpression lines of BIR3 are less sensitive to exogenously applied BL, but the phenotype can be rescued by overexpressing BRI1, demonstrating the negative regulatory function of BIR3 in the BL-pathway (Imkampe et al., 2017). However, BRI1 is not the only ligand-binding receptor BIR3 interacts with: it also forms complexes with FLS2, EFR and PEPR1 to prevent heteromerization with BAK1 (Imkampe et al., 2017). Due to the direct inhibitory effect on complex formation, BIR3 has a strong negative influence on MAMP responses and BL-signaling (Imkampe et al., 2017). An additional function of BIR3, which differs from BIR2, is the stabilizing effect on BAK1. *Arabidopsis* plants, which lack *BIR3*, contain less BAK1 protein levels, although the transcript levels are not altered compared to the wild type. The effect of reduced BAK1 levels might mask a hyperresponsiveness of *bir3* mutants and explain the relatively weak phenotype of *bir3* mutants (Imkampe et al., 2017).

1.1.3 Growth and developmental pathways rely on receptor kinases

A wide range of plant growth and developmental processes are mediated by plasma membrane localized LRR-RLKs, which recognize endogenous hormones or peptide signals (He et al., 2018). One of the best-studied LRR-RLK involved in growth and development is BRI1. It perceives brassinosteroids (BR), which are phytohormones controlling nearly all phases of plant development (Li & Chory, 1997; Belkhadir et al., 2014). This includes numerous cellular processes such as root growth, cell elongation, light and stress responses as well as stomatal development (Zhu et al., 2013). *Arabidopsis* mutants, impaired in BR synthesis or signaling, exhibit an extreme dwarfism, photomorphogenesis in the dark, an altered

distribution of stomata and delayed flowering time (Zhu et al., 2013). In the absence of BR, transphosphorylation events between BRI1 and BAK1 are inhibited by the negative regulator BRI1 KINASE INHIBITOR 1 (BKI1) and BIR3 (Wang & Chory, 2006; Wang et al., 2014; Imkampe et al., 2017). Ligand binding leads to partial release of BIR3, which increases the interaction of BRI1 and BAK1 and the binding causes auto-and transphosphorylation events of the cytoplasmatic kinase domains, which in turn activate downstream signaling (Imkampe et al., 2017). Moreover, BRI1 phosphorylates BKI1, which subsequently dissociates from the plasma membrane to the cytosol (Wang & Chory, 2006). In parallel, BRI1 phosphorylates the RLCK BR SIGNALING KINASE 1 (BSK1), which relays the signal to downstream components (Tang et al., 2008).

Closely related to BRI1 are the LRR-RLKs PHYTOSULFOKINE (PSK) RECEPTOR 1 (PSKR1) and PSKR2. They recognize the secreted peptide hormone PSK, which is a required growth factor for cellular divination and expansion (Wang et al., 2015a). *Pskr1pskr2* seedlings have shorter roots and hypocotyls than wild type plants and overexpression of the receptors lead to enhanced plant growth (Hartmann et al., 2013). It is shown that the responsiveness to PSK also depends on the BR-signaling pathway. The inhibition of BR biosynthesis causes insensitivity to PSK in wild type seedlings as well as in *bri1-9* mutants, which are unable to perceive BR (Hartmann et al., 2013). The BRI1 and the PSK signaling pathway share the co-receptor BAK1 and both interact with RECEPTOR LIKE PROTEIN 44 (RLP44) (Nam & Li, 2002; Wolf et al., 2014; Ladwig et al., 2015; Glöckner et al., 2020). It is reported that the association of the receptor and co-receptor is promoted by the direct interaction with RLP44 (Holzwart et al., 2018; Holzwart et al., 2019; Garnelo Gómez et al., 2021). Thereby it is likely that RLP44 acts as a scaffold to promote the interactions and to maintain signaling specificity (Wolf, 2020; Garnelo Gómez et al., 2021).

Apart from LRR-RLKs also malectin-like RLKs play a role in developmental processes (Escocard de Azevedo Manhães et al., 2021). FERONIA (FER), which has two extracellular malectin-like domains and a catalytically active kinase domain, is involved in multiple cellular processes such as hormone signaling, salt stress tolerance and cell elongation (Franck et al., 2018; Zhang et al., 2020). It was identified as the receptor for multiple RAPID ALKALIZATION FACTOR (RALF) peptides (Haruta et al., 2014; Stegmann et al., 2017; Gronnier et al., 2022). Additionally, FER senses the cell wall integrity through the interaction of the malectin-like extracellular domain with carbohydrates in the cell wall (Li et al., 2016a). Interestingly, FER is also involved in immune responses as *fer* mutants are less sensitive to PAMP treatments with flg22 or elf18 (Stegmann et al., 2017; Franck et al., 2018; Zhang et al., 2020). Together with the GPI-anchored protein LORELEI-LIKE GPI-ANCHORED PROTEIN 1 (LLG1) FER can promote complex formation of FLS2 and

BAK1. The perception of the peptide RALF23 inhibits the flg22 induced heteromerization FLS2 with its co-receptor, which results in a suppressed flg22-induced ROS burst (Stegmann et al., 2017; Xiao et al., 2019; DeFalco & Zipfel, 2021). Thus, FER is proposed to act as a scaffold protein and positive regulator for membrane localized PRRs (Stegmann et al., 2017).

1.2 Nanodomain formation of membrane residing proteins provides signaling platforms

Together with the cell wall, the plasma membrane forms the frontier of the cell and acts as a physical barrier. The plasma membrane is composed of lipids and proteins and forms a signaling platform to perceive and transfere extracellular signals to the cytoplasm (Jaillais & Ott, 2019). The fluid mosaic model proposed that biological membranes are liquid, and that lipids and proteins undergo lateral diffusion without major restrictions (Singer & Nicolson, 1972). According to this model, the membrane composition would exhibit a uniformly distribution. However, the understanding of plasma membrane organization has improved, resulting in a dogma shift of the previous described fluid mosaic model. Clear evidences pointed out that proteins and lipids are heterogeneously distributed within plant membranes and highly compartmentalized into domains of different types and sizes (Gronnier et al., 2018; Jaillais & Ott, 2019; Yu et al., 2020; Martinière & Zelazny, 2021). Clusters of higher-order structures are termed as “membrane nanodomains” or “membrane microdomains” and classified by their size. Thus, nanodomains are defined as submicron protein and/or lipid assemblies in a range of 20 nm to 1 µm and microdomains as significant larger assemblies greater than 1 µm (Ott, 2017). The lipid raft hypothesis proposed lateral heterogeneity of membrane components and that self-assembly of certain lipids can promote protein aggregation and complex formation (Simons & Van Meer, 1988; Yu et al., 2020). Biochemical approaches, which separated biological membranes in detergent-resistant (DRM) and detergent-sensitive fractions, strengthened the concept of membrane compartmentalization (Brown & Rose, 1992; Mongrand et al., 2004; Borner et al., 2005; Morel et al., 2006). DRM cannot be solubilized in nonionic detergents such as Triton X100 in the cold and are enriched in sphingolipids, sterols and associated proteins (Mongrand et al., 2004; Laloi et al., 2006; Lefebvre et al., 2007; Martinière & Zelazny, 2021). However, the usage of detergents might influence lipid segregation and protein aggregations, which might lead to the generation of artifacts in the preparation. It is proposed that DRM do not reflect the *in vivo* repartition of lipids and proteins (Tanner et al., 2011; Martinière & Zelazny, 2021). Thus, the binary nature of DRM fractionation leads to an oversimplification of membrane organization and only partially represent its heterogeneity and diversity

(Tanner et al., 2011; Gronnier et al., 2018; Martinière & Zelazny, 2021). Cell biological approaches like fluorescence microscopy replaced the biochemical fractionation of membranes and additionally to protein and lipid composition, it enables studying membrane dynamics *in vivo.*

1.2.1 BRI1 and FLS2 localize in distinct nanodomains within the plasma membrane

The development of powerful microscopy approaches with increased resolution discovered a number of proteins to be organized in nanodomains (Kleine-Vehn et al., 2011; Jarsch et al., 2014; Bücherl et al., 2017; Jaillais & Ott, 2019; Martinière et al., 2019; Platre et al., 2019). Thereby, heterogeneously distributed proteins appear as puncta-like structures in the plasma membrane (Jaillais & Ott, 2019). By Variable-Angle Epifluorescence Microscopy (VAEM) it was shown for BRI1-GFP and BAK1-mCherry to be uneven distributed within the plasma membrane, promoting the conclusion that the receptors are localized in nanoclusters (Wang et al., 2015b; Hutten et al., 2017). Additionally, Hutten et al. (2017) applied Selective-Surface Observation FRET-FLIM analysis to demonstrated that BRI1 and BAK1 reside in very close proximity within the same nanodomain. Depletion of endogenous ligands or their exogenous application did not affect the distance and the density of the receptors. Consequently, this rose up the assumption of ligand-independent preformed receptor complexes, which could also be supported by additional studies in the field (Bücherl et al., 2013; Hutten et al., 2017; Großeholz et al., 2020). Moreover, live-cell imaging and single-molecule microscopy obtained quantitative analysis data for BRI1 and FLS2 to be localized in different nanodomains (Bücherl et al., 2017). The size and the density of the clusters were comparable for both receptors as well as both appeared to be rather immobile (Bücherl et al., 2017; Hutten et al., 2017). The same heterogenous distribution and cluster formation was shown for BOTRYTIS-INDUCED KINASE 1 (BIK1), a RLCK which is shared in the FLS2 and BRI1 downstream signaling (Lu et al., 2010; Lin et al., 2013; Bücherl et al., 2017). Hence, spatial separation of immune and development receptors might provide signaling specificity.

1.2.2 Remorins and SPFH-domain containing proteins are organizing factors for nanodomains

The formation and the maintenance of nanodomains depend on specific protein-lipid interactions and on a continuum between the cell wall, plasma membrane and the cytoskeleton. Until now it is unclear,

whether a specific lipid environment creates nanodomains through the interaction with proteins or if the opposite is the case. Proteins might bind lipids and actively initiate their clustering (Martinière & Zelazny, 2021). The strong electronegativity of anionic lipids in the inner leaflet of the plasma membrane is crucial for the recruitment of soluble or lipid-anchored proteins (Jaillais & Ott, 2019). Recently it was shown for the Rho GTPase RHO OF PLANTS 6 (ROP6) to be stabilized by the phospholipid phosphatidylserine into plasma membrane nanodomains in response to auxin stimuli (Platre et al., 2019). That proteins can modify their lipid environment was shown by overexpressing REMORIN 1.2 (REM1.2), which led to an induced increase of ordered lipids in the membrane (Huang et al., 2019; Martinière & Zelazny, 2021). Remorins and Stomatin/Prohibitin/Flotillin/HflK/C (SPFH)-domain containing proteins are exclusively associated in DRM and typically used as nanodomain marker proteins in cell-biological approaches (Jaillais & Ott, 2019; Yu et al., 2020; Martinière & Zelazny, 2021). These proteins are hypothesized to be organizing factors for nanodomains and to function as scaffolds for receptor complexes at the plasma membrane (Yu et al., 2020).

Remorins are well characterized nanodomain-resident proteins in plants. *Arabidopsis* contains 16 members, which are subdivided into six groups, based on their N-terminal region (Raffaele et al., 2007). Remorins do not contain a target-peptide or a transmembrane domain but are attached to the inner leaflet of the plasma membrane independent of conventional secretory pathway (Raffaele et al., 2007; Gronnier et al., 2017; Gouguet et al., 2020). Their recruitment to the plasma membrane is mediated by a C-terminal hydrophobic stretch, called the REMORIN C-terminal Anchor (REM-CA) (Gronnier et al., 2017; Gouguet et al., 2020). For *St*REM1.3, a remorin protein from *Solanum tuberosum,* it is shown that the C-terminal anchor REM-CA defines segregation of *St*REM1.3 in nanodomains. Mutations in the REM-CA of *St*REM1.3 caused alterations in the size and density of formed nanodomains (Gronnier et al., 2017). Additionally, sterol and phosphatidylinositol 4-phosphate (PI4P) are shown to mediate the localizations of *St*REM1.3 into the nanodomains (Gronnier et al., 2017). Many of the *Arabidopsis* REMs contain cysteine residues in their REM-CA, which are posttranslational modified by S-acylation. This further contributes to their membrane association, but it is not responsible for their sub- compartmentalization in nanodomains (Konrad et al., 2014; Jaillais & Ott, 2019; Gouguet et al., 2020). Moreover, REMs form higher-order oligomers *via* their coiled-coil domain, which is highly important for their targeting and function (Jaillais & Ott, 2019; Gouguet et al., 2020). The functionality of REMs in the recruitment of receptors into nanodomains was demonstrated in rice (*Oryza sativa*). Ligand induced phosphorylation of *Os*REM4.1 by *Os*BRI1 caused the dissociation of *Os*REM4.1 and *Os*SERK1, allowing the receptor recruitment into the *Os*BRI1/*Os*SERK1 signaling complex (Gui et al., 2016; Jaillais & Ott, 2019). Furthermore, REMs are required

to maintain and to stabilize receptor complexes. In *Medicago truncatula* the primary perception of rhizobia involves the receptor LYSIN MOTIF KINASE 3 (LYK3) (Liang et al., 2018). Upon infection the expression of SYMREM1 is induced. Subsequently the physical interaction of SYMREM1 with LYK3 stabilize the activated receptors in membrane nanodomains, which is indispensable for the downstream signaling and a proper function during host cell infection (Liang et al., 2018). Besides their membrane organization function, REMs are described to be involved in many different pathways, including plant defense against virus and bacteria, symbiosis, hormone signaling and plant development (Martinière & Zelazny, 2021).

Another protein family, which is used as nanodomain marker are SPFH-domain containing protein, also called Band-7 proteins. They are an evolutionary conserved protein family among metazoans, bacteria, fungi and plants (Rivera-Milla et al., 2006). In *Arabidopsis* they are classified into five groups: two stomatin-like, seven prohibitins, three flotillins, one erlin-like protein and four HYPERSENSITIVE INDUCED REACTION (HIR) proteins (Daněk et al., 2016). The SPFH-domain containing proteins generally form oligomers and are localized to diverse cellular membrane (Browman et al., 2007; Gehl & Sweetlove, 2014; Daněk et al., 2016). It is hypothesized that they are involved in the regulation of protein complex assembly and they are often linked to membrane nanodomains (Browman et al., 2007). So far, it remains largely unknown how plant SPFH proteins are targeted to the membrane and how they are recruited into nanodomains (Martinière & Zelazny, 2021).

Prohibitins are primary localized to mitochondrial inner membranes and function in mitochondrial cristae formation. They are suggested to act as universal scaffold by their lipid association in the mitochondrial membrane and thus affecting mitochondrial processes within the mitochondrial membrane (Gehl & Sweetlove, 2014).

Flotillins (FLOT) have been predominantly observed to be localized at the plasma membrane. *At*FLOT1 and *At*FLOT2 fused to GFP cluster in dynamic puncta structures in the plasma membrane of epidermal cells in leaves and roots (Li et al., 2012; Jarsch et al., 2014; Daněk et al., 2016). Additionally, *At*FLOT1 co-localizes with FM4-64 labeled endosomes, which differed from clathrin-coated endosomes, indicating that flotillins define a clathrin-independent endocytosis pathway (Li et al., 2012). FLOTs possess putative sterol binding motifs named CRAC/CARC located within the SPFH-domain (Daněk et al., 2016). This might contribute to the recruitment of FLOTs into sterol-enriched nanodomains in the plasma membrane. Exogenous depletion of sterols with methyl-β-cyclodextrin (mβCD) or sterol-biosynthesis mutants displayed decreased movements of *At*FLOT1-GFP (Li et al., 2012; Cao et al., 2020). Moreover, FLOTs have been shown to play a role in plant-microbe interaction. It was reported for *Mt*FLOT2 and *Mt*FLOT4 to be

involved in nodulation and thus are required for symbiosis (Haney et al., 2011). *At*FLOT1 amiRNA mutants exhibited a role of FLOTs in PAMP triggered pathways. Those mutants showed defects in flg22 induced ROS responses and attenuated levels of callose deposition compared to wild type (Yu et al., 2017a). Additionally, it has been proposed that upon stress or ligand treatment *At*FLOT1 assist endocytosis of the aquaporin PIP2;1, BRI1 and FLS2 (Li et al., 2011; Li et al., 2012; Wang et al., 2015b; Cui et al., 2018).

1.2.2.1 Hypersensitive Induced Reaction proteins – modulators of immunity related signaling complexes?

HYPERSENSITIVE INDUCED REACTION (HIR) proteins are a plant-specific subgroup of the SPFH-domain containing protein family. They were originally discovered in maize but can also be found in algae, rice, wheat, pepper, tomato and Arabidopsis (Daněk et al., 2016). The latter contain four different *HIR* genes: *A*tHIR1 (At1g69840), *At*HIR2 (At3g01290), *At*HIR3 (At5g51570), and *At*HIR4 (At5g62740) (Qi et al., 2011). *A*tHIR1, *At*HIR4 and *A*tHIR2 proteins are most closely related with an amino acid similarity up to 86%. The single isoforms differ in their protein expression pattern. *At*HIR1 is expressed in leaves and some flower parts but absent in root tissue, whereas *At*HIR2 exhibits its highest protein levels in leaves and roots without being expressed in flowers and siliques (Daněk et al., 2016). *At*HIR3 and *At*HIR4 are expressed in nearly all developmental stages in all organs to a certain extent but show the highest amounts in siliques and seeds or the gametophytes and seeds, respectively (Daněk et al., 2016). All four *At*HIR proteins can form homo- and heterooligomers *in vivo,* which was experimentally confirmed for all pair-wise combinations of single *At*HIR isoforms (Qi et al., 2011). As other SPFH-domain containing proteins, the HIR proteins are localized at the inner leaflet of the plasma membrane and were found to be enriched in DRM, suggesting a nanodomain organizing function (Qi et al., 2011). Sterol depletion with mβCD did not alter the association of the HIRs in DRMs, but it caused a significant increase in the dynamics of *At*HIR1 (Kierszniowska et al., 2009; Lv et al., 2017). Interestingly, physical interactions between different nanodomain markers with the HIR proteins have been observed, such as interactions between *At*HIR1 and *At*REM1.3 as well as between *At*HIR2 and *At*FLOT2, but the importance of such protein complexes is unclear (Lv et al., 2017; Junková et al., 2018; Martinière & Zelazny, 2021).

The HIR proteins are described to participate in plant immunity of different plant species and were primary associated with the development of a hypersensitive response (HR) after pathogen attack (Nadimpalli et al., 2000; Martinière & Zelazny, 2021). Overexpression of the pepper *Ca*HIR1 triggered pathogen-independent cell death in *Capsicum annuum* and *N. benthamiana* and caused an increase in callose

deposition (Choi et al., 2011). In accordance with this, overexpression of the rice *Os*HIR1 in *Arabidopsis* caused spontaneous hypersensitive response lesions (Zhou et al., 2010). During bacterial or fungal infections, the expression of the HIR protein is increased (Daněk et al., 2016). Moreover, transcriptional upregulation of *At*HIR1, *At*HIR2 and *At*HIR3 was shown upon elevated levels of the phytohormone SA or after elicitor treatment with flg22, chitin or EF-Tu (Qi et al., 2011; Daněk et al., 2016). Transgenic *Arabidopsis* lines, overexpressing either *At*HIR1 or *At*HIR2, exhibit enhanced resistance to the bacteria *Pseudomonas syringae* pv*. tomato* (*Pst)* DC3000 (Qi et al., 2011). The same effect was observed for overexpression of the rice *Os*HIR1 or the pepper *Ca*HIR1 in *Arabidopsis* (Jung & Hwang, 2007; Zhou et al., 2010). The latter additionally showed increased susceptibility to necrotrophic fungal pathogen *Botrytis cinerea* (Jung et al., 2008). Furthermore, physical interactions of the HIR proteins with LRR proteins were confirmed in several studies by yeast-two-hybrid and Co-IP experiments (Jung & Hwang, 2007; Qi & Katagiri, 2009; Zhou et al., 2009; Qi & Katagiri, 2012). *Ca*HIR1 interacts with *Ca*LRR1 protein in pepper as well as their respective homologs in rice (Jung & Hwang, 2007; Zhou et al., 2009). In *Arabidopsis*, *At*HIR1 and *At*HIR2 bind to NB-LRR protein RESISTANCE TO P. SYRINGAE 2 (RPS2) (Qi & Katagiri, 2009). RPS2 confers resistance to *P. syringae* infections in *Arabidopsis* by binding to RPM1 INTERACTING PROTEIN 4 (RIN4), which is a target of the bacterial effector AvrRpt2 (Bent et al., 1994; Axtell & Staskawicz, 2003; Mackey et al., 2003). Additionally, physical association of *At*HIR2 with FLS2 was shown by Co-IP experiments in *N. benthamiana* (Qi & Katagiri, 2012). The complex formation of HIR2 with key components of the classical PTI-signaling (FLS2), but also with proteins involved in ETI-signaling (RPS2), led to the assumption that HIR2 might provide a signaling platform, cross-linking PTI with ETI signaling (Qi & Katagiri, 2012).

Given examples indicated a clear involvement of the HIR proteins in plant immunity, however their mode of action remains unclear. It is suggested that HIR proteins play a role in the recruitment of proteins in membrane nanodomains as well as in the maintenance of these. The HIR proteins might act as scaffold, promoting protein complex formation of signaling components at the plasma membrane (Qi et al., 2011; Qi & Katagiri, 2012; Martinière & Zelazny, 2021).

1.3 Super resolution microscopy imaging in plant cells

Optical microscopes utilize visible light and lenses to magnify and image cells (Khater et al., 2020). Light can be seen as a point source with an Airy disc pattern, which is also known as point-spread function (PSF) (Henriques et al., 2011). The resolution of optical microscopes, which is defined as the smallest distance where two points can be distinguished, depends on the wavelength of the observed light (λ) and the numerical aperture (NA) of the objective. The diffraction limit (d) of optical microscopy was first described by Abbe and can be expressed by the equation:

$$d = \frac{\lambda}{2\,NA}$$

(Abbe, 1873)

Any point source, that is smaller than the diffraction limit appears with a fixed size and shape. Hence, typical optical microscopes cannot resolve objects smaller than 200 nm (Figure 1-2).

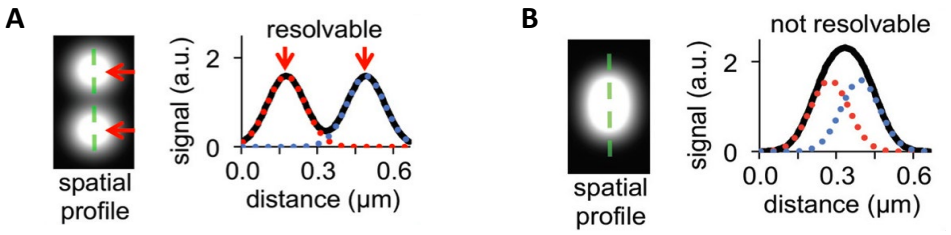

Figure 1-2: The resolution limit of optical microscopy. Two particles viewed in xy plane and their respective signal profile, illustrated in resolvable [**A**] and not resolvable [**B**] distances. The green line marks the intensity profile shown in the plots and red arrows indicate the center of the particles, when they are resolvable. The dotted red and blue line correspond to the upper and lower particle profile. The black line shows the summed profile of both particles. The figure is adapted from Herbert et al. (2012).

As many biological structures are smaller than 200 nm, these are commonly precluded from imaging and analysis. To visualize macromolecular structures at the nanometer scale, much effort was made to develop techniques, whereby higher resolution in microscopy could be achieved. Over the past decades, several super-resolution techniques have been developed, which enable to break the diffraction limit of light. Among these, single-molecule localization microscopy methods (SMLM), such as Photoactivated Localization Microscopy (PALM) and Stochastic Optical Reconstruction Microscopy (STORM) were developed (Betzig et al., 2006; Rust et al., 2006). Both methods obtain single molecule localization by acquisition of multiple images and the usage of special fluorophores, of which only a few can be found in

a stochastically active emission state. In each imaging cycle, only a subpopulation of the fluorophores is activated. This enables the separation of otherwise overlapping PSFs from densely labeled samples. Their localization is determined by approximating the PSF of a single emitter with a 2D Gaussian function and computing its center. By combining the sequential acquired images, a super-resolved image can be reconstructed.

PALM relies on genetically encoded photoactive fluorescent proteins (FP), which feature the ability to change their emission state in a light-dependent manner (Komis et al., 2015; Khater et al., 2020). The transfer of a subset of the FPs into another optically distinguishable state is achieved by pulsed illumination with an activation laser and the detection is carried out by continuous illumination with an excitation laser (chapter 1.3.1). Labelling of proteins with genetically encoded FPs produce translational fusion proteins and thus nonspecific labelling is intrinsically excluded. In theory, it ensures a 1:1 labeling ratio, which in particular enables SMLM (Henriques et al., 2011; Durisic et al., 2014; Wang et al., 2018). Moreover, the intensity and localization of the expression can be controlled by suitable promoters and allows the expression in mutant backgrounds. The labeling is non-invasive and less toxic than organic dyes. Thus, imaging with PALM can be performed in living cells. Contrary to PALM, STORM is primarily based on photo-switching properties of fluorescent organic dyes. The cyanine dye pair Cy3-Cy5 can be used to ensure time wise separation of fluorescence signals. Cy5 is switchable between a fluorescent and a dark state, controlled by light of different wavelengths. The switching is facilitated by the second chromophore Cy3 in a distance-depended manner (Bates et al., 2005; Rust et al., 2006). The labeling is achieved by antibodies and therefore, STORM is performed in fixed samples.

1.3.1 Photoactive fluorescent proteins enable single molecule detection

Labelling proteins with conventional fluorophores, such as GFP or RFP, produce a high signal density, that precludes the detection of single molecules. To perform PALM, it is essential to tag the protein of interest with a photoactive fluorescent protein, which is defined by the ability to change its emission state in response to light with a specific wavelength. Hereby, only a sparse stochastic subset of the FPs undergoes the transition at one time. Photoactive fluorophores can either be reversibly photoswitchable, photoactivatable or photoconvertible (Figure 1-3). Reversibly photoswitchable fluorophores, such as Dronpa or Skylan-NS, can be switched multiple times between a fluorescent and non-fluorescent state. Many switching cycles produce a sharper picture by repeated imaging of the same protein and are

beneficial to resolve structures (Habuchi et al., 2005; Zhang et al., 2016). However, to measure stoichiometry and distributions of proteins, the usage of irreversible photoactivatable or photoconvertible fluorescent proteins are preferable. Photoactivatable fluorophores are natively in a dark state and can be irreversibly turned into an active fluorescent state by illumination with UV light.

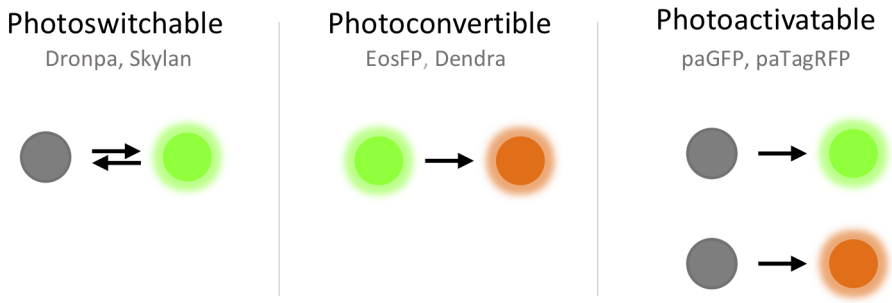

Figure 1-3: Overview of different types of photoactive fluorescing proteins used in super-resolution fluorescence microscopy. Grey circles indicate fluorescing proteins in a non-emitting fluorescent off state. Green and red circles represent fluorophores emitting respectively colored light.

The first photoactivatable fluorophore was photoactivatable GFP (paGFP). It was generated by the amino acid substitution T203H in GFP from *Aequorea victoria* (Patterson & Lippincott-Schwartz, 2002). PaGFP has a dark state and turns into bright green emission at 517 nm upon 405 nm illumination. Like paGFP, photoactivatable mCherry (pa-mCherry) and TagRFP (paTagRFP) are initially dark but become red fluorescent after UV irradiation (Subach et al., 2009; Subach et al., 2010). The generation of a multiplicity of different photoactive fluorophores, which cover a wide range of the visible light spectra, enables various applications of PALM. Additionally, it provides the possibility to combine fluorophores for two color imaging.

1.3.2 Variable Angle Epifluorescence Microscopy facilitates a selective illumination of the plasma membrane of epidermal plant cells

In order to image protein distribution and dynamics at the cell surface, it is crucial to reach a high spatial resolution. Conventional confocal microscopes have limitations in the z-axis resolution and background fluorophore excitation cannot be excluded. To avoid the illumination of background structures, Confocal

Laser Scanning Microscopy (CLSM) microscopy can be complemented with Total Internal Reflection Fluorescence Microscopy (TIRFM) (Ambrose, 1956). While in epifluorescence illumination, the light beam passes upwards through the sample, it is reflected in TIRF (Figure 1-4). The angle of the light beam is modulated in a way that a total reflection of the excitation light is obtained at the interface of coverslip and sample. In this configuration, a part of the light reaches the sample *via* an evanescent wave, which intensity decays exponentially and therefore only illuminates around 100 nm of the sample above the coverslip. This enables a selective visualization of the cell surface regions (Axelrod et al., 1984).

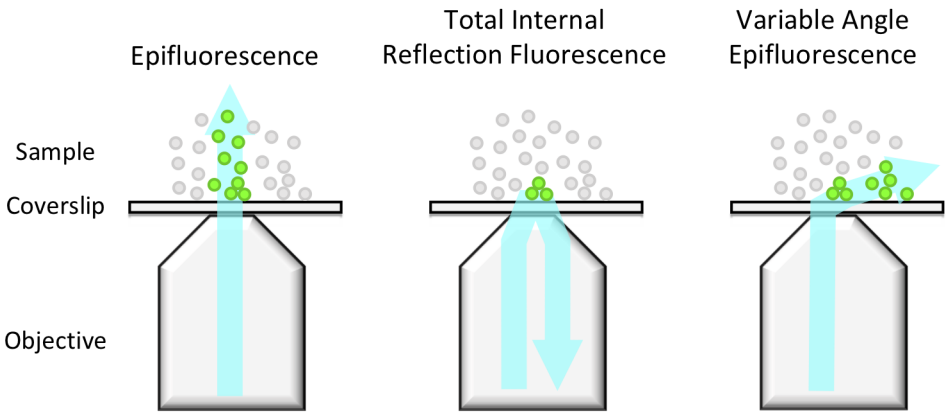

Figure 1-4: Different illumination techniques in fluorescence microscopy. Schematic representation of the laser path (blue) in Epifluorescence, Total Internal Reflection Fluorescence and Variable Ange Epifluorescence microscopy. The illustration is based on Konopka and Bednarek (2008).

TIRFM allows to image the plasma membrane, the cortical cytoskeleton and exo-and endocytosis in adherent mammalian cells (Langhans & Meckel, 2014). However, due to the presence of the cell wall in plants, the plasma membrane is kept at a distance of around 200 nm apart from the coverslip. As consequence, such cellular structures cannot be illuminated in an intact plant cell by TIRFM. To solve this issue, a related technique can be applied: in Variable Angle Epifluorescence Microscopy (VAEM) the light also strikes the coverslip/sample interface at an angle, but it is not totally reflected as it does in TIRFM (Figure 1-4, right). Thereby, VAEM offers a variable illumination depth of the field of view and allows to image selectively the plasma membrane of epidermal plant cells (Konopka & Bednarek, 2008). While this technique does not provide the same background noise repression as TIRFM, it nevertheless produces a higher contrast than epifluorescence illumination and allows the selective illumination of structures deeper than 200 nm within the sample's tissue.

1.3.3 The spatiotemporal organization of proteins can be measured by single-particle tracking Photoactivated Localization Microscopy (sptPALM)

In terms of structure and dynamic, the plasma membrane is characteristically heterogeneous. By performing single-particle tracking (spt), the motions and the heterogeneity of proteins can be analyzed. One particle is imaged over multiple frames and by linking the particles coordinates, trajectories are built in a time-dependent matter. Thus, a map of single particles motions is created (Figure 1-5 A). This technique is limited by the density of observed particles and requires the distance of imaged particles to be wider than the resolution limit. In the case of the usually densely packed plasma membrane, tracking of single molecules is challenging. However, single-particle tracking can be combined with PALM and VAEM, which is termed as sptPALM (Manley et al., 2008). In contrast to PALM, where the localization of one molecule is captured only once, in sptPALM, a single molecule is imaged as long as possible to document its spatiotemporal motion as possible. Imaging has to be performed with low laser intensities to avoid early photobleaching, which reduces the time one molecule can be detected. The different positions of one molecule can be connected to trajectories, which represent the path this particular molecule has moved. Based on the trajectories, quantitative parameters such as the mean square displacement (MSD) and the diffusion coefficient (D) of one protein can be calculated. Three different diffusion types can be distinguished: First, a molecule can follow Brownian motion (free diffusion). Second, it can have a directed diffusion, which could indicate an active motion, where a particle is pulled in a certain direction. Third, a molecule can show a confined diffusion behavior, which could describe a protein being restricted in its mobility when bound in complexes and/or nanodomains (Figure 1-5 B). Thus, the application of sptPALM in live-cell imaging allows the visualization of single proteins with high spatial resolution in plants plasma membrane, and at the same time, it enables to resolve their dynamics and to obtain quantitative information about their mobility behavior.

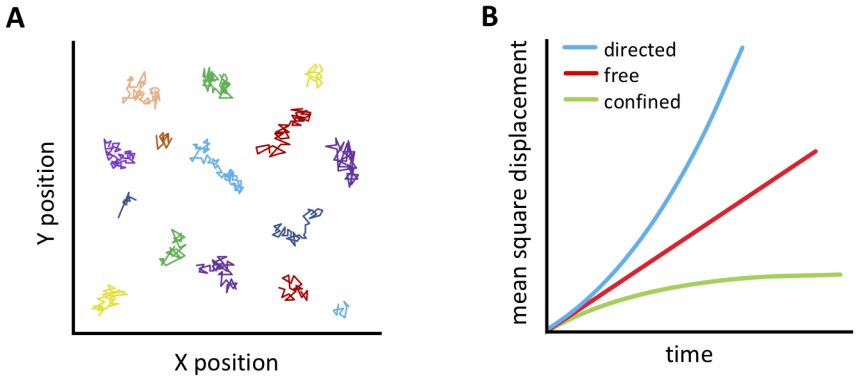

Figure 1-5: Single particles trajectories and mean square displacement plot (MSD). [**A**] Schematic representation of typical particle tracks from single fluorescence tagged proteins moving in living cell membranes. [**B**] Exemplary MSD plots of particles with Brownian movement (free diffusion, red), directed (blue) and confined (green) diffusion behavior.

So far, sptPALM has only been used in few studies in plant science. The first reported studies were performed in 2015, where the dynamical organization of aquaporin PLASMA MEMBRANE INTRINSIC PROTEIN 2;1 (PIP2;1) and the small integral protein LOW TEMPERATURE INDUCIBLE 6a (LTI6a) were analyzed (Hosy et al., 2015). The proteins were tagged with mEos2 and analyzed in transgenic *Arabidopsis* lines. The plasma membrane localized *At*PIP2;1-mEos2 showed a high confined diffusion behavior and was described to be highly immobile. Contrary, LTI6a-mEos2 exhibited a more homogeneous distribution and a higher mobility (Hosy et al., 2015). Additionally, it was reported for CLATHRIN LIGHT CHAIN 2 (CLC2) to have different diffusion types with two distinguishable subpopulations (Martinière et al., 2019). Moreover, diffusion dynamics in response to external stimuli were studied by employing sptPALM. The Rho GTPase RHO OF PLANTS 6 (ROP6) is mobile in a mock treated environment, whereas 25-30 % of ROP6 become rapidly immobile in response treatment with the phytohormone auxin (Platre et al., 2019). In addition, it was demonstrated with sptPALM that external signals resulting from pathogen infection influences the membrane organization of REMORIN 1.3 (REM1.3) (Perraki et al., 2018). REM1.3 displays an immobile and confined behavior under uninfected conditions, whereas upon infection with Potato virus X it shows an increased mobility. Additionally, REM1.3 alters its nanodomain pattern, which was analyzed by Voronoi tessellation-based automatic segmentation of the super-resolved images (Perraki et al., 2018). This mathematical computation enables the visualization of cluster formation and protein distributions.

The published studies analyzing protein dynamics by sptPALM, only observed the mobility behavior of one protein at once. Simultaneous analysis of two different proteins has not been implemented in plant science yet (Jaillais & Ott, 2019; Bayle et al., 2021). The ability to employ dual color sptPALM in a plant system would be a great benefit in order to study complex formations and interactions of two proteins within living cells in real-time. Moreover, dual color sptPALM could give unique mechanistic insights into dynamic molecular processes of membrane organization during, e.g., pathogen perception or developmental processes, which have not been visualized to date. Thus, the development of a dual color sptPALM imaging technique has the potential to fill the gap of missing information about dynamical changes of proteins during signaling transduction in plants.

1.4 Aim of this thesis

Receptor complexes are heterogeneously distributed within the plasma membrane and organized in nanodomains. How their formation is regulated and how the specificity of multiprotein receptor complexes is determined, remains unclear. HIR2, a SPFH-domain containing membrane localized protein, is described to play a regulatory role in the formation of immunity-related receptor complexes. It is part of this thesis to investigate the function of HIR2 and its involvement in the modulation of nanodomain formation. In order to study the spatiotemporal distribution and dynamics of receptor complexes, the aim of this work is to establish and further develop a cutting-edge live-cell super-resolution tool for single and dual color imaging as well as to elucidate the modulation of receptor patterning in response to external stimuli. Applying this technique to HIR2 and immunity related receptor kinases, holds the potential to gain a better understanding of the molecular mechanism of cell surface signaling event determination.

2 MATERIALS AND METHODS

2.1 Material

2.1.1 Organisms

2.1.1.1 Bacterial and fungal strains

Bacterial strains of *Escherichia coli* were used for cloning experiments. The two different strains of *Agrobacterium tumefaciens* were used for plant transformation.

The yeast *Saccharomyces cerevisiae* strains were used for the expression of bait and prey proteins in the mbSUS assay.

Table 2-1: Bacterial and yeast strains

Species	**Strain**	**Genotype**
Escherichia coli	DH5α	F– ϕ80lacZΔ M15 Δ (*lacZYA-argF*) *U169 recA1 endA1 hsdR17* (rK– mK+) *phoA supE44* λ- *thi–1 gyrA96 relA1*
Escherichia coli	One Shot® ccdB Survival™ 2 T1R	F- *mcr*A Δ(*mrr-hsd*RMS-*mcr*BC) Φ80*lac*ZΔM15 Δ*lac*X74 *rec*A1 *ara*Δ139 Δ(*ara-leu*)7697 *gal*U *gal*K *rps*L (Str^R) *end*A1 *nup*G *fhu*A::*IS2*
Agrobacterium tumefaciens	GV3101	T-DNA- vir+ rif^R, pMP90 gent^R
Agrobacterium tumefaciens	AGL1 (pSoup)	C58 RecA (rif R/carb R) Ti pTiBo542DT-DNA (Strep R) Succinamopine (pSoup-tet R)
Saccharomyces cerevisiae	THY.AP4	MATa; *ade2* ⁻, *his3* ⁻, *leu2* ⁻, *trp1* ⁻, *ura3* ⁻; lexA::ADE2, lexA::HIS3, lexA::lacZ
Saccharomyces cerevisiae	THY.AP5	MATα; *ade2* ⁻, *his3* ⁻, *leu2* ⁻, *trp1* ⁻

2.1.1.2 Plants

Transient protein expression was performed in *Nicotiana benthamiana* plants and stable transformation in *Arabidopsis thaliana* Col-0.

2.1.2 Media and Antibiotics

For the respective media, the listed components were dissolved in MQ water and autoclaved at 122°C.

Table 2-2: Media compositions

Medium	**Components**
LB	10 g/l Bacto-Trypton, 5 g/l Bacto-Yeast extract, 5 g/l NaCl, to solidify add 15 g/l Agar
½ MS	2.2 g/l MS-salts (Duchefa), 1% sucrose when indicated (pH 5.7), to solidify add 8 g/l Select-Agar
YPD	20 g/l Peptone, 20 g/l Glucose, 10 g/l Yeast extract (pH 6-6.3), to solidify add 20 g/l Oxoid Agar
CSM	1.7 g/l YNB (without amino acids), 5 g/l $(NH_4)_2SO_4$, 20 g/l Glucose, 0.65 g/l CSM, KH_2PO_4 (pH 6-6.3), to solidify add 20 g/l Oxoid Agar

After autoclaving and cooling down to a temperature of ~60°C, antibiotics were added to the media.

Table 2-3: List of antibiotics

Antibiotic	**Stock**	**Final concentration**	**Solvent**
Kanamycin	50 mg/ml	50 µg/ml	Water
Rifampicin	12,5 mg/ml	50 µg/ml	Methanol
Spectinomycin	50 mg/ml	100 µg/ml	Water
Gentamycin	10 mg/ml	25 µg/ml	Water
Carbenicillin	50 mg/ml	50 µg/ml	Water
Streptomycin	50 mg/ml	2.5 µg/ml	Water
Tetracycline	12.5 mg/ml	2.5 µg/ml	Ethanol

2.1.3 Plasmids

The following listed plasmids were used in this research. Plasmids with the indication “this thesis” were cloned *de novo* as part of this study.

Table 2-4: List of plasmids

Plasmid	Feature	Reference
pBAK1-BAK1-mEos3.2-nosT-Basta-BB10	Expression of BAK1-mEos3.2 for sptPALM	This thesis
pBIR3-BIR3-mEos3.2-nosT-Basta-BB10	Expression of BIR3-mEos3.2 for sptPALM	This thesis
pFLS2-FLS2-mEos3.2-nosT-Basta-BB10	Expression of FLS2-mEos3.2 for sptPALM	This thesis
2x35S-Eos-ROP6	Expression of Eos-ROP6 for sptPALM	Platre et al. (2019)
35S-HIR2-mEos3.2-nosT-pFast-BB10	Expression of HIR2-mEos3.2 for sptPALM	This thesis
Ubi-BIR2-paGFP-nosT-pFast-BB10	Expression of BIR2-paGFP for dual color sptPALM	This thesis
Ubi-BAK1-paTagRFP-nosT-pFast-BB10	Expression of BAK1-paTagRFP for dual color sptPALM	This thesis
HIR2-pK7FWG2	Expression of 35S-HIR2-eGFP *in planta*	This thesis
BAK1-pB7RWG2	Expression of 35S-BAK1-RFP *in planta*	Ladwig et al. (2015)
BIR2-pB7RWG2	Expression of 35S-BIR2-RFP *in planta*	Schlöffel et al. (2020)
BIR3-pB7RWG2	Expression of 35S-BIR3-RFP *in planta*	This thesis
FLS2-pB7RWG2	Expression of 35S-FLS2-RFP *in planta*	Glöckner et al. (2020)
BRI1-pB7RWG2	Expression of 35S-BRI1-RFP *in planta*	Ladwig et al. (2015)
35S-CERK1-mCherry-nosT-pFast-BB10	Expression of 35S-CERK1-mCherry *in planta*	This thesis
CLV1-pB7RWG2	Expression of 35S-CLV1-RFP *in planta*	This thesis
LTI6b-pB7RWG2	Expression of 35S-LTI6b-RFP *in planta*	AG Harter
pUBN-RFP-Dest	Expression of free cytosolic RFP *in planta*	Grefen et al. (2010)
BAK1-pGWB17	Expression of 35S-BAK1-4xmyc *in planta*	Halter et al. (2014)
FLS2-pK7FWG2	Expression of 35S-FLS2-eGFP *in planta*	Mueller et al. (2012)
BIR3-pGWB17	Expression of 35S-BIR3-4xmyc *in planta*	Dissertation S. Schulze
CERK1-pCAMBIA-NLuc	Expression of 35S-CERK1-HA-NLuc *in planta*	Ronja Burggraf

HIR2-pMetYC	Expression of methionine-repressible bait HIR2-Cub-PLV in yeast	Raffaele Manstretta
BIR2-pMetYC	Expression of methionine-repressible bait fusion BIR2-Cub-PLV in yeast	Julia Imkampe
BIR3-pMetYC	Expression of methionine-repressible bait fusion BIR3-Cub-PLV in yeast	Julia Imkampe
HIR2-pxNubA22	Constitutive expression of prey fusion HIR2-Nub-3xHA in yeast	Raffaele Manstretta
BAK1-pxNubA22	Constitutive expression of prey fusion BAK1-Nub-3xHA in yeast	Christopher Grefen
BRI1-pxNubA22	Constitutive expression of prey fusion BRI1-Nub-3xHA in yeast	Christopher Grefen
pNubWT- Xgate	Expression of NubWt protein in yeast	Grefen (2007)
pXNubA22-Dest	Expression of NubA protein in yeast	Grefen (2007)
$HIR2^{G2A}$-pK7FWG2	Expression of 35S-$HIR2^{G2A}$-eGFP *in planta*, myristylation mutant	This thesis
$HIR2^{C6,7S}$-pK7FWG2	Expression of 35S-$HIR2^{C6,7S}$-eGFP *in planta*, palmitoylation mutant	This thesis
$HIR2^{G2AC6,7S}$-pK7FWG2	Expression of 35S-$HIR2^{G2AC6,7S}$-eGFP *in planta*, myristylation and palmitoylation mutant	This thesis
amiHIR2-pGWB2	Expression of artificial microRNA for silencing of *HIR2* in *A. thaliana*	This thesis
amiHIR1-4-pGWB2	Expression of artificial microRNA for silencing of all 4 *HIR* genes in *A. thaliana*	This thesis
HIR2-pDGE347	*zm*Cas9 driven genome editing of HIR2 in *A. thaliana*	This thesis
HIR1-4-pDGE347	*zm*Cas9 driven genome editing of all 4 *HIR* genes in *A. thaliana*	This thesis

2.1.4 Primer

All primers were ordered by Eurofins Genomics. The lyophilized oligonucleotides were diluted to a concentration of 100 µM with nuclease-free water and the working solution had a final primer concentration of 100 pmol/µl.

Table 2-5: List of oligonucleotides

Primer	**Sequence 5´- > 3´**	**Characteristics**
mEos3.2_GG-D-E_F	TTATGGTCTCTAAGGGAATGTCTGCTATCAAGCCT	GoldenGate Cloning D-E Modul LI
mEos3.2 _GG-D-E_R	TTAAGGTCTCTGATTTTATCTTCTAGCGTTATCTGGAA	GoldenGate Cloning D-E Modul LI
GG_D-linker_F	TAGGTCTCAAAGGGAggtggaggaggttctggaggcggtggaagtg	GoldenGate linker before fluorophore
D_linker-Eos3.2_F	aggcggtggaagtggtggcggaggtagcATGTCTGCTATCAAGCCT	GoldenGate for D overhang + linker before fluorophore
Linker-PA-GFP_F	aggcggtggaagtggtggcggaggtagcATGGTGAGCAAGGGCGAA	GoldenGate Cloning D-E Modul LI
paGFP_GG-D-E_R	TTAAGGTCTCTGATTTTATCACTTGTAAAGCTCGTCCA	GoldenGate Cloning D-E Modul LI
Linker-paTagRFP_F	aggcggtggaagtggtggcggaggtagcATGGAACTCATCAAAGAAAACA	GoldenGate Cloning D-E Modul LI
paTagRFP_ D-E_R	TTAAGGTCTCTGATTTTATCAATTGAGCTTGTGCCCG	GoldenGate Cloning D-E Modul LI
pBIR2_GG_A-B_R	TTATGGTCTCTGCGGtattaagtgaggttgaggct	GoldenGate Cloning A-B Modul LI
pBIR2_GG_A-B_F	TTAAGGTCTCTCAGAggatgatgaagtggtttcag	GoldenGate Cloning A-B Modul LI
BIR2-cds_GG_B-D_R	TTATGGTCTCTTCTGAACAATGAAAGAGATCGGCTCA	GoldenGate Cloning B-D Modul LI
BIR2-cds_GG_B-D_F	TTAAGGTCTCTCCTTCACTTTCTCGTTCTCTTGC	GoldenGate Cloning B-D Modul LI
pBIR3_GG-A-B_F	TTATGGTCTCTGCGGGGATTTGGTTATGTCGAATTTT	GoldenGate Cloning A-B Modul LI
pBIR3_GG-A-B_R	TTAAGGTCTCTCAGAgattaaggatggatctagttc	GoldenGate Cloning A-B Modul LI
BIR3-cds_GG-B-D_F	TTATGGTCTCTTCTGAACAATGAAGAAGATCTTCATCACAC	GoldenGate Cloning B-D Modul LI
BIR3-cds_GG-B-D_R	TTAAGGTCTCTCCTTAGCTTCTTGTTTGTTGAAGAC	GoldenGate Cloning B-D Modul LI
HIR2-pENTR_F	CACCATGGGGAATCTTTTCTG	for pENTR/Topo cloning
HIR2-cds_F	ATGGGGAATCT TTCTGTTGC	RT-PCR *hir2-5* Primer 1

HIR2-cds_R	GGAGGCATTGTTGGCCTGT	for pENTR/Topo cloning, RT-PCR *hir2-5* Primer 2
HIR2_GG_B-D_F	TTATGGTCTCTTCTGAACAATGGGGAATCTTTTC TGTTGC	GoldenGate Cloning B-D Modul LI
HIR2_GG_B-D_R	TTAAGGTCTCTCCTTGGAGGCATTGTTGGCCTG	GoldenGate Cloning B-D Modul LI
HIR2-G2A_F	CACCATGGCGAATCTTTTCTGTTGCGTGCT	mutagenesis glycine2 to alanine
HIR2-G2A_R	GATTCGCCATGGTGAAGGGGGCGGCCGC	mutagenesis glycine2 to alanine
HIR2_C6,7S_F	GAATCTTTTCTCTTCCGTGCTTGTGA	mutagenesis cysteine 6 and 7 to serine
HIR2_C6,7S_R	TCACAAGCACGGAAGAGAAAAGATTC	mutagenesis cysteine 6 and 7 to serine
HIR2-G2AC76S_F	CACCATGGCGAATCTTTTCTCTTCCGTGCT	mutagenesis glycine2 to alanine in $HIR2^{C6,7S}$
EF1α_F	GAGGCAGACTGTTGCAGTCG	qPCR
EF1α_R	TCACTTCGCACCCTTCTTG	qPCR
HIR1-300_F	TGTCTTTGATGTGATCCGAGCA	qPCR
HIR1-514_R	CTCTCATTCTAGAAGCAGCATTG	qPCR
HIR2-511_F	AGAGTGGCAGCGAGCGAAA	qPCR, RT-PCR *hir2-5* Primer 3
HIR2-700_R	ACACATCCTTCGCTGACGTC	qPCR, RT-PCR *hir2-5* Primer 4
HIR3-494_F	AAATCAATGCAGCACAAAGGCTC	qPCR
HIR3-645_R	AAAAGTTCAATATGTTCTCCCTCAAT	qPCR
HIR4-177_F	GACAAAGACTAAGGACAATGTGTTT	qPCR
HIR4-327_R	GACACTCGCTCTAATAACATCAA	qPCR
sgRNA1_F	attgTGTGAAGCAATCAGATGTTG	Crispr HIR2
sgRNA1_R	aaacCAACATCTGATTGCTTCACA	Crispr HIR2
sgRNA2_F	attgAGACGGCGCCTGGACCGTGA	Crispr HIR2
sgRNA2_R	aaacTCACGGTCCAGGCGCCGTCT	Crispr HIR2
sgRNA3_F	attgCATGGCAAACAGTGACAACCCGG	Crispr HIR1
sgRNA3_R	aaacGGTTGTCACTGTTTGCCATG	Crispr HIR1
sgRNA4_F	attgTCTGCAGATCAAGCGTGCTG	Crispr HIR1
sgRNA4_R	aaacCAGCACGCTTGATCTGCAGA	Crispr HIR1
sgRNA5_F	attgACACGGTCCGGGACATGTGA	Crispr HIR3
sgRNA5_R	aaacTCACATGTCCCGGACCGTGT	Crispr HIR3
sgRNA6_F	attgACACGGTCCGGGACATGTGA	Crispr HIR3
sgRNA6_R	aaacTCACATGTCCCGGACCGTGT	Crispr HIR3
sgRNA7_F	attgTCAATCAACGGTAGCGATAA	Crispr HIR4
sgRNA7_R	aaacTTATCGCTACCGTTGATTGA	Crispr HIR4
sgRNA8_F	attgCAGAGGCAGGCGATTGTCGA	Crispr HIR4
sgRNA8_R	aaacTCGACAATCGCCTGCCTCTG	Crispr HIR4

Sail-LB	gcttcctattatatcttcccaaattacc	genotyping SAIL_1274_A05 (hir2-5)
a_SAIL_1274_A05	TCAGCAACTCGATGTTCAGTG	genotyping SAIL_1274_A05 (hir2-5)
b_SAIL_1274_A05	CGATTTTTCTCTCGCAAACAG	genotyping SAIL_1274_A05 (hir2-5)
HIR1-cds_F	ATGGGTCAAGCTTTGGGTTG	genotyping CRISPR HIR1-4
HIR1-cds_R	CTCAGCAGCAGAGTTACCCT	genotyping CRISPR HIR1-4
HIR3-cds-320_F	TTAGGGCTTTGGTCCCAATG	genotyping CRISPR HIR1-4
HIR3-cds_R	ACGTCGTTGACCTGAGTACTA	genotyping CRISPR HIR1-4
HIR4-cds_F	ATGGGGAATTTGTTTTGTTGTG	genotyping CRISPR HIR1-4
HIR4-cds_R	TTTGCGGACGAGCCTTGAA	genotyping CRISPR HIR1-4

2.1.5 Antibodies

Following listed antibodies were used for immunoblotting.

Table 2-6: List of primary antibodies

Primary antibody	**Origin**	**Use**	**Provider**
α-GFP	Goat	1:5000	Acris
α-RFP	Mouse	1:1000	Chromotek
α-Myc	Rabbit	1:5000	Sigma-Aldrich
α-HA	Mouse	1:2000	Sigma-Aldrich
α-BRI1	Rabbit	1:5000	Agrisera

Table 2-7: List of secondary antibodies

Secondary antibody	**Conjugate**	**Use**	**Provider**
α-goat IgG	HRP	1:10000	Sigma-Aldrich
α-rabbit IgG	HRP	1:75000	Agrisera
α-mouse IgG	HRP	1:10000	Santa Cruz

2.1.6 Chemicals

Chemicals used in this study were obtained from Carl-Roth, Sigma-Aldrich/Merck, Duchefa and Applichem. Enzymes were purchased from Thermo Fisher Scientific.

2.2 Methods

2.2.1 Molecular Biology Methods

2.2.1.1 Transformation of *Escherichia coli*

Chemical competent *E. coli* cells were transformed by heat shock. Cells stored at -80°C were defrosted on ice and 1-5 µl of plasmid DNA or ligation reaction mix was added. The heat shock was performed at 42°C for 45 s, followed by an incubation on ice of 1 min and the addition of 450 µl LB medium. The suspension was incubated for 1 hour at 37 °C shaking at 230 rpm. Subsequently, 200 µl were plated on selective LB plates and incubated at 37 °C overnight.

2.2.1.2 Transformation of *Agrobacterium tumefaciens*

For the transformation of electro competent agrobacteria (GV3101), 2 µl plasmid DNA were added to the cells, transferred into an electroporation cuvette and electroporated at 1600 V. Following, 450 µl LB medium was added and the cells were transferred back in a tube, followed by a 1.5 hours incubation at 28°C, while shaking at 230 rpm. Afterwards, the cell suspension was plated on LB plates containing respective antibiotics and incubated at 28 °C until colonies grew.

For the transformation of chemical competent agrobacteria (AGL1), the cells were defrosted on ice and 2 µl of plasmid DNA was added. The mixture was incubated for 5 minutes on ice, followed by 5 minutes in liquid nitrogen and 5 minutes heat shocked at 42°C. After adding 450 µl LB medium, the cells were proceed as described above.

2.2.1.3 Extraction of bacterial plasmid DNA

To isolate plasmid DNA, mini preps were performed with GeneJET Plasmid Miniprep Kit (Thermo Scientific) according to the manufacturer's protocol.

2.2.1.4 Extraction of plant genomic DNA

Extraction of genomic DNA was performed according to Edwards protocol (Edwards et al., 1991). A small leaf piece was homogenized in 200 µl Edwards buffer (200 mM Tris/HCl pH 7.5, 250 mM NaCl, 25 mM

EDTA pH 8 and 0.5 % (w/v) SDS) and centrifuged for 5 minutes at 13000 rpm. The supernatant was transferred in a fresh tube, 200 µl isopropanol was added, incubated for 5-45 minutes (depending on the leaf size) at room temperature to precipitate the DNA and subsequently centrifuged for 10 minutes at 13000 rpm at 4°C. The supernatant was discarded, and the pellet washed in 70 % ethanol. After a further centrifugation step of 5 minutes at 13000 rpm, the pellet was air dried and 50 µl of water were added.

2.2.1.5 RNA extraction

RNA from *Arabidopsis* leaves was extracted using the RNeasy Plant mini Kit of Qiagen according to the manufacturer's protocol.

2.2.1.6 Reverse transcription

For reverse transcription of RNA to cDNA the SuperScript IV Reverse Transcriptase (Thermo Scientific) was used, and the reaction was performed with 1 µg RNA, as described in the manufacturer's protocol.

2.2.1.7 Polymerase Chain Reaction (PCR)

To amplify DNA fragments for cloning purposes, the proofreading polymerase Phusion (Thermo Scientific) was used according to the protocol provided by the manufacturer. PCR reactions for genotyping or colony PCRs were performed with an in-house produced *Taq* polymerase. The master mix contained 1x reaction buffer (67 mM Tris, 16 mM $(NH_4)_2SO_4$, 2.5 mM $MgCl_2$, 0.01% Tween, pH 8.8), 125 µM dNTP mix, 0.5 µM forward and reverse primer, 0.5 µl *Taq* polymerase and 1-2 µl DNA. The amplification protocol was as follows: Initial denaturation for 3 min at 95°C, 30 cycles of denaturation (30 s, 95°C), primer annealing (30 s at primer melting temperature (T_m) minus 3°C) and elongation (1 min/kb at 72°C) and finished with 5 min final elongation step at 72°C.

2.2.1.8 Colony PCR

In order to analyze bacterial colonies after plasmid transformation, a single colony was picked with a 10 µl pipette tip and mixed in a PCR tube with 20 µl master mix, followed by an *Taq*-based PCR as described above.

2.2.1.9 Site-directed mutagenesis PCR

To modify single bases in plasmid DNA, a site-directed PCR was performed. For this, overlapping forward and reveres primers, containing the desired base exchanges, were designed and used in a PCR, in which the full plasmid was amplified.

2.2.1.10 DNA agarose gel electrophoresis

To separate DNA fragments by their size, the DNA samples were mixed with 5x DNA loading buffer (10 mM Tris pH 7.5, 60 mM EDTA, 60 % (v/v) glycerol, 0.25 % bromphenol blue) and loaded on an 1 % (w/v) agarose gel, mixed with 1x TAE buffer (40 mM Tris, 50mM acetic acid, 1 mM EDTA pH 8.5) and DNA stain peqGreen (dilution 1:5; Peqlab). The electrophoresis was performed at 120 V. As standard the GeneRuler 1 kb DNA ladder (Thermo Scientific) was used, and the DNA was visualized by UVP GelStudio PLUS (Analytik Jena).

2.2.1.11 In-gel purification of DNA

DNA extraction from agarose gels was performed using the Gel extraction kit of Machery-Nagel (NucleoSpin Gel-and PCR clean-up), according to the manufacturer's protocol.

2.2.1.12 Cloning strategies

As part of this work, different cloning techniques were utilized in order to assemble new plasmids. These are described in the following.

Golden Gate cloning

Golden Gate cloning was performed according to(Binder et al., 2014). Deviating to the system described in the publication, no N-tag module was used. The B-overhang was instead added to the module containing the gene of interest at its N-terminal end. Level I modules were obtained by blunt-end ligation into pCR1.2 (Thermo Scientific) vector.

Gateway cloning

The Gateway cloning technology (Thermo Scientific) were used according to the manufacturer's protocol. To generate entry clones either pENTR/D-TOPO or the pCR8/GW/TOPO cloning kit was used. A-overhangs, which had to get attached, 7.9 µl of PCR amplicons, 1 µl 10 mM dATP, 1 µl 10x *Taq*-buffer and 0.1 µl *Taq* polymerase were incubated for 10 min at 72°C. The TOPO reaction was transformed into *E. coli* cells. To transfer the gene of interest into an expression vector, LR reaction was performed using the Gateway LR Clonase II Enzyme Mix (Thermo Scientific).

Cloning of CRISPR/Cas9 constructs

CRISPR/Cas9 constructs were cloned according to (Stuttmann et al., 2021). Target sites were chosen using three different online tools: CCTop (Stemmer et al., 2015), ChopChop (Labun et al., 2019) and CRISPR-P 2.0 (Liu et al., 2017).

Cloning of artificial microRNA silencing constructs

Artificial microRNA cloning was performed according to the online WMD3-Web MicroRNA Designer (Version 3.2©, Copyright 2005-2018 Max Planck Institute for Developmental Biology, Tübingen. http://www.weigelworld.org). Target search parameters did not allow off-targets and target sequences were cloned by site-directed mutagenesis in the endogenous miR319a precursor. The destination vector pGWB2 served as expression vector. The target sequences and primers used for cloning of the amiRNA constructs are listed below.

Table 2-8: List of sequences for generating amiRNA constructs

	Sequence 5´- > 3´	
HIR2 amiRNA	TCTAGTTGTACTACCCCTCGG	
primer for cloning	I miR-s	gaTCTAGTTGTACTACCCCTCGGtctctcttttgtattcc
	II miR-a	gaCCGAGGGGTAGTACAACTAGAtcaaagagaatcaatga
	III miR*s	gaCCAAGGGGTAGTAGAACTAGTtcacaggtcgtgatatg
	IV miR*a	gaACTAGTTCTACTACCCCTTGGtctacatatatattcct
HIR1/HIR2/HIR3/HIR4 amiRNA	TGTGTCAAAGTACTGAGTCAC	
primer for cloning	I miR-s	gaTGTGTCAAAGTACTGAGTCACtctctcttttgtattcc
	II miR-a	gaGTGACTCAGTACTTTGACACAtcaaagagaatcaatga
	III miR*s	gaGTAACTCAGTACTATGACACTtcacaggtcgtgatatg
	IV miR*a	gaAGTGTCATAGTACTGAGTTACtctacatatatattcct

2.2.1.13 DNA sequencing

For DNA sequencing the sanger sequencing light run service of Eurofins Genomics was utilized. The results were analyzed by aligning the received sequences to the reference gene sequence using the software CLC Main Workbench (8.0.1 Qiagen).

2.2.1.14 Quantitative real-time PCR

For quantitative real-time PCR (qPCR) reactions, cDNA (chapter 2.2.1.6) was mixed with SYBR Green Fluorescein Mix (Thermo Scientific) according to the manufacturer's protocol and intron-intron spanning primers. The PCR reaction was measured with the CFX384 Real-Time PCR detection system (BioRad).

2.2.2 Biochemical methods

2.2.2.1 Protein extraction from leaf tissue

To extract proteins from leaf tissue, the plant material was ground in liquid nitrogen either in a mortar or by usage of the TissueLyser LT (Qiagen). For rapid extraction, the leaf material was mixed with 3x SDS-loading buffer (312.5 mM Tris/HCl pH 6.8, 10% (w/v) SDS, 10 mM DTT 50% (v/v) glycerol, 0.05% (w/v) bromophenol blue). Alternatively, 800 µl ice-cold extraction buffer (10% glycerol, 150 nM Tris/HCl,

pH 7.5, 1 mM EDTA, 150 mM NaCl, 10 mM DTT, 0.2% Nonidet P-40, 2% PVPP, 1 tablet of proteinase inhibitor cocktail (Roche) per 10 ml solution) were added to 200 mg of leaf powder. The mixture was incubated at 4°C on a rotor for 1 hour. Following, the extract was centrifugated at 5 000 x g for 20 min at 4°C. The supernatant was filtered through one layer of Miracloth (Roche), mixed with 3x SDS-loading buffer and boiled for 5 min at 59°C.

2.2.2.2 SDS-Polyacrylamide gel electrophoresis (SDS-PAGE)

Protein extracts (see chapter 2.2.2.1) were separated by SDS-PAGE. After samples were boiled, 20 µl were loaded on a SDS-polyacrylamide (5% stacking gel (1.3 ml H_2O, 0.34 ml acrylamide-bisacrylamide mix (37.5:1), 0.5 ml 1 M Tris pH 6.8, 20 µl 10% SDS, 20 µl 10% Ammonium persulfate (APS) and 2 µl Tetramethylethylenediamine (TEMED)) and 8% separation gel (2.3 ml H_2O, 1.3 ml acrylamide-bisacrylamide mix (37.5:1), 1.3 ml 1.5 M Tris pH 8.8, 50 µl 10% SDS, 50 µl 10% APS and 3 µl TEMED)). The Mini-PROTEAN Tetra Cell (BioRad) system was used. The electrophoresis was performed at 200 mA per gel for ~1 hour in 1x SDS running buffer (25 mM Tris base, 192 mM glycine, 0.1% (w/v) SDS). As size standard, 5 µl of prestained protein ladder PageRuler (Thermo Scientific) was used. The gel was further processed for immunoblot analysis (see chapter 2.2.2.3).

2.2.2.3 Immunoblot analysis

By SDS-PAGE separated proteins were transferred to a nitrocellulose membrane (GE Healthcare) using the BioRad Tetra Blotting Module. The transfer was performed at 100 V for 1 hour in cold 1x transfer buffer 5 mM Tris base, 192 mM glycine, 20% ethanol). The membrane was blocked in 5% milk (w/v) PBS-T (137 mM NaCl, 27 mM KCl, 10 mM Na_2HPO_4, 2 mM KH_2PO_4, pH 7.4, 0.1% Tween 20) buffer for 1 hour at room temperature. Following, the membrane was incubated with first antibody (diluted in milk/PBS-T buffer) at 4°C overnight. The next day, the membrane was washed three times for 10 minutes in PBS-T and incubated for 1 hour with the secondary antibody and subsequently washed three times in PBS-T. Afterwards, the membrane was incubated in ECL prime reagent (GE Healthcare) and the proteins detected with Amersham Imager 600 (GE Healthcare) imaging system.

2.2.2.4 Co-immunoprecipitation (Co-IP)

For Co-IP experiments, proteins were extracted as described before (chapter 2.2.2.1). Agarose beads (Chromotek) were washed three times with GTEN buffer (10% glycerol, 150 mM Tris/HCl, pH 7.5, 1 mM EDTA, 150 mM NaCl, 10 mM DTT, 0.2% Nonidet P-40) and added to the filtered protein extract, of which 30 µl were kept before to detect input levels. The mixture with the beads was incubated for 1 hour at 4°C on a rotor. Following, the beads were washed two times with buffer A 50 mM Tris/HCl, pH 7.5, 150 mM NaCl) and once with buffer B (50 mM Tris/HCl, pH 7.5, 50 mM NaCl). The supernatant was removed by centrifugation for 2 minutes at 2500 x g. The eluate bonded proteins from the beads, 3xSDS-loading buffer was added and boiled for 5 minutes at 95°C.

2.2.2.5 Isolation of microsomal fractions

In order to extract microsomal fractions, 200 mg leaf tissue was ground on liquid nitrogen and homogenized in 600 µl lysis buffer (0.33 M sucrose, 20 mM Tris-HCl pH 7.5, 1 mM EDTA, 10 mM DTT and 1 tablet of proteinase inhibitor cocktail (Roche)). The lysate was centrifuged at 5000 x g for 10 minutes at 4°C. The supernatant was centrifuged at 42000 rpm for 45 minutes. The pellet containing the microsomal proteins as well as the supernatant containing soluble proteins were resuspended in 3x SDS loading buffer and processed as described for SDS-PAGE (chapter 2.2.2.2) and Immunoblot analysis (chapter 2.2.2.3).

2.2.2.6 Measurement of reactive oxygen species (ROS) production

Oxidative burst was measured based on a luminol assay. For that, five to six-week-old *A. thaliana* leaves were cut into equal squares and floated in H_2O overnight. One piece was transferred in one well of a 96-well plate, containing 90 µl substrate solution (5 µM luminol L-012 (Wako) and 2 µg/ml peroxidase). Before adding of the elicitor, background measurement was performed for 10 minutes). The ROS burst was measured by luminescence detection for at least 30 minutes in the luminometer (Centro LB 960, Berthold Technologies).

2.2.2.7 Mating-based split-ubiquitin system (mbSUS)

For analysis of direct protein-protein interactions, the mbSUS was performed according to Grefen 2009 and Grefen, 2014.

2.2.2.8 Predictions for posttranslational modifications

To predict posttranslational lipidation modifications, the online tools NBA-Palm (http://nbapalm.biocuckoo.org/) (Xue et al., 2006), CCPalm 4.0 (http://gpspalm.biocuckoo.cn/) (Ning et al., 2020) and ExPASy Myristoylator (https://web.expasy.org/myristoylator/) (Bologna et al., 2004) were used.

2.2.3 Plant methods

2.2.3.1 Plant growth conditions

Arabidopsis thaliana plants were grown under short day conditions (8 hours light, 16 hours darkness, 22°C, 110mE$m^{-2}s^{-1}$ and 60% relative humidity) in a growth chamber und used for functional assays. *Arabidopsis* plants, grown in long day conditions (16 hours light, 8 hours dark), were either used for seed production or stable genetic transformations. *N. benthamiana* plants were grown in the greenhouse under long day conditions.

2.2.3.2 Transient transformation of *Nicotiana benthamiana*

For transient protein expression in *N. benthamiana*, Agrobacterium mediated transformation was used. For this, *A. tumefaciens*, carrying the expression cassette for the protein of interest, was cultivated in 5-10 ml liquid culture (LB medium containing respective antibiotics) at 28°C and 220 rpm overnight. The cells were harvested by centrifugation at 4000 x g for 10 minutes. The pellet was resuspended in 10 mM $MgCl_2$ and diluted to a final OD_{600}=0.5 and mixed in the ratio 1:0.7 with the silencing inhibitor p19 (Voinnet et al., 2003) and after addition of 150 µM acetosyringone, incubated for at least 90 minutes at room temperature. The suspension was infiltrated with a needless syringe into the abaxial leaf site of four-week-old tobacco plants. The leaves were harvested 2 to 3 days post infiltration.

2.2.3.3 Stable transformation of *Arabidopsis thaliana*

For stable transformation, the flowers of one-month old *Arabidopsis* plants were dipped into an Agrobacteria suspension (OD_{600}=0.8 in 5 % (w/v) sucrose, 0.02 % (v/v) Silwet-L77) for 5 minutes and stored in a humid environment for 16-24 hours.

2.2.3.4 Seed sterilization

Seed sterilization was achieved by incubation in 70 % EtOH for 10 minutes at room temperature, while rotating. Following, the seeds were washed twice with 100 % EtOH and air dried.

2.2.3.5 Seed selection

Transgenic seeds carrying a Kanamycin resistance were grown on ½ MS plates containing 50 µg/ml Kanamycin and grown under short day conditions for 10 days until resistant seedlings were easily distinguishable from non-resistant by green open cotyledons.

The seeds carrying the FastRed fluorescent marker were selected using the Axio Zoom V16 microscope (Zeiss) with the filter set 63 HE. The identified fluorescent seeds were planted into soil.

2.2.4 Microscopy

2.2.4.1 Confocal laser scanning microscopy

Confocal laser scanning microscopy (CLSM) was performed either at the SP8 confocal laser scanning microscope (Leica Microsystems GMBH) with LAS X software or with the LSM880 (Zeiss, software ZENblack). Images were taken by using a 63x/1.2 water-immersion objective and 40x/1.2 water-immersion objective, respectively. eGFP was exited at 488 nm and the emission was detected in a range of 500-550 nm; RFP was excited at 561 nm with an emission spectrum of 600-650 nm.

For Fluorescence Resonance Energy Transfer-Fluorescence Lifetime Imaging Microscopy (FRET-FLIM) analysis, donor and acceptor proteins were transiently expressed in *N. benthamiana* and imaged with the SP8 in combination with SymPho Time 46 software (PicoQuant) as described in Pruitt et al. (2021). The GFP fluorescence lifetime τ [ns] was obtained by bi-exponential curve fitting in a defined region of interest

covering the plasma membrane. As cell death is shown to correlate with high amplitude A [2] values, data were only included when A [1] [kCnts] to A [2] [kCnts] ratio was above 1.5.

2.2.4.2 Super resolution microscopy

In order to perform single-particle tracking photoactivated localization microscopy (sptPALM) experiments, a TIRF/VAE microscope built by Sven zur Oven-Krockhaus was used. The software is based on a self-written MATLAB script (zur Oven-Krockhaus, 2021). Details for the used filters can be found in Table 2-9.

Table 2-9: Filter details used for sptPALM

Fluorophore	Long pass filter	Band pass filter
mEos3.2	LP 568 (RazorEdge, Semrock, LP02-568RS-25)	BP 580/25 (ET Bandpass, AHF Analysentechnik AG, F49-580)
paGFP	LP 488 (RazorEdge, AHF Analysentechnik AG, F76-488)	BP 525/50 (BrightLine HC, AHF Analysentechnik AG, F37-516)
paTagRFP	LP 568 (RazorEdge, Semrock, LP02-568RS-25)	BP 607/36 (BrightLine HC, AHF Analysentechnik AG, F39-607)

The sptPALM experiments were performed in transiently transformed *Nicotiana benthamiana*, expressing the protein of interest coupled with a photoconvertible or photoactivatable fluorophore (mEos3.2, paGFP or paTagRFP). Imaging was performed two to three days after transformation. Leave pieces with a size of around 0.5 cm^2 were placed between two cover slips and imaged in water, mock or peptide solutions. The epidermal cells were brought into focal plane in transmitted light mode, followed by epifluorescence and imaged with VAEM. The number of emitting fluorophores was controlled by UV light intensity.

For single-particle tracking 2000 or 5000 frames were measured with an acquisition time of 0.05 s/frame and a window size of 128x128 pixel. For the tracking analysis, a maximal linking distance of 300 nm and a maximal gap closing of 4 frames were set. The minimal track length contained 8 data points. The mean square displacement (MSD) and the apparent diffusion coefficient were calculated from the tracking information. For the cluster analysis, a minimal track length of 3 data points was used and the data were further proceed in the SR-Tesseler software (Levet et al., 2015) to build Voronoi diagrams. Here, polygons, based on the localized molecules, were created and computed as one object. Thresholds for the cluster

definition were a density factor of 2 and a minimal localization number of 5. The cluster diameter was calculated based on the assumption of a circular cluster area.

2.2.5 Statistical analysis

Statistical analysis was performed using the software JMP (16.0.0 SAS institute) and Microsoft Excel (2019). Statistically significant differences were indicated by asterisks (* $p < 0.05$, ** $p < 0.01$, *** $p < 0.001$). The data from FLIM measurements and diffusion coefficients of sptPALM data were tested for normal Gaussian distribution and non-parametric distributed data sets were analyzed with by a two-tailed, all-pair Kruskal-Wallis test followed by a Steel-Dwass post hoc correction. Statistical analysis for cluster sizes were calculated for log normal distributed data by Z-score method according to Zhou et al. (1997).

3 RESULTS

3.1 PART A: Functional characterization of HYPERSENSITIVE INDUCED REACTION 2

LRR-RLKs are heterogeneously distributed within the plasma membrane and compartmentalized into nanodomains (Bücherl et al., 2013; Bücherl et al., 2017; Hutten et al., 2017). Only little is known how LRR-RLKs are recruited into nanodomains and how these are maintained. SPFH-domain containing proteins are described to be involved in protein complex assemblies and are proposed to be organizing factors for nanodomains by promoting protein complex formation of signaling components at the plasma membrane (Browman et al., 2007; Qi et al., 2011; Qi & Katagiri, 2012; Yu et al., 2020; Martinière & Zelazny, 2021). HYPERSENSITIVE INDUCED REACTION 2 (HIR2) belongs to the protein family of SPFH-domain containing proteins, and the first part of this thesis focused on studying its function and its involvement in membrane organization of immunity receptor complexes.

3.1.1 HIR2 serves as multi-interactor for different receptor kinases

HIR2 was identified in interactome analysis of BIR2 and BIR3 by LC/ESI-MS/MS and hypothesized to be a potential candidate for scaffolding immune-receptor complexes into nanodomains (Halter et al., 2014; Schulze, 2020). To confirm these interaction, Co-IP experiments, FRET-FLIM and mbSUS analysis were performed and additional potential interaction partner of HIR2 were investigated.

To analyze the interaction of HIR2 with BIR2, fusion proteins of HIR2-GFP and BIR2-RFP were transiently co-expressed under the constitutively active 35S promoter in *N. benthamiana* and Co-IP experiments were performed. In order to suppress the RNA silencing machinery, p19 was co-expressed with the respective proteins and p19 alone served as a negative control. HIR2-GFP served as target protein for the immunoprecipitation and a co-immunoprecipitation with BIR2-RFP was detectable. A weak unspecific binding of BIR2-RFP was visible in the control (Figure 3-1 A).

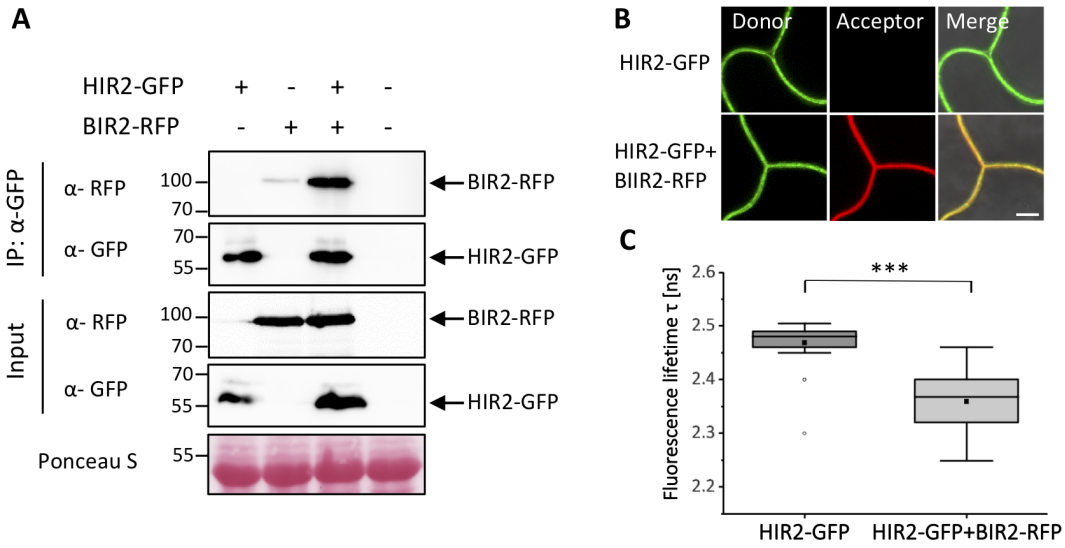

Figure 3-1: HIR2 shows interaction with BIR2 in Co-IP and FRET-FLIM. For interaction analysis, 35S-HIR2-GFP and 35S-BIR2-RFP were transiently expressed in *N. benthamiana.* [**A**] Co-IP of HIR2-GFP and BIR2-RFP was performed with GFP beads. Precipitated HIR2-GFP and co-immunoprecipitated BIR2-RFP were detected with α-GFP and α-RFP antibodies, respectively. Inputs were taken prior to the IP and detected as mentioned above. Infiltration of p19 only served as negative control. Ponceau S staining indicates protein loading. [**B**] CLSM images of a representative part of the plasma membrane, which were used for FRET-FLIM. The measurements were performed in *N. benthamiana* leaves transiently expressing 35S-HIR2-GFP as donor alone and co-expressing with 35S-BIR2-RFP as acceptor. [**C**] The average GFP fluorescence lifetime τ [ns] was obtained by bi-exponential curve fitting in a defined region of interest covering the plasma membrane and shown in the Boxplot. The center line indicates the median and the square indicates the mean. The bounds of the box show the 25th and the 75th percentiles, the whiskers indicate a range within 1.5 × IQR, outliers are displayed by open circles. Significant differences were analyzed with Kruskal-Wallis test followed by a Steel-Dwass post hoc correction and indicated by asterisks ($p<0.001$ ***). The scale bar represents 5 µm and applies to all images. Donor HIR2-GFP: $n= 34$; Acceptor BIR2-RFP: $n= 34$. Experiments were performed on three independent days.

Furthermore, the spatial proximity of HIR2 and BIR2 was investigated by FRET-FLIM measurements. HIR2-GFP served as donor and BIR2-RFP as acceptor. The fusion proteins were transiently expressed under the constitutively active 35S promoter in *N. benthamiana.* The fluorescence lifetime of the donor HIR2-GFP showed an average of 2.47 ns (± 0.04). Co-expression of HIR2-GFP with BIR2-RFP showed their co-localization at the plasma membrane and a significant reduction in the fluorescence lifetime to a mean value of 2.37 ns (± 0.05) was detectable (Figure 3-1 B, C). The results from these protein interaction data demonstrated a complex formation of HIR2 and BIR2.

Next, the association of HIR2 with BIR3 was investigated. Co-IP experiments were performed with transiently co-expressed 35S-HIR2-GFP and 35S-BIR3-myc fusion proteins in *N. benthamiana.* The protein tags and the target protein for the pulldown were chosen differently than in the interaction analysis with BIR2 to facilitate co-immunoprecipitation at best.

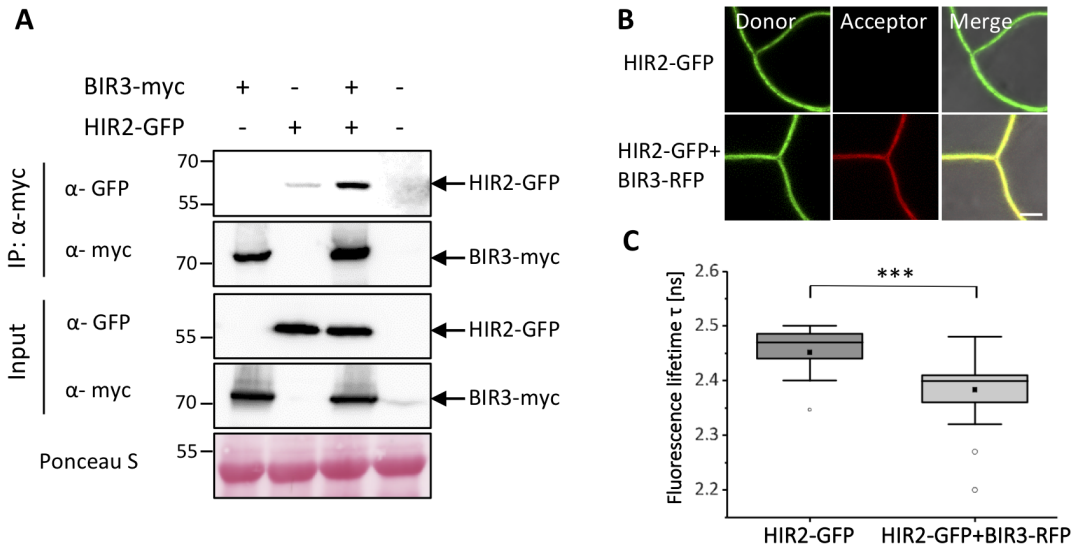

Figure 3-2: HIR2 shows interaction with BIR3 in Co-IP and FRET-FLIM. [**A**] For Co-IP interaction analysis, 35S-BIR3-myc and 35S-HIR2-GFP were transiently expressed in *N. benthamiana* and IP was performed with Myc beads. Precipitated BIR3-myc and co-immunoprecipitated HIR2-GFP were detected with α-myc and α-GFP antibodies, respectively. Inputs were taken prior to the IP and detected as mentioned above. Infiltration of p19 only served as negative control. Ponceau S staining indicates protein loading. [**B**] CLSM images of a representative part of the plasma membrane, which were used for FRET-FLIM. The measurements were performed in *N. benthamiana* leaves transiently expressing 35S-HIR2-GFP as donor alone and co-expressing with 35S-BIR3-RFP as acceptor. [**C**] The average GFP fluorescence lifetime τ [ns] was obtained by bi-exponential curve fitting in a defined region of interest covering the plasma membrane and shown in the Boxplot. The center line indicates the median and the square indicates the mean. The bounds of the box show the 25th and the 75th percentiles, the whiskers indicate a range within 1.5 × IQR, outliers are displayed by open circles. Significant differences were analyzed with Kruskal-Wallis test followed by a Steel-Dwass post hoc correction and indicated by asterisks ($p<0.001$ ***). The scale bar represents 5 µm and applies to all images. Donor HIR2-GFP: n= 36; Acceptor BIR3-RFP: n= 45. Experiments were performed on three independent days.

The pulldown was performed with BIR3-myc as target protein and a co-precipitation with HIR2-GFP was detected by immunoblotting. Thereby, a weak unspecific binding of HIR2-GFP to Myc-beads was detected (Figure 3-2 A). To quantify the molecular interaction of HIR2 and BIR3 by FRET-FLIM, 35S-HIR2-GFP and 35S-BIR3-RFP were transiently expressed in tobacco leaves (Figure 3-2 B). The expression of HIR2-GFP alone served as donor control, which had an average fluorescence lifetime of 2.45 ns (± 0.07). Co-expressing HIR2-GFP with the acceptor BIR3-RFP showed a significant reduction of fluorescence lifetime to 2.37 ns (± 0.06) (Figure 3-2 C).

These results demonstrated a close spatial proximity as well as a potential physical interaction of HIR2 with BIR2 and BIR3, which confirmed the LC/ESI-MS/MS results (Halter et al., 2014; Schulze, 2020).

The BIR proteins constitutively interact with the co-receptor BAK1 and serve as negative regulators of PAMP induced signaling pathways (Halter et al., 2014; Imkampe et al., 2017). In presence of the bacterial flagellin peptide, BAK1 gets released from BIR2, allowing BAK1 to interact with the ligand binding LRR-RLK FLS2 (Halter et al., 2014). The interaction of HIR2 and FLS2 was previously shown by Qi and Katagiri (2012) by Co-immunoprecipitation and verified in this work by FRET-FLIM measurements (Supplemental figure 1).

After confirming the interaction of HIR2 with BIR2 and BIR3 as well as with FLS2, it was analyzed whether HIR2 interacts with BAK1. The association of HIR2 with BAK1 was investigated by Co-IP experiments. Fusion proteins of HIR2-GFP and BAK1-myc were transiently expressed under the constitutively active 35S promoter in *N. benthamiana.* As negative control, the silencing suppressor p19 was used as described above. In addition, the involvement of the peptide flagellin 22 (flg22) on the interaction of HIR2 and BAK1 was analyzed. For this, 100 nM of flg22 were infiltrated in tobacco leaves expressing both proteins of interest before harvesting. To verify the activity of the peptide, the association of FLS2-GFP and BAK1-myc were used as control.

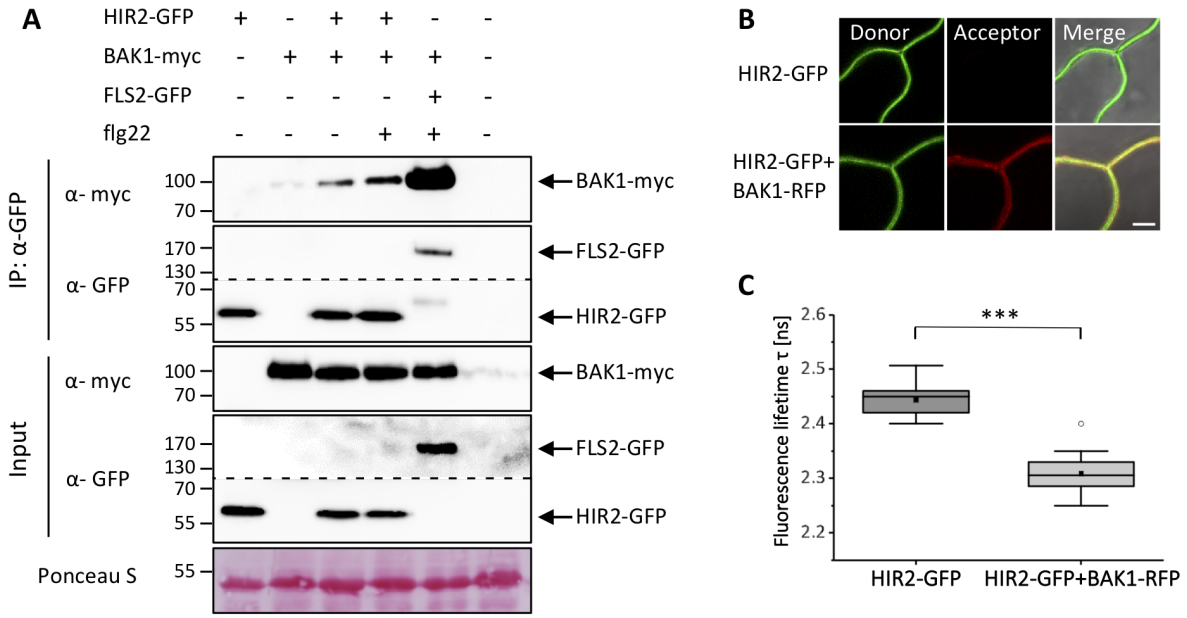

Figure 3-3: HIR2 shows interaction with BAK1 in Co-IP and FRET-FLIM. [**A**] For Co-IP interaction analysis, 35S-HIR2-GFP and 35S-BAK1-myc were transiently expressed in *N. benthamiana* and IP was performed with GFP beads. Precipitated HIR2-GFP and co-immunoprecipitated BAK1-myc were detected with α-GFP and α-myc antibodies, respectively. The effect of flg22 treatment on the interaction was analyzed by additional infiltration of the flg22 peptide (100 nM). The interaction of FLS2-GFP and BAK1-myc served as positive control for flg22 treatment. Inputs were taken prior to the IP and detected as mentioned above. Infiltration of p19 only served as negative control. Ponceau S staining indicates protein loading. The dotted lines indicate cut of the same blot.

[**B**] CLSM images of a representative part of the plasma membrane, which were used for FRET-FLIM. The measurements were performed in *N. benthamiana* leaves transiently expressing 35S-HIR2-GFP as donor alone and co-expressing with 35S-BAK1-RFP as acceptor. [**C**] The average GFP fluorescence lifetime τ [ns] was obtained by bi-exponential curve fitting in a defined region of interest covering the plasma membrane and shown in the Boxplot. The center line indicates the median and the square indicates the mean. The bounds of the box show the 25th and the 75th percentiles, the whiskers indicate a range within 1.5 × IQR, outliers are displayed by open circles. Significant differences were analyzed with Kruskal-Wallis test followed by a Steel-Dwass post hoc correction and indicated by asterisks ($p<0.001$ ***). The scale bar represents 5 µm and applies to all images. Donor HIR2-GFP: n= 42; Acceptor BAK-RFP: n= 30. Experiments were performed on three independent days.

BAK1-myc was co-immunoprecipitated with HIR2-GFP and FLS2-GFP (Figure 3-3 A). Treatment with the PAMP flg22 did not influence the interaction of HIR2-GFP and BAK1-myc. Confocal laser scanning microscopy showed the co-localization of HIR2 and BAK1 at the plasma membrane. To confirm their association, FLIM measurements were performed. For this, HIR2-GFP and BAK1-RFP were transiently expressed in *N. benthamiana* and fluorescence lifetime of GFP was measured. The donor control HIR2-GFP had an average fluorescence lifetime of 2.45 ns (± 0.03). In samples where HIR2-GFP was co-expressed with the acceptor BAK1-RFP, a significant decrease in fluorescence lifetime to 2.31 ns (± 0.04) was detected (Figure 3-3 C), indicating a close proximity of these two proteins.

Furthermore, the association of HIR2 with an LRR-RLK, which is not involved in plant immunity, was investigated. After confirming the interaction of HIR2 with BAK1 and BIR3, which are both involved in brassinosteroid signaling by interaction with the brassinosteroid receptor BRI1, the interaction of HIR2 and BRI1 was tested (Li et al., 2002; Nam & Li, 2002; Imkampe et al., 2017).

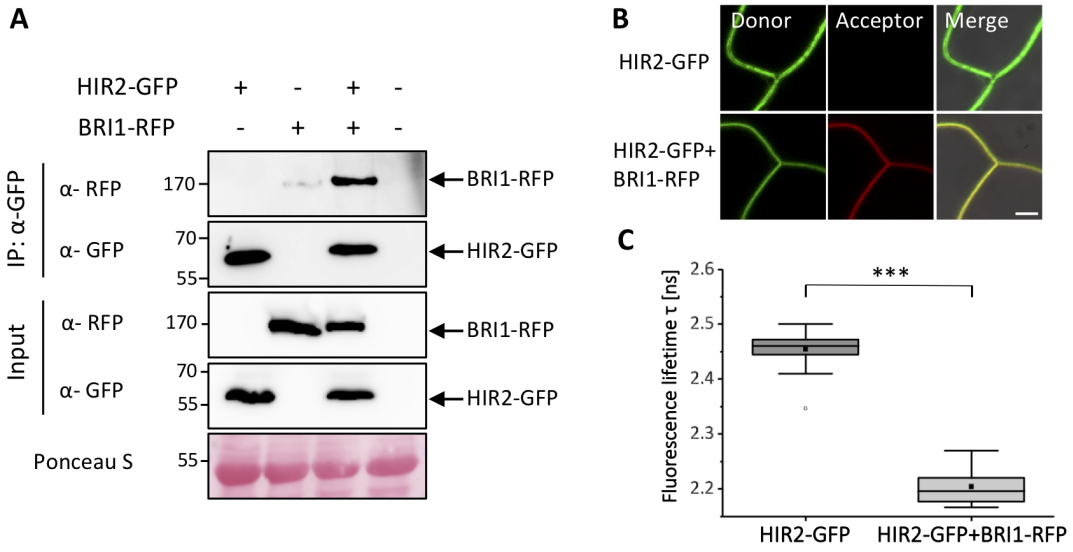

Figure 3-4: HIR2 shows interaction with BRI1 in Co-IP and FRET-FLIM. For interaction analysis, 35S-HIR2-GFP and 35S-BRI1-RFP were transiently expressed in *N. benthamiana*. [**A**] Co-IP of HIR2-GFP and BRI1-RFP was performed with GFP beads. Precipitated HIR2-GFP and co-immunoprecipitated BRI1-RFP were detected with α-GFP and α-RFP antibodies, respectively. Inputs were taken prior to the IP and detected as mentioned above. Infiltration of p19 only served as negative control. Ponceau S staining indicates protein loading. [**B**] CLSM images of a representative part of the plasma membrane, which were used for FRET-FLIM. The measurements were performed in *N. benthamiana* leaves transiently expressing 35S-HIR2-GFP as donor alone and co-expressing with 35S-BRI1-RFP as acceptor. [**C**] The average GFP fluorescence lifetime τ [ns] was obtained by bi-exponential curve fitting in a defined region of interest covering the plasma membrane and shown in the Boxplot. The center line indicates the median and the square indicates the mean. The bounds of the box show the 25th and the 75th percentiles, the whiskers indicate a range within 1.5 × IQR, outliers are displayed by open circles. Significant differences were analyzed with Kruskal-Wallis test followed by a Steel-Dwass post hoc correction and indicated by asterisks ($p<0.001$ ***). The scale bar represents 5 µm and applies to all images. Donor HIR2-GFP: *n*= 16; Acceptor BRI1-RFP: *n*= 19. Experiments were performed on three independent days.

The fusion proteins 35S-HIR2-GFP and 35S-BRI1-RFP were transiently expressed in tobacco and used for Co-IP experiments as well as for FRET-FLIM measurements. As negative control for unspecific binding of proteins to the beads during immunoprecipitation p19 only was used. The Co-IP experiments revealed that HIR2 is interacting with BRI1 (Figure 3-4 A). The localization to the plasma membrane was shown by confocal laser scanning microscopy for both proteins and fluorescence lifetime differences in the samples were analyzed. HIR2-GFP expressed as donor control had a mean fluorescence lifetime of 2.45 ns (± 0.03). Co-expression with the acceptor BRI1-RFP significantly decreased the GFP lifetime to 2.16 ns (± 0.05) (Figure 3-4 C). The fluorescence decay indicates a close distance of both proteins at the plasma membrane and validated the results of the Co-IP experiments.

After confirming that the interactome of HIR2 is not restricted to immunity related LRR-RLKs, as shown by the association with BRI1, interaction analysis with a Lysin motif (LysM) kinase was performed. For this,

the chitin receptor CERK1 was chosen as it seems to signal BAK1 independent (Miya et al., 2007; Couto & Zipfel, 2016; Yu et al., 2017b). To investigate the interaction by Co-IP experiments, fusion proteins of HIR2-GFP and CERK1-HA were transiently expressed under the constitutive active 35S promoter in *N. benthamiana*.

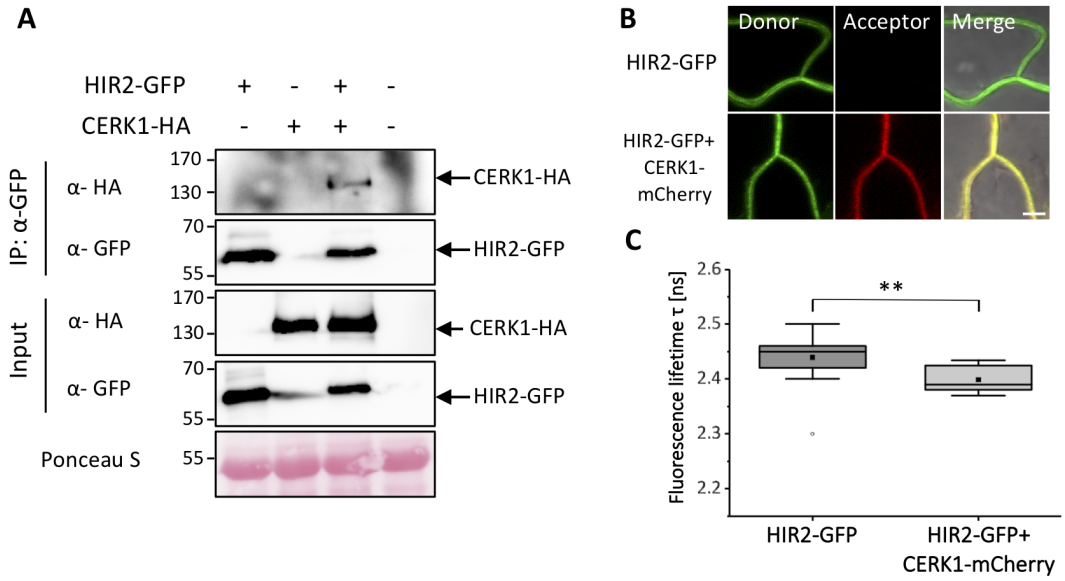

Figure 3-5: HIR2 shows interaction with CERK1 in Co-IP and FRET-FLIM. [**A**] For Co-IP interaction analysis, 35S-HIR2-GFP and 35S-CERK1-HA were transiently expressed in *N. benthamiana* and IP was performed with GFP beads. Precipitated BIR3-myc and co-immunoprecipitated HIR2-GFP were detected with α-GFP and α-HA antibodies, respectively. Inputs were taken prior to the IP and detected as mentioned above. Infiltration of p19 only served as negative control. Ponceau S staining indicates protein loading. [**B**] CLSM images of a representative part of the plasma membrane, which were used for FRET-FLIM. The measurements were performed in *N. benthamiana* leaves transiently expressing 35S-HIR2-GFP as donor alone and co-expressing with 35S-CERK1-mCherry as acceptor. [**C**] The average GFP fluorescence lifetime τ [ns] was obtained by bi-exponential curve fitting in a defined region of interest covering the plasma membrane and shown in the Boxplot. The center line indicates the median and the square indicates the mean. The bounds of the box show the 25th and the 75th percentiles, the whiskers indicate a range within 1.5 × IQR, outliers are displayed by open circles. Significant differences were analyzed with Kruskal-Wallis test followed by a Steel-Dwass post hoc correction and indicated by asterisks ($p<0.01$ **). The scale bar represents 5 µm and applies to all images. Donor HIR2-GFP: n= 21; Acceptor CERK1-mCherry: n= 9. Experiments were performed on three independent days.

A small amount of CERK1-HA protein was co-immunoprecipitated with HIR2-GFP (Figure 3-5 A). FRET-FLIM was measured to further confirm the findings of the previous experiments. HIR2-GFP and CERK1-mCherry fusion proteins were transiently expressed in *N. benthamiana*. The donor HIR2-GFP showed a mean fluorescence lifetime of 2.44 ns (± 0.04). When HIR2-GFP was co-expressed with the acceptor protein CERK1-mCherry, the fluorescence lifetime decreased to a mean value of 2.39 ns (± 0.02) (Figure 3-5 C).

While protein interactions detected in Co-IP experiments are not inevitably direct interactions, since the binding could be mediated by a third protein (Mackay et al., 2007), and a decrease in fluorescent lifetime measured by FRET-FLIM analysis indicate a close spatial proximity of two proteins *in vivo,* a split-ubiquitin based assay was additionally performed in yeast (mbSUS).

Full length proteins of HIR2, BAK1, BIR2/3, BRI1 and CERK1 were either fused to a N-terminal (Nub, "Prey") or C-terminal (Cub, "Bait") half of ubiquitin and expressed in haploid yeast strains. After mating, the diploid cells were grown on CSM media containing adenine and histidine (CSM Leu$^-$ Trp$^-$ Ura$^-$) to verify the presence of the transformed constructs. The putative interactions were analyzed by growth on selective media CSM$^-$ and CSM$^-$ containing 50 µM methionine, which represses the expression of the Cub fusion protein (Grefen, 2007). The NubWT protein, which can spontaneously re-assemble with the Cub-protein and its interaction is supposed to be independent of bait and prey proteins, was used as positive control (Grefen, 2007; Grefen et al., 2009). The NubA served as negative control, where a N-terminal mutation prevents the reconstruction of the ubiquitin halves to a whole protein (Grefen, 2007).

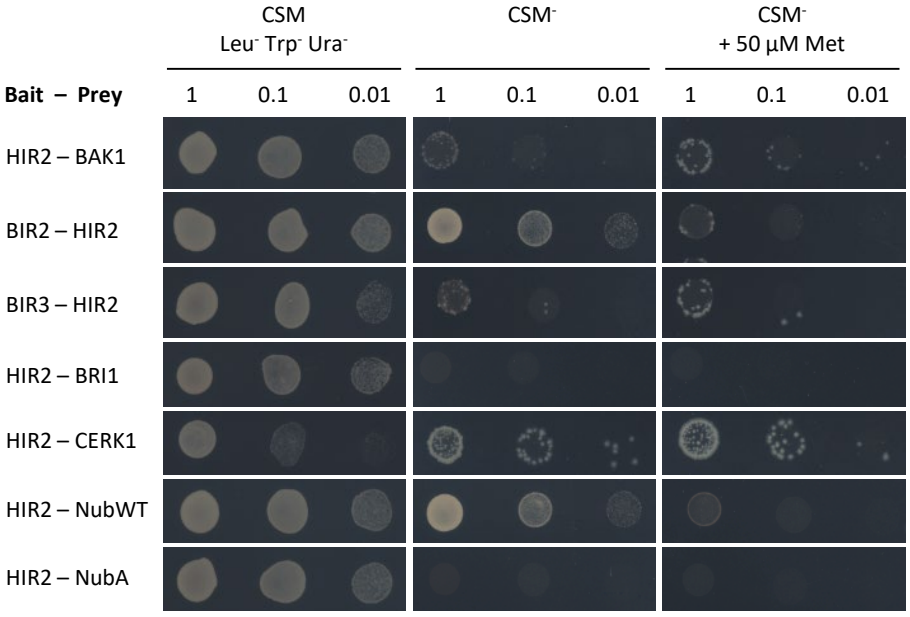

Figure 3-6: HIR2 directly interacts with immunity related receptor kinases. Growth assay of mated yeast, carrying the plasmids for expression of the indicated proteins either as "Bait" or "Prey". The yeast was dropped in three different concentrations (OD_{600}= 1; 0.1; 0.01) on selective media for vector transformation (CSM-Leu$^-$, Trp$^-$, Ura$^-$). For selection of positive interactions, yeast was dropped on nutrient deficient CSM$^-$ medium (Leu$^-$, Trp$^-$, Ura$^-$, Ade$^-$, His$^-$) and CSM$^-$ with addition of 50 µM methionine in three different concentrations (OD_{600}= 1; 0.1; 0.01). The expression of NubWT protein served as positive control and the NubA protein was used as negative control. Growth was documented after one day for vector selection and after two days for interaction selection. The assay was performed at least three times with similar results.

The yeast dropped in serial dilutions (OD_{600}= 1; 0.1; 0.01) on vector selective media, (CSM-Leu$^-$, Trp$^-$, Ura$^-$) showed growth for all transformed fusion-proteins. On the nutrient deficient media (CSM$^-$, CSM$^-$ + 50 µM Met) BIR2 expressed together with HIR2 showed a strong growth of the yeast. Weaker growth occurred for the tested protein-protein interaction of HIR2 with BAK1, alike for HIR2 with BIR3 and HIR2 with CERK1. The co-transformation of HIR2-Cub and BRI1-Nub did not lead to growth of the yeast. The mbSUS approach revealed a direct interaction of HIR2 with BAK1, BIR2/3 and CERK1, but not for HIR2 with BRI1.

All performed experiments to analyze potential interaction partners of HIR2, clearly pointed to the conclusion that HIR2 is associated with different receptor kinases at the plasma membrane. HIR2 can interact with different LRR-RLKs as well as with the LysM RLK CERK1. Additionally, it was demonstrated that HIR2 interaction partners are not exclusively restricted to immunity related components.

3.1.2 Creating a functional knock-out mutant of *HIR2*

Prior to this work, four T-DNA lines for HIR2 were investigated by Raffaele Manstretta (*hir2-1* (SALK_092306), *hir2-2* (SALK_124393), *hir2-3* (SALK_033877) and *hir2-4* (SALK_095926C)). Gene expression analysis of the different T-DNA lines were performed and only *hir2-2* appeared to be a full knock-out mutant, because no transcript of *HIR2* was detected (Manstretta, unpublished). The plants showed a reduced ROS response after flg22 and elf18 treatment (Manstretta, unpublished). However, complementation experiments did not rescue the phenotype and it was assumed that it was caused by a second site mutation (Manstretta, unpublished). The line was backcrossed in wild type Col-0 background and whole-genome sequencing was performed. No additional T-DNA insertions were detected. It could not be ruled out that point mutations or epigenetic effects caused the phenotype. The dubiety of the genetic background of this line, led to the decision not to continue working with *hir2-2* and different approaches were used to generate knock-out lines of *HIR2*.

3.1.2.1 Silencing of the *HIR* genes by artificial microRNA led to transcriptional upregulation

The stable expression of artificial micro RNAs (amiRNA) is an effective way to cause gene silencing in plants (Schwab et al., 2006). This genetic tool benefits from the endogenous plant silencing machinery, whereby natural micro RNAs (miRNAs) lead to a transcriptional repression or a posttranscriptional degradation of

the target genes' mRNA (Bartel, 2004; Schwab et al., 2006). To knockdown the *HIR* genes in *Arabidopsis*, two different amiRNAs were engineered by using the online tool WMD3-Web MicroRNA Designer (http://www.weigelworld.org) and the protocol published by Schwab et al. (2006). The first amiRNA was designed to specifically target *HIR2.* Due to the sequence similarity of the *HIR* gene family, it was likely that they act redundantly and the second amiRNA was designed to target all four *HIR* genes simultaneously. The precursors of the amiRNAs were expressed under the constitutive active 35S promoter and stably transformed in Col-0.

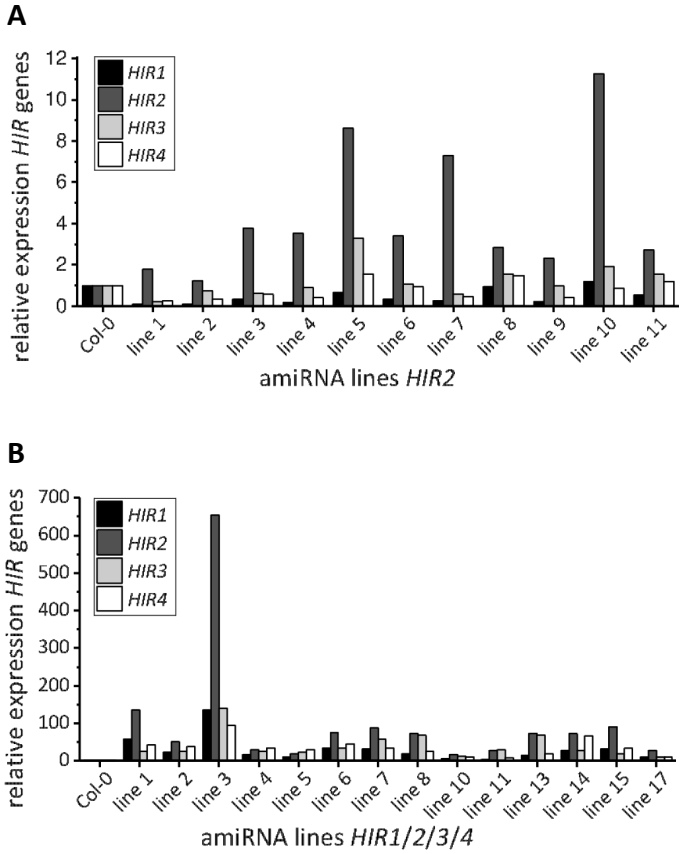

Figure 3-7: Expression of artificial microRNA is not causing silencing of the *HIR* genes. The amiRNA precursors were transformed into Col-0 background and overexpressed by the 35S promoter. The transcript levels were measured by quantitative RT-PCR, normalized against EF1α and compared to Col-0 wild type level, which were set to 1. [**A**] Relative expressions level of *HIR* genes in amiRNA lines targeting either HIR2 or [**B**] all four *HIR* genes.

Quantitative analysis of the transcript levels of the *HIR* genes were performed in T1 generation. The transcript levels of the transgenic plants were compared to the ones in Col-0 plants, which were set to a

value of 1. Surprisingly, all 11 independent amiRNA-HIR2 lines had elevated transcript levels of *HIR2.* Line 10 showed the highest level of *HIR2* transcript, which was more than 10 times higher than in wild type plants. For the levels of *HIR1*, *HIR3* and *HIR4* no consistent trend was visible in the tested lines, however some plants showed reduced levels for these genes (Figure 3-7 A). Likewise, for plants transformed with amiRNA-HIR1/2/3/4 a similar trend was observable. 14 independent lines were analyzed and a universal upregulation of all *HIR* genes was measured (Figure 3-7 B).

The expression of artificial microRNAs targeting the genes of the *HIR* family lead to an unexpected effect of upregulation instead of silencing. To rule out technical issues, the melting curves were analyzed. One distinct peak for the amplified products were visible, excluding the amplification of non-specific products or the presence of primer-dimer. Moreover, the primer sequences were blasted against the *Arabidopsis* genome to reassure gene specificity. Furthermore, amplification of genomic DNA was excluded by different approaches: (i) DNAse treatment was performed during RNA purification to digest residual DNA. (ii) The primers were designed to span exon-exon junctions, which avoids binding on genomic DNA. (iii) The genomic DNA of the plants expressing the amiRNA was isolated and a control PCR with the primer pairs used for the qPCR performed, which did not result in amplicons. Additionally, protein levels could have been determined by Western Blot analysis with HIR2 specific antibodies to identify whether the high transcript levels correspond with high protein amounts, since regulatory mechanism occur after mRNA transcription and steady-state transcript abundances only partially predict protein abundances (De Sousa Abreu et al., 2009; Vogel & Marcotte, 2012). By this, it could be identified whether the plants can be used as HIR2 overexpressing lines. However, this approach failed to produce a functional knockdown line for *HIR2*.

3.1.2.2 Generating *HIR2* knock-out by CRISPR/Cas9

Previously described approaches to gain a functional knockout or knockdown mutant of *HIR2* failed. Additionally, genome editing by CRISPR/Cas9 was performed according to the system described by Ordon et al. (2017) and Stuttmann et al. (2021) to generate deletion mutants of *HIR*s in *Arabidopsis*. In order to achieve deletions in HIR2, two single guide RNAs (sgRNA), which were located within the coding sequence of HIR2, were designed (CRISPR/Cas9-HIR2) (Figure 3-8 B). To generate quadruple mutants, containing deletions in all four *HIR* genes, multiplex genome editing with 8 different sgRNAs was performed. Thereby, two sgRNA were targeting one *HIR* gene each (CRISPR/Cas9-HIR1/2/3/4) (Figure 3-8).

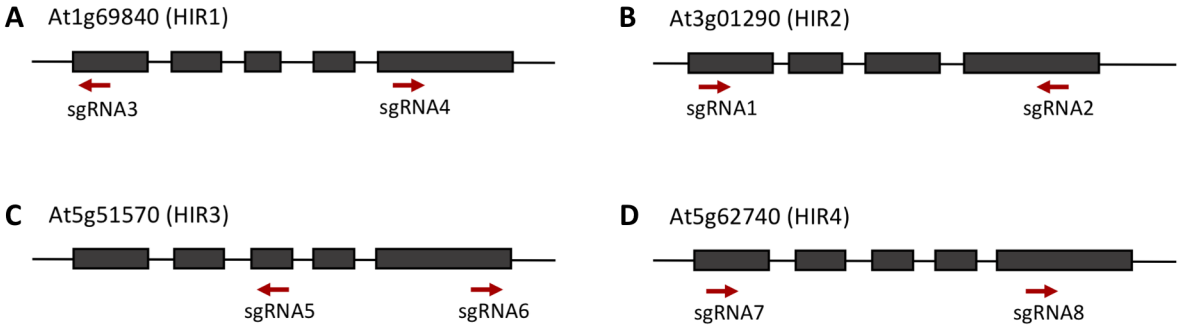

Figure 3-8: Schematic representation of the *HIR* genes of *Arabidopsis thaliana* with sgRNA target sites. The *HIR* genes are shown from 5' end on the left to 3' end on the right. The black boxes represent exons and red arrows indicate the location of the sgRNAs. [**A**] gDNA HIR1 with sgRNA3, starting at base number 867 in exon 1 and sgRNA4, starting at base number 1664 in exon 5. [**B**] gDNA HIR2 with sgRNA1, starting at base number 264 in exon 1 and sgRNA2, starting at base number 1286 in exon 4. [**C**] gDNA HIR3 with sgRNA5, starting at base number 1345 in exon 3 and sgRNA6, starting at base number 1854 in exon 5. [**D**] gDNA HIR4 with sgRNA7, starting at base number 515 in exon 1 and sgRNA8, starting at base number 1453 in exon 5. The sgRNA1 and sgRNA2 were used as target sites for the CRISPR/Cas9-HIR2 construct and all eight sgRNAs were used as target sites for the CRISPR/Cas9-HIR1/2/3/4 construct.

Arabidopsis thaliana Col-0 plants were stably transformed with the constructs for CRISPR/Cas9-HIR2 and CRISPR/Cas9-HIR1/2/3/4, respectively. Primary transformants of the T1 generation were selected by the FastRed selection marker. Strongly red fluorescent seeds were planted on soil and their number was determined. The selection was performed twice for different batches of transformation events. The seed number was counted consecutively. Around 80% of the transformants did not germinate. This was the case for transformants with the CRISPR/Cas9 constructs targeting *HIR2*, as well as for transformants aiming for multiplex deletions. The germinated seedlings were analyzed by PCR and sequencing whether deletions in the targeted gene occurred (Supplemental figure 2 A, B). CRISPR/Cas9-HIR1/2/3/4 plant 7 had a heterozygous deletion of 840 base pairs in *HIR1* (Supplemental figure 2 C). Additional plants with deletions in one of the *HIR*s could not be obtained.

To examine factors causing the low germination rate, transformed T1 seeds were again selected, sterilized by Ethanol and transferred to ½ MS plates. The untransformed siblings served as control. The plates were incubated for two days at 4°C and subsequently transferred to short-day growth conditions. After two weeks of incubation, none of the seeds germinated. This might have indicated that the low germination rate is due to technical issues, but time limitations of the project did not allow to repeat the

transformation of the CRISPR/Cas9 constructs to fresh Col-0 plants. However, repeating this experiment is highly recommendable in order to gain *HIR2* knockout mutants, which will allow studying its function.

3.1.2.3 Preliminary characterization of the T-DNA line *hir2-5*

Previously described T-DNA lines did not provide functional knock-out mutants for HIR2. An additional insertion line was analyzed. The T-DNA insertion of *hir2-5* (SAIL_1274_A05) is located within Exon3 (Figure 3-9 A). Two homozygous plants were identified, and their offspring used for first characterizations. The lines were named *hir2-5* #2 and *hir2-5* #7. The transcript levels were examined by PCR with reverse transcription. The mutants showed no amplicons for *HIR2* full-length, which was seen for Col-0 plants. Amplification of a C-terminal region of *HIR2* revealed that truncated mRNA transcript was produced in the mutants (Figure 3-9 B). This might be due to a transcription start site within the inserted T-DNA.

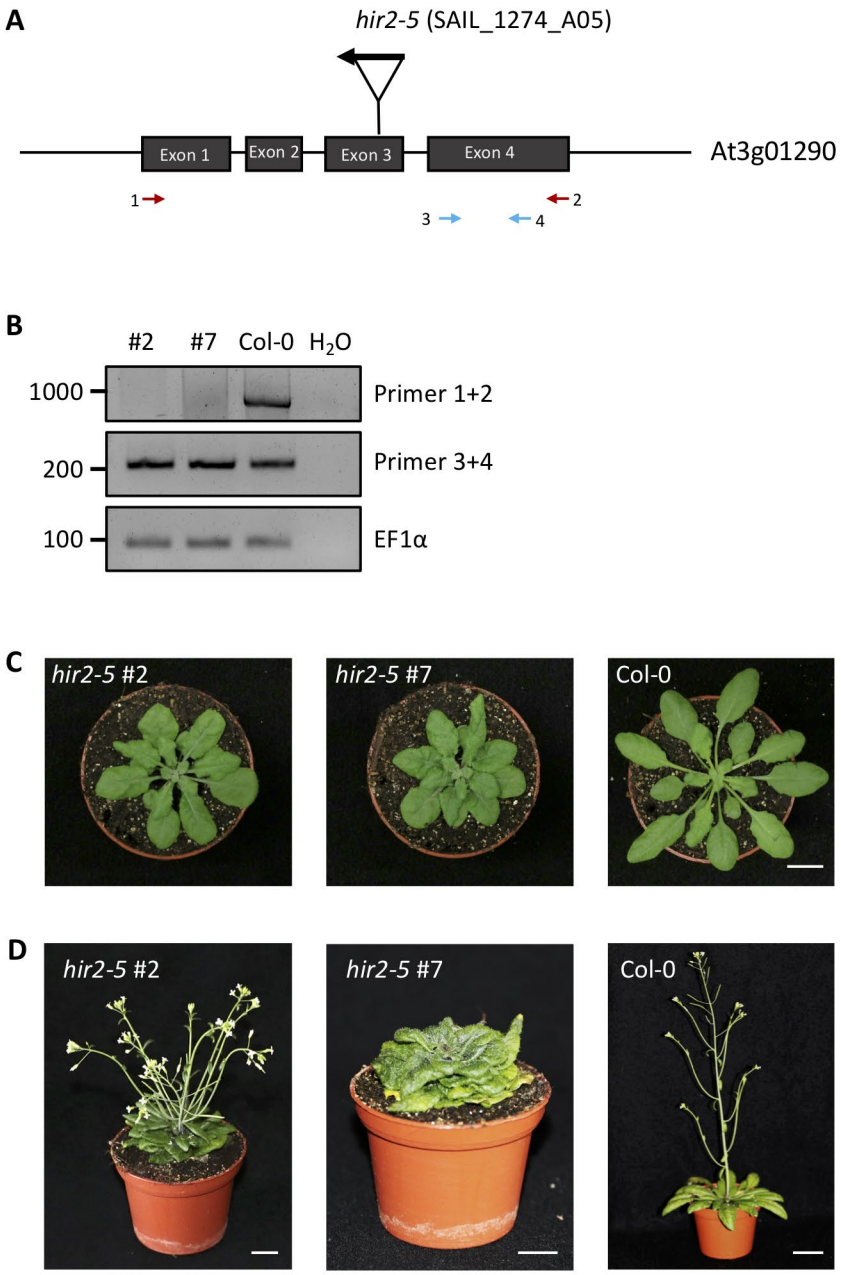

Figure 3-9: T-DNA line *hir2-5*. [**A**] Exon-intron structure of *HIR2* and position of the T-DNA insertions site (*hir2-5)* in the *HIR2* gene. Red arrows indicate primers used to test for full-length transcript and the primer pair used to amplify the C-terminus of *HIR2* are indicated by blue arrows. [**B**] RT-PCR analysis of HIR2 and EF1α (control) transcript in two *hir2-5* plants and Col-0 with the primer pairs indicated in [A]. [**C**] Morphology of two *hir2-5* plants and Col-0. The plants were grown for 5 weeks under short day conditions. The scale bar represents 1 cm and applies to all images [**D**] Morphology of two 3-month-old *hir2-5* plants, which were grown 5 weeks in short-day conditions and subsequently transferred to long-day conditions. The scale bar represents 1 cm. Col-0 plant were grown like the mutant plants, but the picture was obtained of 2-month-old plant. The scale bar represents 2 cm.

The morphology of *hir2-5* plants, grown for five weeks under short day conditions, showed visible differences to Col-0 plants. The petioles of the mutant plants were less elongated, and the rosette diameter was decreased compared to wild type plants. The leaves were thickened and with a curled appearance. (Figure 3-9 C). The plants were transferred to long-day conditions in order to induce flowering and seed production. They exhibited likewise a stunted and bushy phenotype. Interestingly, *hir2-5* #2 plants showed differences in the flowering time compare to the *hir2-5* #7 plants. The *hir2-5* #2 plants had short inflorescences and produced siliques with fertile seeds, whereas *hir2-5* #7 did not grow any inflorescences in the time period of 3 month (Figure 3-9 D). However, the plants were grown in long day conditions for longer and the *hir2-5* #7 plants produced fertile seeds as well. Quantifications of the flowering time and measurements of the plant sizes would contribute to a more detailed characterization of the *hir2-5* T-DNA insertion lines in future.

In order to analyze whether the *hir2-5* mutants are impaired in PAMP responses, a ROS assay was performed as first experiment. Elicitation with 100 nM flg22 peptide was used to activate the FLS2 pathways and to trigger ROS production. The ROS burst in Col-0 plants served as control and followed a typical kinetic (Figure 3-10 A). Likewise, flg22 triggered a ROS response in *hir2-5* mutant plants, although less relative light units were measured compared to the wild type (Figure 3-10 B). This might indicate a decreased sensitivity in the mutant plants to flg22 (Figure 3-10).

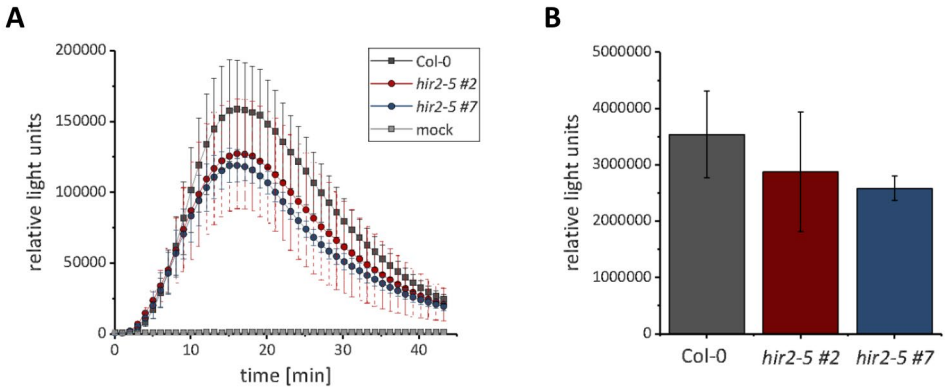

Figure 3-10: Flg22 induced ROS production in *hir2-5* mutant plants. Leave pieces of two homozygous *hir2-5* and Col-0 plants were treated with 100 nM flg22 peptide. ROS production was measured by a luminol-based approach and represented by relative light units. [**A**] The measured relative light units of the single time points were plotted over a time series of 45 minutes. The graphed mock control was performed on Col-0 leave pieces. Additional controls are not shown in the graph. [**B**] The total amount of relative light units of the first 45 minutes after flg22 elicitation was summed up and means plotted in a bar graph. Statistical analyses were performed with Kruskal-Wallis test followed by a Steel-Dwass post hoc correction and no significant differences were obtained. The data of both graphs are means (Col-0: n=4 ± SD; *hir2-5* #2: n= 6± SD; *hir2-5* #7: n= 3 ± SD).

However, the experiment was only performed once with a low replicate number of leave pieces and the indicated data are only preliminary results. Experimental repetitions were limited due to the temporal scope of this thesis. Thus, the results have to be taken with caution.

3.1.3 Analysis of PAMP response in HIR2 overexpression mutants

Although the identification of HIR2 specific interactors led to the suggestion of a potential role of HIR2 in immunity signaling pathways, further studies were required to characterize its function. To get a better understanding of biological processes HIR2 might be involved, stable *Arabidopsis* overexpressing lines have been generated. For this, 35S-HIR2-GFP was stably transformed in *A. thaliana* Col-0 plants and the overexpression determined by confocal laser scanning microscopy. Six independent lines, which showed a strong and clear fluorescent signal at the plasma membrane of epidermal leaf cells, were chosen for further analysis (Figure 3-11 A). Additionally, the expression level was verified by immunoblotting. All six lines showed equivalent HIR2-GFP amounts (Figure 3-11 B). Morphological, the plants did not differ from wild type (data not shown).

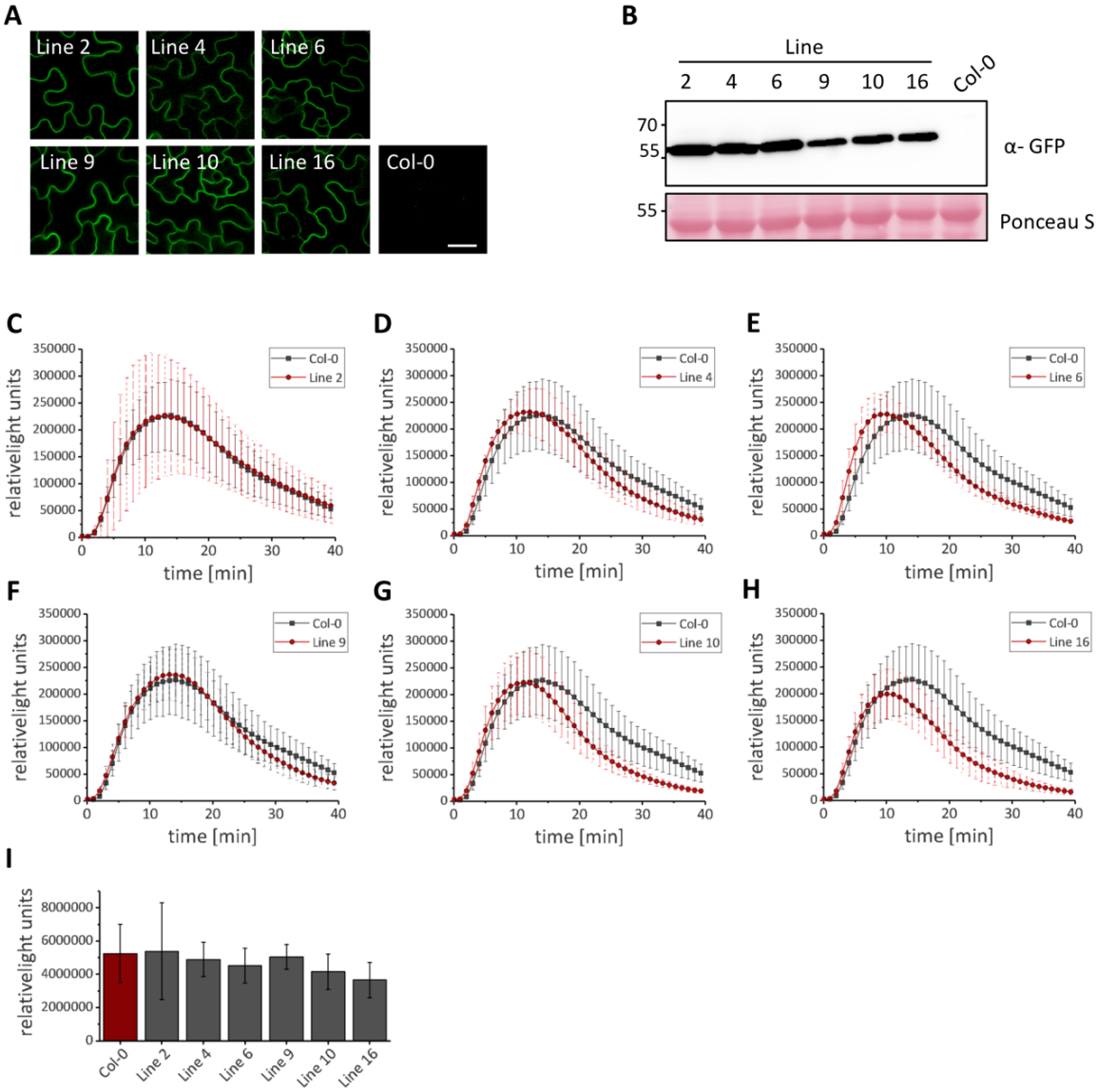

Figure 3-11: Overexpression of HIR2 seemed not to alter flg22 triggered ROS production. 35S-HIR2-GFP was stably transformed in *A. thaliana* Col-0. [**A**] Six independent HIR2-GFP overexpression lines were identified by confocal laser scanning microscopy. The scale bar represents 20 µm and applies to all images. [**B**] Expression levels of six HIR2 overexpression lines were analyzed by Western blot. HIR2-GFP was detected with α-GFP antibodies. Ponceau S staining showed protein loading. [**C-H**] Flg22 induced ROS production in Col-0 and HIR2 overexpression lines was measured by a luminol-based approach and represented by relative light units. The ROS responses of the six lines are separately plotted with the same wild type measurement. Leave pieces were treated with 100 nM flg22 peptide. Results show the means with standard deviation (n=8 ± SD). [**I**] Total ROS production of the six HIR2 overexpression lines and Col-0. The relative light units, which were obtained in the first 40 min after flg22 elicitation, were summed of each *Arabidopsis* line and the mean values were illustrated in the bar graph (n=8 ± SD). No significant differences were obtained by statistical analyses with Kruskal-Wallis test followed by a Steel-Dwass post hoc correction.

To test whether HIR2 affects PAMP responses, elicitor triggered ROS production was measured in HIR2-overexpression lines. The FLS2 pathway was activated using 100 nM flg22 as elicitor. The ROS production

of Col-0 plants were used as control. The ROS burst followed a typical kinetic in the Col-0 control plants with a peak after 10 minutes of elicitor treatment. The ROS production of 35S-HIR2-GFP plants from line 2, 4 and 9 did not differ from Col-0 (Figure 3-11 C, D, F). The ROS production in the lines 6, 10 and 16 showed slightly later maximum compared to the wild type response (Figure 3-11 E, G, H). The ROS production of the mutant plants were compared to the same wild type response. Additionally, the total ROS production in the first 40 minutes after flg22 elicitation were calculated for Col-0 and the six HIR2-overexpression lines. The mean values were compared, but no significant differences in ROS production were obtained (Figure 3-11 I).

Temporal limitations of the project only led to preliminary data. Further experiments are necessary to be able to determine whether elevated protein amounts of HIR2 affect flg22 triggered immune responses.

3.1.4 N-terminal motifs partially confer association of HIR2 to the plasma membrane

HIR2 is localized on the cytosolic surface of the plasma membrane although it does not carry a transmembrane domain (Qi et al., 2011). This led to the question how HIR2 is associated with the membrane. Until now it is not known how plant SPFH proteins are targeted to the plasma membrane (Martinière & Zelazny, 2021). Lipid modifications, by which fatty acid chains are covalently attached to the protein, are required to anchor soluble proteins to the membranes (Hemsley, 2015). Experimental data indicated that HIR2 is palmitoylated (Hemsley et al., 2013). To investigate the necessity of post-translational lipid modifications for the proper localization of HIR2, potential myristoylation and palmitoylation sites were mutated.

In-silico models predicted HIR2 to by myristoylated at glycine 2 and to be palmitoylated at cystine 6 and 7 (NBA-Palm (http://nbapalm.biocuckoo.org/ (Xue et al., 2006), CCPalm4.0 (http://gpspalm.biocuckoo.cn/) (Ning et al., 2020) and ExPASy Myristoylator (https://web.expasy.org/myristoylator/) (Bologna et al., 2004)). To prevent a potential myristoylation, glycine 2 was mutated to an alanine. Cysteine 6 and 7 were mutated to two serine residues, thus hindering HIR2 to be palmitoylated at these positions. Additionally, a triple mutant carrying all three amino acid exchanges was created. To analyze the localization pattern of the different mutants, the constructs were transiently expressed under the constitutive active 35S promoter in *N. benthamiana* and imaged by confocal laser scanning microscopy. BRI1-RFP was co-expressed to serve as a plasma membrane marker. In order to cause plasmolysis, the tobacco cells were treated with 0.5 M mannitol solution prior to imaging.

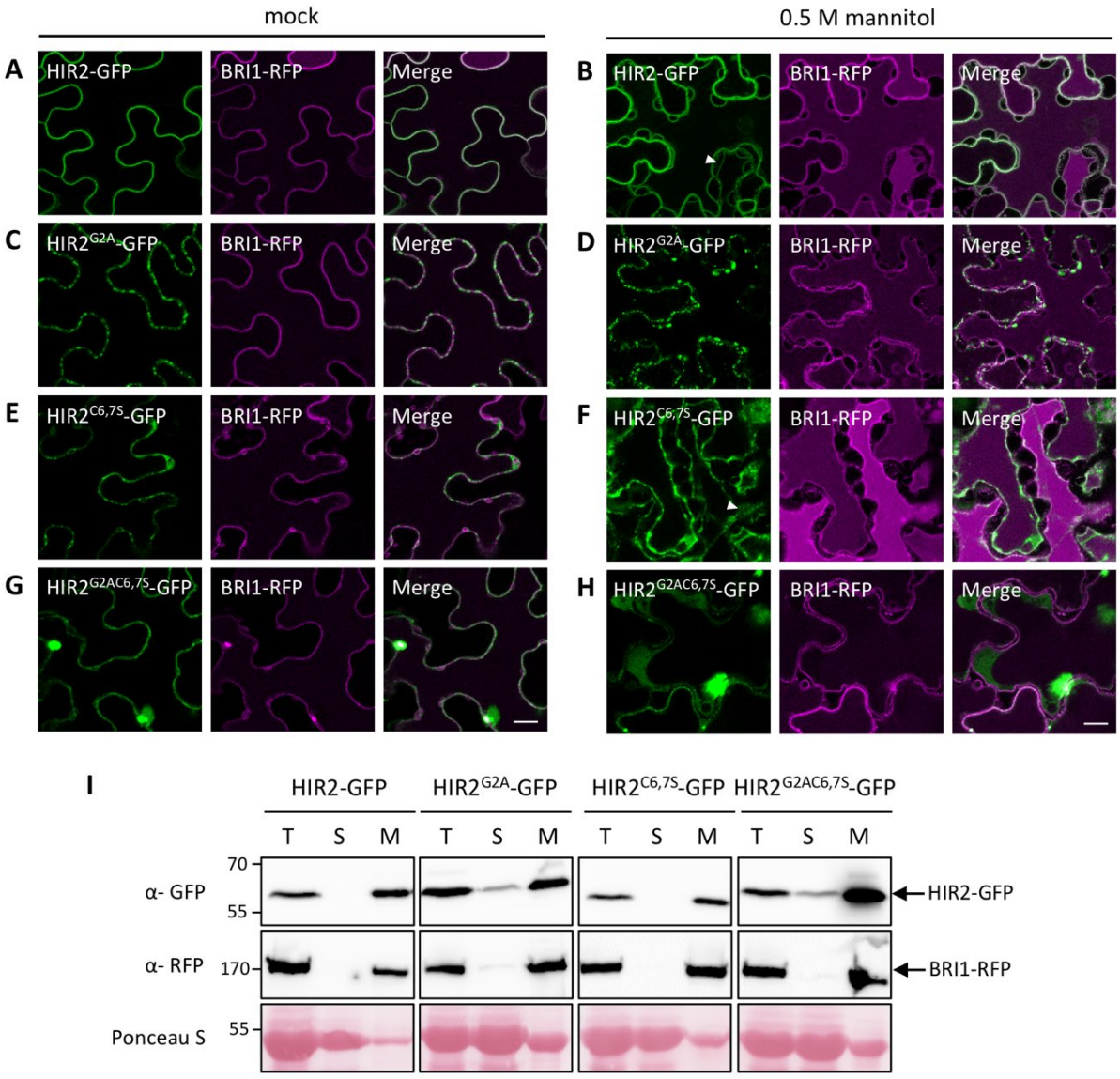

Figure 3-12: Mutation in predicted lipid modification sites alters the localization pattern of HIR2. Wild type HIR2-GFP and mutated variants were transiently expressed in *N. benthamiana*. BRI1-RFP was co-expressed as plasma membrane marker. [**A-H**] Confocal laser scanning microscopy images of epidermal leaf cells with mock treatment or mannitol treatment (plasmolysis). [A, B] wild type HIR2-GFP, (white triangle marks Hechtian strands), [**C, D**] predicted myristoylation site mutant HIR2^{G2A}-GFP, [**E, F**] predicted palmitoylation site mutant HIR2^{C6,7S}-GFP (white triangle marks potential ER structures) and [G, H] triple mutatoin HIR2^{G2AC6,7S}-GFP. Scale bars represent 20 µm and applies to all images. [**I**] Extracts of total (T), soluble (S) and microsomal (M) protein fractions were analyzed by immunoblotting. HIR2-GFP variants are detected with α-GFP antibody and BRI1-RFP with α-RFP antibody. Ponceaus S staining indicates protein loading.

The wild type HIR2-GFP protein showed a co-localization with BRI1-RFP. Following plasmolysis, the formation of Hechtian strands was visible, which demonstrated the plasma membrane localization as well (Figure 3-12 A, B). The predicted myristoylation site mutant HIR2^{G2A}-GFP appeared in an irregular speckled pattern, which clearly differed compared to the wild type. After plasmolysis, a formation of aggregates was visible, which did not completely co-localized with the RFP signal of BR1 (Figure 3-12 C, D). The predicted palmitoylation site mutant HIR2^{C6,7S}-GFP showed only partly a co-localization with BRI1 and a slightly speckled pattern. Moreover, Hechtian strands did not appear after plasmolysis, which indicated a disruption of the plasma membrane localization. Nevertheless, HIR2^{C6,7S}-GFP might to be localized to other membrane systems such as the ER (Figure 3-12 E, F). The triple mutant HIR2^{G2AC6,7S}-GFP formed huge fluorescent bodies and had a clearly visible cytoplasmatic localization in plasmolyzed cells as well as nuclear localization (Figure 3-12 G, H).

Total, soluble and microsomal protein fractions of *N. benthamiana* transiently expressing the different mutants were analyzed by western blot. HIR2-GFP and HIR2^{C6,7S}-GFP were detected in microsomal fractions, whereas HIR2^{G2A}-GFP and HIR2^{G2AC6,7S}-GFP showed a light band in the soluble fraction as well as in the microsomal fraction. The transmembrane protein control BRI1-RFP was completely detected in microsomal fractions (Figure 3-12 I).

These results implicated that the amino acid substitutions of the predicted myristoylation and palmitoylation sites in HIR2 altered its localization pattern and partially confer association of HIR2 to the plasma membrane. However, none of the mutations led to an entire loss membrane association and additional determining factor might be involved in localizing HIR2 to the plasma membrane.

3.2 PART B: Analysis of receptor dynamics and nanocluster formation by sptPALM

Receptors and membrane-associated proteins feature lateral dynamics and heterogeneously distribution within the plasma membrane (Jaillais & Ott, 2019). Most of the published studies analyzing the dynamics and nanocluster formation of receptors utilized GFP- or mCherry- based imaging methods, which are restricted by the resolution limit (Abbe, 1873; Bücherl et al., 2013; Hutten et al., 2017; Gronnier et al., 2022). Single emitters cannot be resolved, and thus imaging of single molecules cannot be ensured. However, live-cell imaging single-particle tracking Photoactivated Localization Microscopy (sptPALM) enables mapping of the spatial and temporal motion of individual proteins (Manley et al., 2008).

The second part of the thesis focused on the implementation, application and improvement of sptPALM *in planta* to probe the lateral mobility of immunity-related proteins within the plasma membrane as well as studying ligand-induced alterations in the organization and dynamics of singling components.

3.2.1 Integration of the fluorophore mEos3.2 for single color sptPALM in plants

SptPALM utilizes genetically encoded photo-controllable fluorescent proteins, which can be stochastically switched or converted into a temporarily active state. The fluorophore mEos is photoconvertible with an active fluorescent state in green and can be photoconverted to red by irradiation with UV light at 405 nm. In previously published work, sptPALM experiments were performed with proteins fused to the fluorophore mEos2 (Hosy et al., 2015; Gronnier et al., 2017; Platre et al., 2019). However, mEos2 was described to form dimers or higher-order oligomers when it is used to label membrane proteins (Zhang et al., 2012). To avoid the possibility of oligomer formation, the improved version mEos3.2 was used in this work. It was described to be truly monomeric, brighter and to mature faster (Zhang et al., 2012). When starting this work, no information was published on the usage of mEos3.2 in plants. To utilize the fluorophore in plants, it was codon optimized (kindly provided by Klaus Harter) and its suitability for plant expression was analyzed.

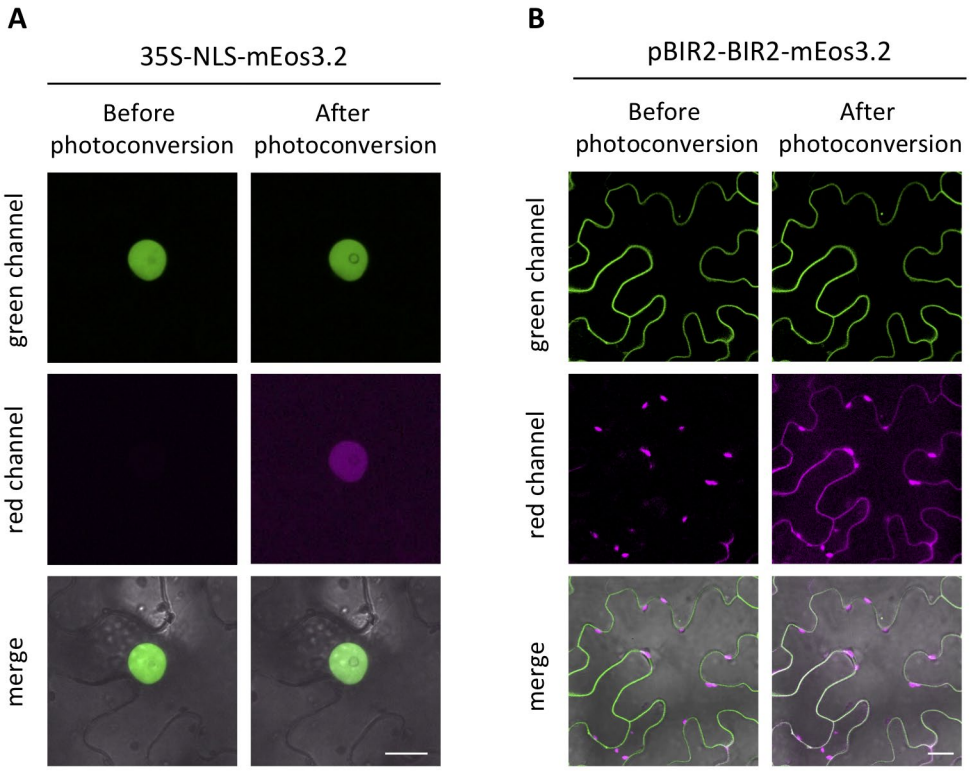

Figure 3-13: Photoconversion of mEos3.2 expressed in the nucleus and in the plasma membrane of epidermal leaf cells of *N. benthamiana*. Confocal laser scanning microscopy images of transiently expressed [**A**] 35S-NLS2-mEos3.2 and [**B**] pBIR2-BIR2-mEos3.2 in tobacco epidermal leaf cells are shown. The fluorescence of mEos3.2 was imaged in the green and the red channel before and after photoconversion by UV light at 405 nm. The images of both channels were merged with brightfield images. The scale bars represent 20 µm and applies to all corresponding images.

Since the cellular compartments differ in their physical properties, such as pH, and this might influence the functionality of chromophores, mEos3.2 expression was investigated in the nucleus as well as at the plasma membrane. For a nuclear localization, mEos3.2 was tagged with a nuclear localization sequence (NLS), transiently expressed under the constitutively active 35S promoter in *N. benthamiana* and imaged by confocal laser scanning microscopy. The green fluorescence of mEos3.2 was visible in the nucleus. Before photoconversion, the chromophore only emitted fluorescence in green and not in red. After exposing the sample for a few seconds with UV light at 405 nm, mEos3.2 molecules were photoconverted and red fluorescence was detectable in the nucleus (Figure 3-13 A). Furthermore, mEos3.2 was fused to the C-terminus of BIR2 to locate it to the cytosolic side of the plasma membrane. The fusion protein was transiently expressed under the control of the BIR2 promoter in *N. benthamiana* and imaged by confocal laser scanning microscopy. As well as for the nuclear expression, BIR2-mEos3.2 was visible in its green

form at the plasma membrane, whereas it did not show fluorescence in the red channel. Irradiation with UV light was necessary to photoconvert a subpopulation of fluorophores into a red fluorescent state (Figure 3-13 B). It is to be noted, that the intensity of the red fluorescence was much lower compared to the one of the green form. At times, the red fluorescence signal was not strong enough to detect it at the plasma membrane by confocal laser scanning microscopy.

Furthermore, fusion proteins of the LRR-RLKs FLS2-mEos3.2, BAK1-mEos3.2 and BIR3-mEos3.2 were transiently expressed under the control of their native promoter in *N. benthamiana* as well as HIR2-mEos3.2 fusion protein under the control of the constitutive active 35S promoter. Confocal laser scanning microscopy imaging was performed, where mEos3.2 was detected in its native green form. This revealed that the fusion proteins of FLS2-mEos3.2, BIR3-mEos3.2 and HIR2-mEos3.2 were well expressed at the plasma membrane. The signal of BAK1-mEos3.2 was usually weak but sufficient for imaging (Figure 3-14 top). Next, the samples were imaged by Variable Angle Epifluorescence Microscopy (VAEM), which displayed the plasma membrane as plane structure (Konopka & Bednarek, 2008). The fluorophore mEos3.2 was photoconverted to its red isoform by shot irradiation with the 405 nm laser. Bright and distinct particles were clearly visible for all fusion proteins (Figure 3-14 middle). Moreover, by adjusting the UV light intensity, the amount of photoconverted mEos3.2 molecules was controllable, providing a considerable number of molecules per frame to facilitate further analysis. The motions of the single molecules imaged by VAEM were mapped by building trajectories out of 2000 frames with the analysis software described in zur Oven-Krockhaus (2021) (Figure 3-14 bottom). The obtained trajectories of single molecules provide quantitative parameter for the molecular displacement and the diffusion coefficient of the individual proteins and allows to analyze their spatiotemporal dynamics within the plasma membrane.

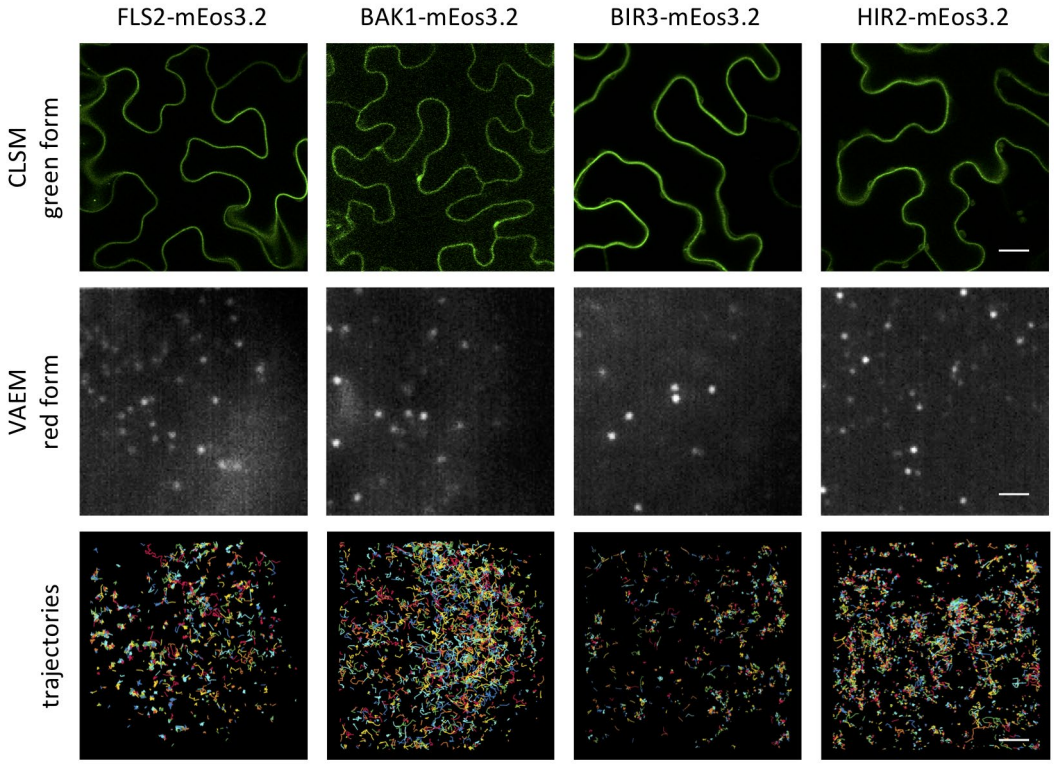

Figure 3-14: Expression of mEos3.2 fusion proteins in *N. benthamiana* and application of sptPALM. The LRR-RLKs FLS2, BAK1 and BIR3 were C-terminally tagged with mEos3.2 and transiently expressed under the control of their native promoter in *N. benthamiana*. HIR2-mEos3.2 fusion protein was expressed under the control of the constitutive active 35S promoter. The native green form of mEos3.2 was imaged by confocal laser scanning microscopy (CLSM) and illustrated in the top row. The scale bar of CLSM images represents 20 µm and applies to all respective images. VAEM images were taken and summed up z-projections of 25 frames are shown in the middle row. Trajectories of the respective single molecules were obtained from 2000 frames and shown in the bottom row. The scale bar of VAEM images and trajectories represent 2 µm and apply to all respective images.

These experiments proved separate objectives: (i) The successful expression of the mEos3.2 in plant cells, which might improve accuracy of single molecule detection due to its monomeric nature. (ii) The functionality of the fluorophore in different cellular compartments such as the nucleus as well as at the plasma membrane. (iii) The ability to photoconvert a subset of the fluorophores into a red-fluorescent state and to control their number by the UV light intensity. (iv) The capability to track positions of single molecules through time by mapping the trajectories. Thus, the results showed the successful integration of the fluorophore mEos3.2 and its application to perform sptPALM in plants.

3.2.2 Analysis of the influence of PAMP treatment on the mobility of membrane proteins

In absence of the ligand flg22, BIR3 interacts constitutively with BAK1 as well as with FLS2. Upon flg22 treatment, BAK1 is released from BIR3 and forms a heteromeric complex with FLS2 (Imkampe et al., 2017). It is proposed that these proteins reside in preformed complexes and are organized by scaffold proteins (Bücherl et al., 2017; Hutten et al., 2017). The nanodomain formation might be determined by HIR2. To get a deeper insight in the dynamics the receptors are undergoing during the process of ligand perception, their diffusion behavior was measured by sptPALM.

The fusion proteins FLS2-mEos3.2, BAK1-mEos3.2, BIR3-mEos3.2 and HIR2-mEos3.2, which were described in the previously chapter (chapter 3.2.1), were transiently expressed in *N. benthamiana.* Their spatiotemporal dynamics were analyzed either in mock or in flg22 (100 nM) treated sample by sptPALM. Videos of single fluorescent particles were recorded by VAEM. Tracks of the motion of the particles were drawn, in which different colors represent different tracked particles. Emerging of the trajectories, MSD (mean squared displacement) plots were obtained, and the first four data points were fitted by a linear regression in order to calculate the diffusion coefficient (D) (Hosy et al., 2015) (MSD data not shown). The log(D) values from super resolved particles of different cells were plotted as histogram, showing the percentage of the occurrences of log(D). Moreover, the mean diffusion coefficient of the single cells was calculated.

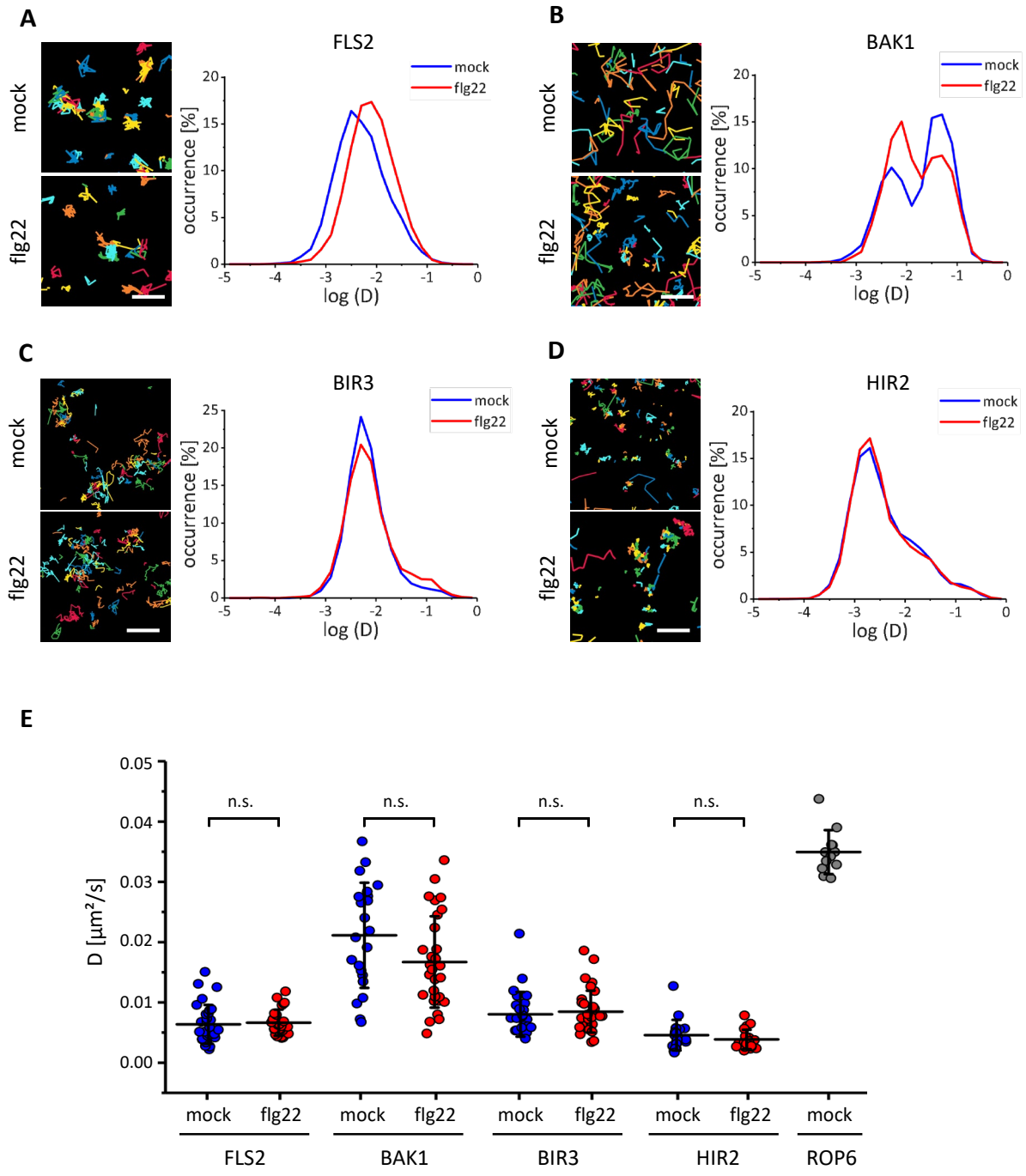

Figure 3-15: Effect of flg22 treatment on protein dynamics of immunity related proteins in the plasma membrane. Fusion proteins of [**A**] FLS2-mEos3.2, [**B**] BAK1-mEos3.2, [**C**] BIR3-mEos3.2 and [**D**] HIR2-mEos3.2 were transiently expressed in *N. benthamiana* and either treated with 100 nM flg22 peptide or mock treatment. The mobility behavior of each protein was analyzed by sptPALM. Trajectories of single molecules and the respective diffusion coefficients (D) were calculated. Occurrence of D of single molecules are shown in histograms [**A-D**] and means of D of single cells are represented in the scatter box chart (mean ± SD) [**E**]. ROP6-mEos2 served as control for a mobile protein. Scale bars represent 0.5 µm and apply to all images. Significant differences were analyzed with Kruskal-Wallis test followed by a Steel-Dwass post hoc correction ($p>0.05$ not significant (n.s.)). The experiments were performed at least in duplicates. FLS2-mock: *n*= 32 cells, 496208 localizations; FLS2-flg22:

n= 31 cells, 775121 localizations; BAK1-mock: *n*=22 cells, 1231761 localizations; BAK1-flg22: *n*= 30 cells, 327290 localizations; BIR3-mock: *n*= 26 cells, 210104 localizations; BIR3-flg22: *n*= 34 cells, 301305 localizations; HIR2-mock: *n*= 19 cells, 628370 localizations, HIR2-flg22: *n*= 19 cells, 674347 localizations. ROP6-mock: *n*= 12 cells, 570737 localizations.

The fusion proteins FLS2-mEos3.2, BAK1-mEos3.2, BIR3-mEos3.2 and HIR2-mEos3.2 were transiently expressed in *N. benthamiana* and either treated with mock treatment or with 100 nM flg22 peptide. The experiments were repeated on at least three independent days and the data were pooled for the analysis. The trajectories of FLS2 illustrated the protein to be quite restricted to the area it was moving in. After treating the sample with flg22, the histogram of FLS2 showed to have a slightly increases log(D), however this was not significant. The median diffusion coefficient changed from mock D= 0.0053 $\mu m^2/s$ (*n*= 31 cells, 775121 localizations) to flg22 treated samples with D= 0.006 $\mu m^2/s$ (*n*= 32 cells, 496208 localizations*)* (Figure 3-15 A, E). Tracking the motion of the co-receptor BAK1 revealed that it occurred in two distinct populations with different mobilities. These were displayed in a bimodal distribution with two peaks in the histogram, where relatively more BAK1 molecules exist in a population with higher mobility. Treatment with flg22 clearly changed the mobility behavior of BAK1, at which the slower population relatively increased. The distribution of the mean D of the different cells was scattered with maximal values around D= 0.03 $\mu m^2/s$ and minimal values around D= 0.006 $\mu m^2/s$. The median diffusion coefficient for mock treated samples was D= 0.021 $\mu m^2/s$ (*n*=22 cells, 1231761 localizations) and D= 0.016 $\mu m^2/s$ (*n*= 30 cells, 327290 localizations) for samples treated with the flg22 peptide, without displaying statistically significant changes (Figure 3-15 B, E). Since the values of the diffusion coefficient of BAK1 displayed a wide spread, a secondary analysis was performed comparing the replicates. The distribution of the data was similar between the measuring days (Supplemental figure 3). Since the complex of BAK1 and BIR3 is released in presence of flg22, the diffusion behavior of BIR3 was analyzed in response to flg22 treatment. The log(D) of BIR3 occurred to be unimodally distributed with one peak, which was unaltered after flg22 treatment. The mean diffusion coefficient of BIR3 of mock treated plants was D= 0.0073 $\mu m^2/s$ (*n*= 26 cells, 210104 localizations) and by adding flg22 to the sample it had a mean D= 0.0078 $\mu m^2/s$ (*n*= 34 cells, 301305 localizations), which did not significantly differ (Figure 3-15 C, E). Furthermore, the diffusion behavior of HIR2 was analyzed. Trajectories of HIR2 revealed a striking limited area in which one particle resided in the membrane. Comparison of flg22 treated cells with mock treated cells, displayed a nearly identical distribution of the log(D) from HIR2. The median diffusion coefficient with D= 0.0038 $\mu m^2/s$ (*n*= 19 cells, 628370 localizations) for mock treated and D= 0.0034 $\mu m^2/s$ (*n*= 19 cells, 674347 localizations) for flg22 treated cells did not indicate alterations in the mobility behavior of HIR2 after addition of the

peptide flg22 (Figure 3-15 D, E). Comparing the mobilities of the different membrane proteins, it was noticed that all occurred to be highly immobile. To exclude errors in the mobility measurements of the proteins due to the transient expression of the proteins in tobacco or due to technical restriction of the microscope setup, the mobility behavior of the GTPase Rho of Plants 6 (ROP6) was measured as control. ROP6 is reported to be a highly mobile protein in the plasma membrane (Platre et al., 2019). Eos2-ROP6 (kindly provided by Yvon Jaillais) was transiently expressed in *N. benthamiana* and the diffusion coefficient was obtained as described before. For ROP6 a median diffusion coefficient of D= 0.035 $\mu m^2/s$ (*n*= 12 cells, 570737 localizations) was measured. The values were approximately 10 times higher as measured for HIR2. The mobility of ROP6 was significant faster compared to FLS2, BAK1, BIR3 and HIR2. Moreover, the activity of flg22 peptide was verified by ROS measurement (Supplemental figure 4). Considering the results of these control experiments, the reliability of the data obtained by sptPALM measurements was proven.

Taken together, it was shown that FLS2 is immobile and did not change its mobility behavior due to flg22 perception. Likewise, BIR3 and HIR2 are immobile and their dynamics do not change in response to flg22 treatment. However, it was shown for BAK1 to exists in two distinct populations and a treatment with flg22 triggered a switch of these populations, whereas the occurrence of the slower BAK1 population increased.

3.2.3 Investigation of PAMP induced alterations in nanocluster formation

The previous chapter described the dynamics and the spatiotemporal distribution of different immunity related proteins during flg22 perception. However, this did not provide information about complex formation and nanocluster shaping of the signaling components.

To get a better understanding of the molecular mechanism of protein compartmentalization during pathogen perception, sptPALM data were analyzed using Voronoi tessellation. To generate Voronoi diagrams, the center point of the trajectories of the super-resolved particles were computed and polygons surrounding those were created. The area of the polygons is based on the local density of the molecules (Levet et al., 2015; Gronnier et al., 2017). This is encoded by color temperature, whereby a high density was represented by dark color. Thus, the polygon size quantifies the spatial distances of neighboring molecules and enables a reconstruction of protein accumulation. By this, cluster formation of proteins can be visualized in living cells (Gronnier et al., 2017; Platre et al., 2019).

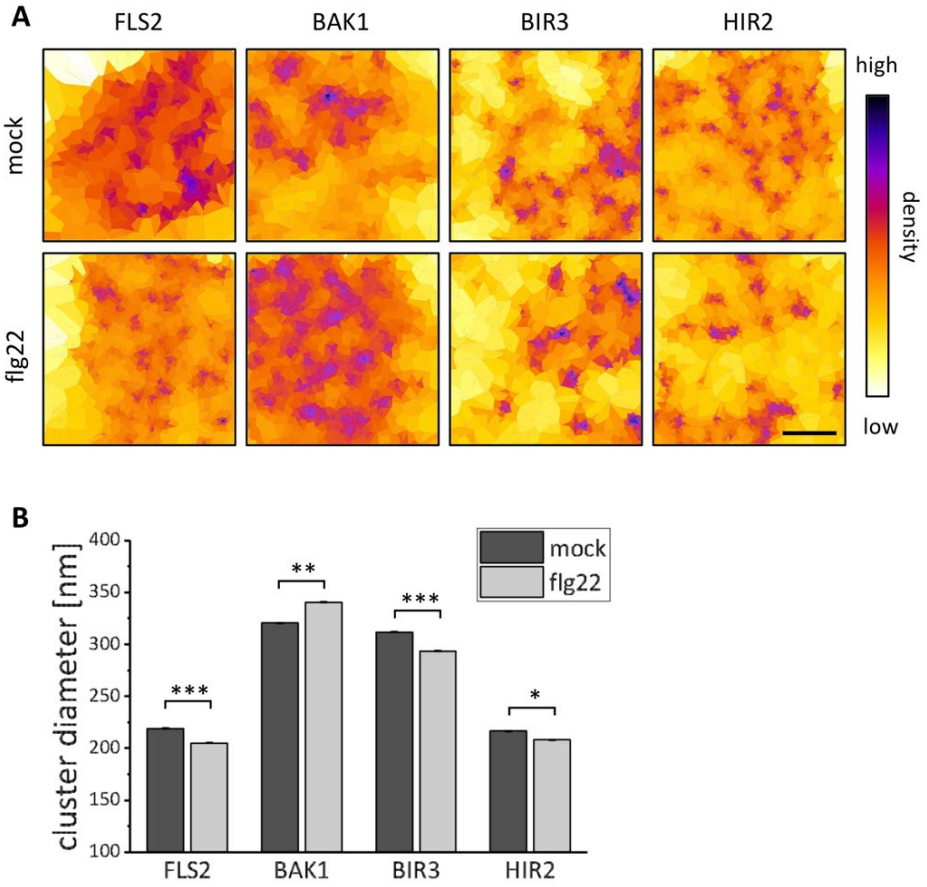

Figure 3-16: Cluster sizes of immunity related plasma membrane proteins were influenced by flg22. The sptPALM data of mock and flg22 treated samples, expressing FLS2-mEos3.2, BAK1-mEos3.2, BIR3-mEos3.2 and HIR2-mEos3.2, were analyzed using Voronoi tessellation-based segmentation. Voronoi diagrams are generated based on trajectories of super-resolved images by SR-Tesseler. [**A**] The Voronoi diagrams illustrated an uneven protein distribution within the membrane and the formation of distinct nanoclusters. Polygon sizes are based on protein density, which were encoded by color temperature, whereby high densities are represented by dark colors. A representative section of the cell was pictured. The scale bar represents 2 µm and applies to all images. [**B**] Mean cluster diameters were calculated based on the area of Voronoi polygons, which were defined as cluster by the software SR-Tesseler. The cluster sizes followed a log normal distribution and statistical analyses were performed by Z-score method according to Zhou et al. (1997). Significant differences are indicated by asterisks (p <0.05 *; p<0.01 **; p<0.001 ***) (FLS2-mock: *n*=328 ± SD; FLS2-flg22: *n*=450 ± SD; BAK1-mock: *n*=125 ± SD; BAK1-flg22: *n*=219 ± SD; BIR3-mock: *n*=318 ± SD; BIR3-flg22: *n*=354 ± SD; HIR2-mock: *n*=688 ± SD; HIR2-flg22: *n*=718 ± SD).

The membrane organization of FLS2, BAK1, BIR3 and HIR2 was analyzed. For all fusion proteins, the previously described sptPALM data were reanalyzed by Voronoi tessellation. Voronoi diagrams were generated for flg22 and mock treated samples. Furthermore, the cluster sizes were calculated and the mean diameter size diagramed. The relative frequency of the cluster sizes followed a log normal

distribution and statistical analyses were performed by the Z-score method according to Zhou et al. (1997) (Supplemental figure 5). The mosaic pattern in the Voronoi diagrams illustrated membrane areas with high protein accumulation and regions with a minor density of the analyzed fusion protein. This indicated that the receptor kinases FLS2, BAK1 and BIR3 as well as HIR2 form distinct clusters in the membrane. The mean cluster diameter of mock treated FLS2-mEos3.2 had a size of 219 nm and their size drastically decreased after flg22 perception. Contrariwise, the diameter of BAK1-mEos3.2 clusters significantly increased from 320 nm to 340 nm and was approximately 1.5 times larger compared to clusters of FLS2. Treatment of BIR3-mEos3.2 expressing cells with the peptide flg22 caused a significant decrease in the mean cluster diameter of BIR3 from 310 nm to 290 nm. The dimensions of BIR3 clusters were comparable with BAK1 nanodomains in their size. Alike FLS2 and BIR3, flg22 treatment led to a reduction in the cluster sizes of HIR2- mEos3.2 in the imaged cells. The mean diameters changed from 217 nm to 208 nm. However, the peptide did not affect the cluster size formation of HIR2-mEos3.2 as severe as for the analyzed receptor kinases (Figure 3-16).

In summary, the analysis demonstrated that the described proteins are heterogeneously distributed in the plasma membrane and reside in distinct nanodomains. Moreover, the nanodomains differ in their dimensions among various proteins and occur in specific sizes. The receptors involved in the perception of flg22 did not respond alike relating to cluster formation. The nanodomains of FLS2 and BIR3 decreased in their size, whereas BAK1 clusters became larger. Additionally, this indicated that ligand perception and activation of signaling cascades are causing obvious changes in the membrane organization of LRR-RLKs.

3.2.4 Establishment of dual color sptPALM for simultaneous mobility analysis of two different proteins in *planta*

Single color sptPALM enables studying the temporal and spatial dynamics of membrane proteins *in vivo*. However, only one protein can be analyzed at one time. To date, no sptPALM technique is available to image the dynamics of two proteins simultaneously in living plant cells (Bayle et al., 2021).

Therefore, as part of this work, a dual color sptPALM technique was developed, which can be applied in a plant system. This method will allow studying the motions of two different proteins at the same time and alterations in membrane organization of two distinct proteins can be visualized in real-time. Thus, dual color sptPALM will help to get a better understanding of dynamic behaviors of proteins related with each

other and their stochiometric ratio. Moreover, it will enable a more precise analysis of nanodomain compositions within the plasma membrane.

Single color sptPALM experiments utilized the photoconvertible fluorophore mEos3.2. The ability of photo-conversation from green to red fluorescence is a benefit in single color sptPALM, but it makes it unusable for dual color imaging. However, photoactivatable fluorophores suit ideal for this application. They feature a dark state and fluorescence can be triggered by to activating light. Photoactivatable variants of GFP (paGFP) and TagRFP (paTagRFP) were already used in animal systems to perform sptPALM and have been selected in terms of their photostability, maturation time and photoactivation efficiency (Subach et al., 2010). PaGFP has been used in plants science studies before but it has not been combined with another fluorescent protein for multicolor imaging (Martinière et al., 2012; McKenna et al., 2019; Bayle et al., 2021). So far, no studies have been published, expressing paTagRFP in plants. In order to develop dual color sptPALM, paGFP and paTagRFP were implemented equivalently in the establishment.

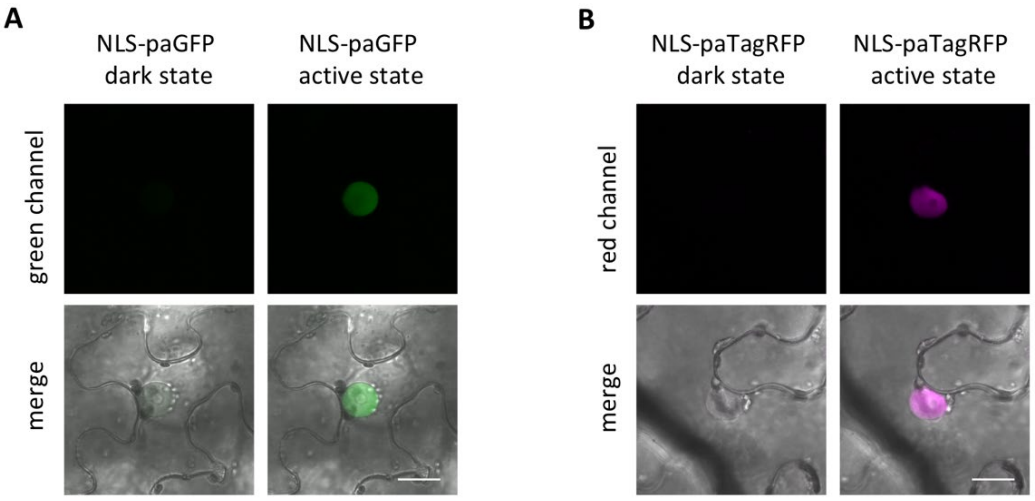

Figure 3-17: Photoactivation of paGFP and paTagRFP. [**A**] 35S-NLS-paGFP and [**B**] 35S-NLS-paGFP were transiently expressed in *N. benthamiana* and imaged by CLSM. Nuclei were imaged before and after photoactivation of the respective fluorophore. Photoactivation was achieved by exposing the sample to UV light at 405 nm. The scale bar represents 20 µm and applies to all images.

The photoactivable fluorophores paGFP and paTagRFP were plant codon optimized (kindly provided by Klaus Harter) and fused to a nuclear localization signal (NLS). The fusion proteins were transiently expressed in *N. benthamiana* under the control of the constitutively active 35S promoter and imaged by

confocal laser scanning microscopy. Nuclei were imaged in brightfield, while the fluorophores were in their dark state. Following, the samples were illuminated with 405 nm ultraviolet light for a short time to transfer the fluorophores into an active fluorescent state. The photoactivation of paGFP was clearly detectable in the nuclei. During UV irradiation, the fluorescence signal was rapidly activated and decreased slowly after turning off the activation laser (Figure 3-17 A). When samples expressing 35S-NLS-paTagRFP were imaged before photoactivation, the chromophore did not display any fluorescence in the nucleus. Illumination with activating light activated the fluorescence of paTagRFP (Figure 3-17 B). Thereby, an increase of the fluorescent signal was clearly visible with continuing UV light irradiation and the photoactivation time occurred to be slower than for paGFP.

To study if the fluorophores are also functional at plant plasma membranes, the photoactivatable fluorophores were C-terminally fused to membrane localized receptor kinases and transiently expressed in *N. benthamiana*. First, BIR2-paGFP and BAK1-paTagRFP were expressed under the control of their native promoters. Imaging by confocal laser scanning microscopy did not display an appropriate expression level and by VAEM the signal-to-noise ratio was too low for proper recognition of the single molecules by the analysis software. The expression of the fusion proteins in adequate amounts for dual color sptPALM was unexpectedly challenging and had to be optimized. To enhance the signal and the protein amounts, the 35S promoter was used to drive the expression of BIR2-paGFP and BAK1-paTagRFP. Thereby, the expression level of the fusion proteins and the fluorescent signal were visibly increased. However, the overexpression of BAK1 led to a severe cell death in the epidermal leaf cells (He et al., 2007; Kemmerling et al., 2007; Domínguez-Ferreras et al., 2015), which made the samples almost unusable for imaging and unusable for studying biological functions of the protein. Therefore, BIR2-paGFP and BAK1-paTagRFP were expressed under the control of Ubiquitin1 promoter, which was described to have an intermediate expression strength (Holtorf et al., 1995). The co-expression, driven by the Ubiquitin promoter, minimized the occurring cell death and a weak but distinct signal of the fusion proteins at the plasma membrane was detectable by confocal laser scanning microscopy (Figure 3-18).

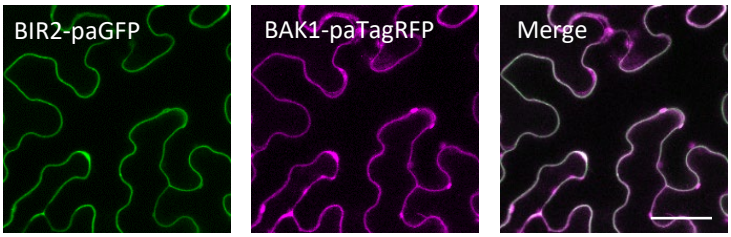

Figure 3-18: The novel fluorophores paGFP and paTagRFP function at plant plasma membranes. The fluorophores paGFP and paTagRFP were C-terminally fused to the membrane localized receptor kinases BIR2 and BAK1, respectively. The fusion proteins were transiently co-expressed in *N. benthamiana* under the control of the Ubiquitin1 promoter and imaged by confocal laser scanning microscopy. BIR2-paGFP and BAK1-paTagRFP showed fluorescence at plasma membrane. Merged images indicate the co-localization of both proteins. Scale bar represents 50 µm and applies to all images.

Samples expressing both proteins at sufficient levels were used to perform dual color sptPALM. The image acquisition and processing were conducted as described previously for single color sptPALM. The signal emitted from the sample was separated into two colored channels by an image splitter. The VAEM images were pictured next to each other on the same camera chip. By this, it was succeeded to visualize single molecules of BIR2-paGFP and BAK1-paTagRFP simultaneously. BIR2-paGFP single molecules were visible and clearly distinguishable from the background, whereas BAK1-paTagRFP single molecules emerged in fewer numbers. The background in the red channel appeared with a higher noise-to-signal ratio compared to the green channel (Figure 3-19 A). By zooming in the VAEM images, the contrast was enhanced, and the fluorescent particles were better visible (Figure 3-19 B). This was sufficient for the analysis software to localize the particles and to track their motions. On account of an unequal number of imaged proteins, the pictured trajectories of BIR2-paGFP and BAK1-paTagRFP differed in their quantity and density (Figure 3-19 C). By merging the trajectories, an evaluation of a spatiotemporal co-localization of BIR2 and BAK1 might be possible, but further development of the analysis software is required beforehand.

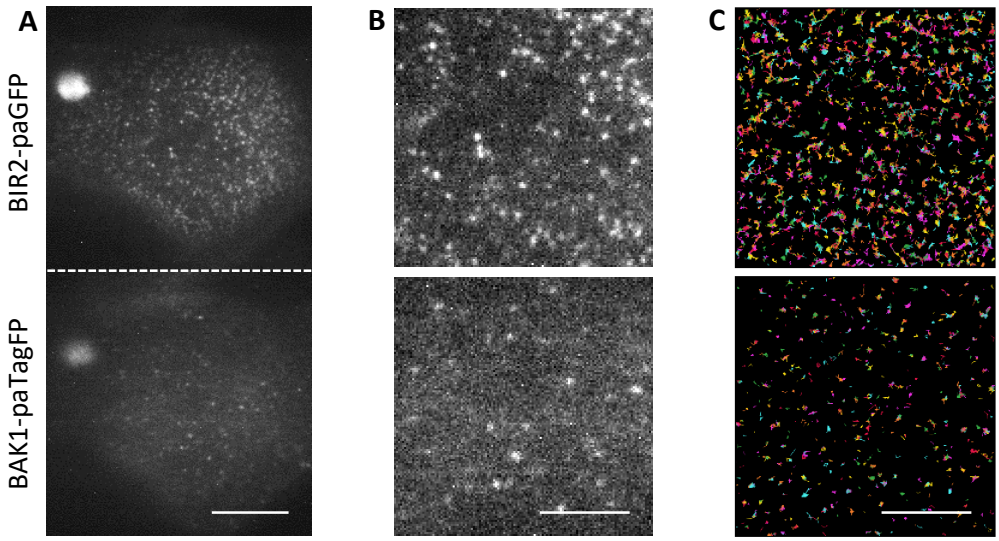

Figure 3-19: Dual color sptPALM of BIR2-paGFP and BAK1-paTagRFP. Ubi1-BIR2-paGFP and Ubi1-BAK1-paTagRFP were transiently co-expressed in *N. benthamiana* and imaged by VAEM. [**A**] Dual color VAEM raw image of BIR2-paGFP and BAK1-paTagRFP. VAEM images, displaying the same cell, showing separated simultaneously captured projections of BIR2-paGFP and BAK1-paTagRFP single molecules. Scale bar represents 10 µm. [**B**] Zoomed in view of a corresponding VAEM image range. Scale bar represents 5 µm. [**C**] Corresponding trajectories computed from 300 frames. Arbitrary coloring for each protein. Scale bar represents 5 µm.

In brief, these experiments showed the successful application of the two novel photoactivatable fluorophores paGFP and paTagRFP *in planta* and their application for sptPALM. Their expression and photoactivation was functional in the nucleus as well as localized at the plasma membrane. Moreover, simultaneously imaging of single paGFP- and paTagRFP-tagged proteins was achieved. For the first time, these results showed the simultaneously dynamics of two different proteins in real-time by sptPALM in living plant cells. The established application of dual color sptPALM will give rise of new possibilities to study the spatiotemporal membrane organization and dynamical relations of two proteins during signaling transduction in plants. By this work, primary and major steps were taken in order to perform dual color sptPALM in plants.

4 DISCUSSION

Plants utilize cell surface located receptors to perceive extracellular signals such as PAMPs or hormones (Escocard de Azevedo Manhães et al., 2021). It is known that the two well described LRR-RLKs FLS2 and BRI1 are heterogeneously distributed within the plasma membrane and thereby forming distinct nanodomains (Bücherl et al., 2017). It is proposed that the compartmentalization of membrane residing proteins into nanodomains and their assembly in preformed complexes serve as signaling platforms (Bücherl et al., 2013; Bücherl et al., 2017; Hutten et al., 2017). The multifunctional co-receptor BAK1 is shown to reside in different pools of preformed receptor complexes: On the one hand, BAK1 constitutively interacts with its negative regulators BIR2 and BIR3 and on the other hand BAK1 resides ligand-independent in preformed signaling complexes with the ligand-binding receptor BRI1 and BIR3 (Bücherl et al., 2013; Halter et al., 2014; Hutten et al., 2017; Imkampe et al., 2017; Großeholz et al., 2020). The formation, the maintenance and the spatiotemporal dynamics of such preformed complexes is largely unknown. New insights into the nanoscale dynamics of BAK1 and FLS2 were recently published by Gronnier et al. (2022), who hypothesized that BAK1 might dynamically associate with various nanodomains.

Until now, it remains elusive how the plasma membrane nanoscale organization is regulated, and the molecular determination of such a complex protein assembly is only starting to be identified (Gronnier et al., 2018).

4.1.1 What is the function of HIR2?

HYPERSENSITIVE INDUCED REACTION (HIR) proteins are plant-specific and conserved proteins, which belong to the SPFH-domain containing protein family. *Arabidopsis* contains four different *HIR* genes, which share high homology and HIR2 is described as the most abundant in leaves (Qi et al., 2011; Daněk et al., 2016). HIR2 is localized on the cytosolic side of the plasma membrane and found to be enriched in detergent-resistant membranes, which have been associated with membrane nanodomains (Qi et al., 2011). Moreover, HIR2 was shown to be involved in the plant immune response as its transcription is upregulated after elicitor treatment with the peptide flg22 and it can interact with different types of immune receptors FLS2 and RPS2 (Qi et al., 2011). Also, it was described to be involved in the RPS2-mediated ETI response (Qi et al., 2011). However, it is unclear how HIR2 proteins function in the immune

response. Furthermore, it is known that HIR2 can form homo- and heterooligomers with all HIR proteins, which has been suggested to be necessary for the stabilization of some SPFH-domain containing protein at the membrane (Browman et al., 2007; Qi et al., 2011). Evidence for the function of HIR proteins are given by stomatin-like and flotillin-like homologs from animals, which also belong to the SPFH-domain containing proteins. They are demonstrated to bind lipids and to form putative scaffolds to provide spatially and temporally stable platforms for the assembly of multiprotein complexes within membranes (Langhorst et al., 2005; Gehl & Sweetlove, 2014).

Therefore, HIR2 is hypothesized to act as scaffolds to assist the organization of immunity receptors in specific nanodomains within the plasma membrane (Qi et al., 2011).

4.1.2 HIR2 interacts with receptor kinases of multiple signaling pathways and with intracellular NLRs

HIR2 was identified by Qi and Katagiri (2009) through a biotinylated affinity tag-based approach in a complex with the NLR-type resistance protein RPS2 and its interaction was confirmed in *Arabidopsis* and *N. benthamiana* by using Co-IP and FRET analyses (Qi & Katagiri, 2009; Qi et al., 2011). The same authors demonstrated a physical interaction of HIR2 with the LRR-RLK FLS2 by Co-IP experiments in *N. benthamiana* and speculated that HIR2 might provide a signaling platform, potentially linking PTI with ETI receptors (Qi & Katagiri, 2012). Additionally, HIR2 was identified in the BIR2 interactome by performing LC/ESI MS/MS (Halter et al., 2014). Later, using the same technique, HIR2 was also found in the interactome of BIR3 (Schulze, 2020). BIR2 and BIR3 are negative regulators of the flg22-induced signaling pathway by interacting with BAK1 and preventing its interactions with FLS2 in the absence of the ligand (Chinchilla et al., 2007; Halter et al., 2014; Imkampe et al., 2017). Moreover, HIR2 was recently found in the interactome of the NLR CONSTITUTIVE SHADE-AVOIDANCE 1 (CSA1) by mass spectrometry analyses, and their interaction was confirmed by Co-IP experiments in *N. benthamiana* (AG Kemmerling, unpublished). CSA1 is involved in the BAK1- and BIR- mediated cell death and it was proposed to guard BAK1 BIR3 complexes in order to activate ETI-responses in the absence of BIR3 or BAK1 (Schulze et al., 2021).

This study confirmed the physical interaction of HIR2 with the small receptor kinases BIR2 and BIR3, as well as with BAK1 by multiple, independent interaction experiments (Co-IP, FRET-FLIM and mbSUS). Additionally, the interaction of HIR2 with FLS2 was confirmed in this work by FRET-FLIM analyses (Qi &

Katagiri, 2012). Moreover, it was shown by the same three interaction analysis approaches that can form complexes with the LysM-RLK CERK1, which is essential for the perception of fungal chitin (Miya et al., 2007). The CERK signaling pathway is proposed to signal independently of the co-receptor BAK1, although crosstalk between the receptors was reported (Miya et al., 2007; Couto & Zipfel, 2016; Yu et al., 2017b; Gong et al., 2019). Further interaction analysis revealed an association of HIR2 to the brassinosteroid receptor BRI1, which controls growth of plants. Although a direct interaction was not shown by the mbSUS assay, a close spatial proximity was demonstrated by FRET-FLIM analysis and it can be suggested that HIR2 and BRI1 reside in one complex at the plasma membrane.

These data revealed that HIR2 has a broad interaction spectrum. It is neither restricted to LRR-RLK signaling pathways nor is it exclusively dependent on BAK1-regulated signaling pathways, as both was shown by the interaction with the LysM-RLK CERK1. Besides the interaction with PTI receptor kinases, HIR2 was shown to be associated with different intracellular NLR proteins, which are typically implicated in ETI signaling. Additionally, HIR2 does not only interact with receptors of the immune system; it is also associated to developmental receptor kinases. How HIR2 is involved in the immunity and/or developmental signaling pathways has to be elucidated in the future.

4.1.3 The difficulty of obtaining a null mutant of *HIR2*

In order to understand the function of HIR2, it was important to generate a genetically stable null-mutant of HIR2. Previous to this thesis, four different T-DNA insertion lines of *HIR2* were analyzed. The *hir2-2* (SALK_124393) mutant appeared to be a full knock-out mutant and showed impairment in ROS signaling in response to PAMP treatment (Manstretta, unpublished). However, complementation experiments did not rescue the observed phenotype, and no additional T-DNA insertions were identified. It could not be ruled out that point mutations or epigenetic effects caused the phenotype, so *hir2-2* was not used for additional characterizations. Further analyzed *HIR2* T-DNA insertion lines did either still translate the *HIR2* full-length transcript (*hir2-4* (SALK_095926C)) or a truncated mRNA transcript (*hir2-1* (SALK_092306) and *hir2-3* (SALK_033877) (Manstretta, unpublished).

It is important to mention that Qi et al. (2011) examined the function of HIR2, among others, on the basis of *hir2-1*. The mutant was used to test RPS2-mediated ETI by *Pst* DC3000 AvrRpt2 growth assays, which showed an enhanced bacterial growth phenotype (Qi et al., 2011). However, neither complementation of the mutant line was performed nor the transcript upstream of the T-DNA insertion site was analyzed. The

authors could only suggest that the phenotype is caused by the mutation (Qi et al., 2011). Raffaele Manstretta identified *hir2-1* to produce a truncated mRNA, lacking the C-terminus and it is not known whether the translated protein is functional. Therefore, one has to be aware that the published *hir2-1* mutant might not be a full knock-out mutant.

In the scope of this work, alternative approaches were used to generate a functional *HIR2* mutant. Artificial microRNA lines targeting *HIR2* were created. Additionally, amiRNA constructs targeting all four *HIR* genes were designed, since it was suspected that the HIRs might function redundantly due to their high sequence homology. Unexpectantly, instead of silencing, the plants turned out to overexpress the *HIR* transcripts. Although technical issues have been largely excluded, this cannot be ruled out with certainty as the cause of this observation. Until now, no certain explanation can be given for that effect and only speculations could be drawn.

Furthermore, CRISPR/Cas9 lines targeting either *HIR2* or all four *HIR* genes were generated. The transformants of the T1 generation showed a low germination rate and only a small number of plants were analyzed. For none, a deletion in *HIR2* was identified. Due to time limitations of the project, this could not have been repeated.

In addition, a preliminary characterization of the T-DNA insertion line *hir2-5* (SAIL_1274_A05) was performed as part of this work. RT-PCR analyses indicated no amplicons for *HIR2* full-length but revealed a truncated mRNA of the C-terminal region, which might be transcribed due to a transcription start site within the inserted T-DNA. The growth deficiency phenotype of the *hir2-5* plants and their flg22-triggered ROS response will be discussed in the following chapters. However, complementation of *hir2-5* is necessary to ensure the described growth phenotype is caused by the T-DNA insertion in *HIR2,* and further characterizations are required to be able to state a function of HIR2 in developmental and immunity signaling pathways.

Until now, no full knock-out mutant of *HIR2* has been identified. Due to the difficulties in obtaining null mutants, it can be hypothesized that HIR2 is essential and early loss might be lethal. In that case, the other HIRs would not function redundantly as it was presumed. If knocking-out *HIR2* is lethal, inducible constructs of the amiRNA or the CRISPR/Cas9 could be generated. Alternatively, the function of HIR2 could be studied with mutants, in which HIR2 proteins are not able to localize correctly at the plasma membrane. As HIR2 are described to form homo-oligomers, these might interact with endogenous HIR2 and disrupt their function in a dominant-negative way.

4.1.4 The role of HIR2 in the plant immune response

The HIR proteins are described to be involved in plant immunity in several plant species. However, the underlying mechanism of how HIR proteins function in immune responses is not understood yet (Zhou et al., 2010; Choi et al., 2011; Qi et al., 2011; Li et al., 2019; Martinière & Zelazny, 2021). Primary, HIRs were associated with the development of a hypersensitive response (HR) (Nadimpalli et al., 2000; Martinière & Zelazny, 2021). Overexpression of the pepper *Ca*HIR1 triggered a pathogen-independent cell death in *Capsicum annuum* and *N. benthamiana,* as well as the overexpression of the rice *Os*HIR1 in *Arabidopsis* caused spontaneous hypersensitive response lesions (Zhou et al., 2010; Choi et al., 2011). The pathogen-independent development of an HR led to the suggestion that HIR proteins are involved in ETI-signaling. In *Arabidopsis*, HIR2 was described to function in a RPS2-mediated immune response as the *hir2-1* mutants showed reduced resistance against *Pst* DC3000 AvrRpt2 (Qi et al., 2011). As discussed before, these results have to be taken with care as the mutants seemed not to be a full knock-out line (Manstretta, unpublished). Furthermore, it was suggested that HIR2 is involved in PTI responses. Transcriptional upregulation of *HIR2* was described after flg22 treatment in Col-0 plants and an interaction with FLS2 was reported (Qi et al., 2011; Qi & Katagiri, 2012). Moreover, enhanced resistance against the bacteria *Pst* DC3000 was observed in *Arabidopsis* overexpressing HIR2-YFP-HA (Qi et al., 2011). Thus, it was hypothesized that HIR2 functions in PTI as well as in ETI signaling pathways (Qi & Katagiri, 2012).

The involvement of HIR2 in PTI signaling was investigated as part of this thesis. The FLS2 signaling pathway was triggered by flg22 in *hir2-5* and Col-0 plants. In preliminary results, the *hir2-5* plants showed a slightly, but not significant, lower ROS production than the wild type. Additional experiments have to be conducted to verify this result. Since a stronger impairment in the ROS response would have been expected, it might be considered that the truncated C-terminal transcript of *HIR2* in *hir2-5* translates a partially functional protein, which is involved in the observed ROS response. Also, whether the ROS response is caused by a redundancy of the HIR proteins, thus masking, e.g., the effect in the *hir2-5* line, or an actual non-participation of HIR2 in the FLS2 pathway has to be clarified in the future.

The ROS production in response to flg22 elicitation was measured in *Arabidopsis* overexpressing HIR2-GFP. No clear differences in the ROS burst were detectable in the HIR2 overexpression plants compared to wild type. It has been described that the co-activation of PTI and ETI leads to higher ROS production compared to those with activation of PTI alone, particularly in a phase of five to fifteen hours after PAMP elicitation (Ngou et al., 2021). As HIR2 was proposed to positively regulate ETI, it can be hypothesized that

overexpressing HIR2 activates ETI signaling and differences in ROS burst would appear in later phases than those monitored in this work.

The overexpression of HIR2-GFP did not cause macroscopic cell death symptoms as it was described for the overexpression of *Os*HIR1 and *Ca*HIR1 in *Arabidopsis* plants (Zhou et al., 2010; Choi et al., 2011). Neither did the transient expression of 35S-HIR2-GFP in *N. benthamiana* cause an HR nor did the HIR2-amiRNA lines, which strongly overexpressed *HIR2*, show macroscopic lesions on the leaves. Also, the development of an HR was not described by Qi et al. (2011) for the HIR2 overexpression in stable *Arabidopsis* lines. The closest homolog of *Ca*HIR1 in *Arabidopsis* is *At*HIR4*,* which has been studied rarely so far. Whether the overexpression of *At*HIR4 is causing spontaneous cell death in *Arabidopsis* has to be shown in future work. Thus, the different HIR proteins might have diverse functions.

4.1.4.1 Does HIR2 enhance plant immunity?

For a long time, PTI and ETI were seen as two independent systems in the plants' defense, but the discussion if and how PRR- and NLR-mediated immunity diverges has been risen in the community. Recent publications were able to show that the boundaries between these two distinct immune systems are fading. Ngou et al. (2021) and Yuan et al. (2021) reported in independent studies that the activation of PTI or ETI alone is insufficient to provide a robust immunity. The authors showed that PTI is required for induced bacterial resistance mediated by multiple NLRs and that both systems potentiate each other, which explained observed similarities in downstream defense-outputs between PTI and ETI (Ngou et al., 2021; Yuan et al., 2021).

HIR2 interacts with two different types of NLRs, with the CC-NLR RPS2 and the TIR-NLR CSA1 (Qi & Katagiri, 2009; AG Kemmerling, unpublished). HIR2 might be involved in the activation of ETI by the described NLRs, thereby conferring bacterial resistance (Qi et al., 2011).

Moreover, it was shown that the activation of NLRs causes an upregulation of PTI signaling components such as *BAK1*, *FLS2* and *CERK1* (Ngou et al., 2021; Yuan et al., 2021). Does an NLR-mediated signaling maybe also require the upregulation of HIR2? Indeed, upregulation of *HIR2* upon elevated SA levels and after flg22 elicitation was reported (Qi et al., 2011; Daněk et al., 2016). Thus, future research might reveal whether the overexpression of HIR2 activates ETI responses and contributes to enhancing PRR-mediated resistance.

Until now, the role of HIR2 in the plant immune response remains elusive. Despite the interaction with different RLKs and the two NLRs RPS2 and CSA1 it is unclear how HIR2 is involved in PTI or ETI. Further research with the *hir2-5* mutant and HIR2 overexpressing lines is needed to address whether HIR2 is a positive regulator in ETI and contributes to the enhancement of PRR-mediated resistance.

4.1.5 Is HIR2 pivotal for developmental pathways?

Nearly all phases of plant growth and development are controlled by brassinosteroids (BR), which are recognized by the LRR-RLK BRI1 (Li & Chory, 1997; Belkhadir & Chory, 2006; Santiago et al., 2013; Belkhadir et al., 2014). Hormone binding to the extracellular domain of BRI1 and the complex formation of BRI1 with the co-receptor BAK1 are essential to initiate downstream signaling (Li et al., 2002; Nam & Li, 2002; Belkhadir & Chory, 2006). The BR signaling is negatively regulated by BIR3, which directly interacts with BRI1 and BAK1 in a competitive manner (Imkampe et al., 2017; Großeholz et al., 2020). Mutants, which are impaired in BR synthesis show a dwarf phenotype due to the lack of cell elongation, which can be rescued by the exogenous application of brassinolide (BL) (Choe et al., 1998). Alike, *bri1* mutants show dwarfism and impairments in several developmental processes such as delayed flowering time, reduced male fertility, and altered photomorphogenesis (Kwon & Choe, 2005; Sun et al., 2017). Numerous *bri1* mutant alleles have been identified, which differ in the severity of their morphological alterations (Sun et al., 2017). Moreover, *Arabidopsis* plants with mutations in the *BAK1* gene display a compact rosette with round leaves and short petioles, which resembles a weak *bri1* phenotype (Nam & Li, 2002). The observed growth defects in *bak1* mutants are related to the insensitivity to BR and can be restored by exogenous application of BL (Kemmerling et al., 2007).

First phenotypical characterizations of *hir2-5* mutants showed clear morphological differences to wild type plants. The *hir2-5* plants exhibited dark green, thickened leaves that grew compactly due to shortened petioles. The stunted phenotype strongly resembles the phenotype of weak *bri1* mutants. Does *hir2-5* mimic the *bri1*-mutant phenotype? Whether *hir2-5* is impaired in the BR-biosynthesis pathway or in the BR-signaling pathway has to be clarified in future. If exogenous treatment with BL can complement the phenotype, the first is the case. If BL application does not affect the morphogenesis of *hir2-5* plants, the latter is applicable.

Since interaction analyses of HIR2 revealed associations to BRI1 as well as to BAK1 and BIR3, it can be hypothesized that *hir2-5* is hampered (i) in the receptor assembly or (ii) the activation of the downstream signaling: Exemplary, *hir2-5* could mimic *bri1-301* or *bri1-705* mutants.

The *bri1-301* has an amino acid substitution in the cytoplasmic kinase domain of BRI1 and shows a reduced protein abundance due to a reduced stability of the receptor (Lv et al., 2018). The truncated HIR2 protein could cause a destabilization of BRI1 and BAK1 at the plasma membrane, leading to the similarities in the stunted phenotype of *hir2-5* and *bri1-301*. Analysis of the protein abundance of BRI1 and BAK1 in *hir2-5* could give evidence whether the protein stability is affected in the mutants or not.

The *bri1-705* is a subtle allele with a mutation in the extracellular domain of BRI1, which disrupts the interaction between BRI1 and BAK1 (Sun et al., 2017). Assuming HIR2 is involved in maintaining BRI1 and BAK1 in a preformed complex, *hir2-5* mutants could be impaired in the formation of the heteromeric complex between the ligand-binding receptor and its co-receptor and thereby affected in BRI1 downstream signaling. Interaction analysis of the association of BRI1 and BAK1 in *hir2-5* could reveal an involvement of HIR2 in the complex formation.

Moreover, for weak *bri1* alleles *bri1-5* or *bri1-301,* which are impaired in the initiation of the BR signaling pathway, it was shown that overexpression of BAK1 can partially rescue the growth deficiencies, whereas the overexpression of a kinase-inactive version of BAK1 caused a dominant negative phenotype. Contrary overexpression of the kinase-inactive BAK1 in *bri1-705* failed to generate dominant-negative mutants, which indicated that the interaction of BRI1 and BAK1 is disrupted (Sun et al., 2017). The overexpression of BAK1 or a kinase-inactive version of BAK1 in *hir2-5* could indicate whether HIR2 functions by maintaining the stability of the receptor complexes or is involved in the signaling activation.

Currently, the involvement of HIR2 in the BR-signaling pathway can only be hypothesized and further studies, which take the discussed variables into account, have to be conducted. Also, complementation lines of the *hir2-5* mutants are necessary to ensure the described phenotype is solely caused by the mutation in *HIR2*. However, HIR2 is an eligible candidate to mediate the ligand independent complex formation of BRI1, BAK1 and BIR3 within a nanodomain (Bücherl et al., 2013; Hutten et al., 2017; Imkampe et al., 2017; Großeholz et al., 2020).

4.1.6 Does HIR2 act as a scaffold protein?

Scaffold proteins are central players in regulating the spatiotemporal organization of proteins in a heterogeneous environment and are able to offer compartmentalization (Su et al., 2020). The function of scaffold proteins can be described as the ability to bring two or more proteins into a relatively stable configuration by having multiple protein-protein interaction modules (Garbett & Bretscher, 2014). Thereby they form physical platforms to facilitate the complex formation of receptors with downstream signaling proteins (Su et al., 2020). Moreover, scaffold proteins have been described to act as "diffusion traps" for ligand-binding receptors, e.g., in synapses cells of mammalians where the interaction of the neurotransmitter receptor GlyR with the cytoplasmatic scaffold gephrin is responsible for the inhibition of the lateral receptor diffusion and the accumulation in clusters (Maynard & Triller, 2019).

The nanoscale dynamics and the cluster formation of HIR2 were analyzed by sptPALM and Voronoi-based segmentation. HIR2 showed a heterogeneous distribution and formation of distinct clusters within the plasma membrane. It showed a confined and immobile diffusion behavior with a diffusion coefficient of D= 0.0034 $\mu m^2/s$, which was the slowest measured value in this study and its mobility remained unaffected by external stimulation with flg22.

In order to study the impact of HIR2 on the diffusion of membrane localized receptor kinases, it would be of interest to analyze the spatiotemporal organization of HIR2-interacting proteins in *HIR2* deficient mutants or in mutants where these interactions are disrupted.

The static and immobile diffusion behavior, as well as the broad interaction spectrum of HIR2 indicate characteristic features of scaffold proteins, thus supporting the hypothesis that HIR2 to acts as a scaffold and stabilizes interacting receptor kinases in functional nanodomains.

4.1.7 Does HIR2 assist endocytosis of receptor kinases upon signaling activation?

Receptor kinases such as FLS2 and BRI1 are described to be internalized upon ligand perception by two independent pathways. They undergo endocytosis *via* clathrin-dependent processes or mediated by flotillin 1 (FLOT1), which is reported to function in a clathrin-independent manner (Robatzek et al., 2006; Irani et al., 2012; Li et al., 2012; Di Rubbo et al., 2013; Wang et al., 2015b; Mbengue et al., 2016; Cui et al., 2018; Liu et al., 2020). The closest homolog of FLOT1, FLOT2 was described to form a complex with HIR2 (Junková et al., 2018). Analysis of cluster formation of HIR2 and the ligand-binding receptor FLS2 revealed

a reduction in the cluster sizes upon flg22 treatment, which might occur due to internalization of the receptor complexes. Based on the close similarity of the FLOT1 and FLOT2 isoforms, it is possible that FLOT2 might function like its homolog, and HIR2 might contribute to stress-induced endocytosis *via* FLOT2 by stabilizing its interacting receptor kinases such as FLS2 and BRI1 in nanodomains (Daněk et al., 2016).

Future research could address whether the observed reduction in cluster sizes is dependent on endocytosis either in a clathrin-dependent or a clathrin-independent manner *via* FLOTs. Moreover, the involvement of HIR2 in endocytic pathways could be studied in the future.

4.1.8 How is HIR2 associated to the plasma membrane?

The association of soluble proteins to the plasma membrane can be mediated by protein-protein interactions with other membrane-residing proteins or protein-lipid interactions (Konrad et al., 2014). The latter is mediated by posttranslational lipid modifications, such as myristoylation or palmitoylations. HIR2, which belong to the SPFH-domain containing protein family, is localized at the plasma membrane and found to be enriched in nanodomains (Qi et al., 2011). So far, it is not known how members of the SPFH-domain containing protein family, and especially HIR2, is associated to the plasma membrane and how the recruitment into nanodomains is determined (Martinière & Zelazny, 2021). Since proteomic studies indicated that some family members are modified by myristoylation and palmitoylation, lipidation might be involved in targeting these proteins to the membrane (Hemsley et al., 2013; Majeran et al., 2018; Martinière & Zelazny, 2021). Additionally to the proteomic data, palmitoylation of the HIRs was verified by biochemical approaches (Hemsley, 2015). The importance of the SPFH-domain for membrane association was shown for the mammalian flotillin proteins. Truncated FLOT1 proteins, containing the N-terminus of the SPFH-domain with myristoylation and palmitoylation sites, were shown to localize properly to the membrane, whereas the deletion of the entire SPFH-domain led to an accumulation of the protein in soluble fractions (Morrow et al., 2002; Neumann-Giesen et al., 2004). This indicated that the N-terminal lipidation motifs of the SPFH-domain of flotillin proteins are necessary for the localization at the plasma membrane (Daněk et al., 2016).

In this study, mutations in predicted lipidation sites of HIR2 were introduced to prevent potential myristoylation and/or palmitoylation. Transient expression of these mutated proteins did not cause a total loss of the plasma membrane localization; however, mis-localizations were visible for the single mutants HIR2^{G2A}-GFP and HIR2^{C6,7S}-GFP and the triple mutant HIR2^{G2AC6,7S}-GFP. The partly cytosolic and ER

localization, as well as the formation of protein aggregations, indicate a distinct function of the lipidation motifs for the association of HIR2 to the plasma membrane, although the modification sites seem not to be exclusively responsible for this process.

Studies investigating the effect of lipid modifications in the context of protein localization showed, that myristoylation is necessary but insufficient for anchoring proteins stably into the membrane and stabilization of the membrane localization may be further strengthened through proximal second reversible modification, such as palmitoylation (Stael et al., 2011; Ranf et al., 2014; Majeran et al., 2018). Mutating the myristoylation site e.g., in the RLCK CAST AWAY (CST) caused only a partial redistribution of the protein to the cytoplasm, which was also observed for mutation in predicted palmitoylation sites. Mutations in both sites did not cause an additional redistribution of $CST^{G2A\ C4S}$-GFP to the cytoplasm (Burr et al., 2011). Similar observations have been shown in this work, as neither the mutation of the predicted myristoylation or the palmitoylation site in HIR2, nor the triple mutation caused a complete delocalization into the cytosol. It is hypothesized that palmitoylation sites in the vicinity of a myristoylated glycine might have a regulatory role in relocating and stabilizing proteins within the plasma membrane; this might also apply to HIR2 (Hemsley, 2015; Turnbull & Hemsley, 2017; Majeran et al., 2018). Palmitoylation is mediated by Palmitoyl-Acyl-Transferases (PATs), which are located in the plasma membrane (Batistič, 2012). Therefore, it is conceivable that palmitoylation of HIR2 might occur after it is targeted to the plasma membrane in order to anchor HIR2 itself in distinct compartments. Since palmitoylation is an enzymatically reversible modification, HIR2 might exist in two different pools: with and without modification. These differentiations might guide the protein to locate in distinct clusters within the membrane (Majeran et al., 2018). In addition to lipid modifications, the capability of HIR2 to form oligomers might play a role in its membrane localization and recruitment into nanodomains (Qi et al., 2011; Martinière & Zelazny, 2021). It is possible that complex formation with endogenous HIR2 homologs from tobacco or interactions with membrane localized LRR-RLKs in *N. benthamiana* did promote an association of the mutated HIR2 isoforms to the plasma membrane. Indeed, remorins (REM), which are described to have similar functions regarding their ability to organize plasma membrane nanodomains, form higher order oligomers (Bariola et al., 2004; Martinez et al., 2019; Yu et al., 2020). It was demonstrated that fatty acid modifications at cysteine residues of remorins are not the key determinant for their localization, but the formation of trimeric complexes is essential for their recruitment into the plasma membrane (Konrad et al., 2014; Martinez et al., 2019). The oligomerization of the REMs is facilitated by a coiled-coil domain upstream of the C-terminal anchor REM-CA (Martinez et al., 2019). Furthermore, it was shown for mammalian flotillins to be organized in tetrameric complexes as well, which

depends on coiled-coil structures outside the SPFH-domain (Solis et al., 2007). *In silico* predictions identified coiled-coil regions within the HIR proteins C-terminal of the SPFH-domain (except of HIR3) (Daněk et al., 2016), indicating that the localization and the recruitment of HIR2 to the plasma membrane might also be mediated by oligomerization *via* a coiled-coil domain. Further research regarding the role of the coiled-coil domain might give a deeper insight into the process of HIR2 membrane recruitment and nanodomain formation. Deletion of the putative domain sequence might cause alterations in the cellular localization of HIR2 and/or influences the formation of homo-and heterooligomers. This could provide a better understanding of the mode of action of HIR2. Additionally, it would be interesting to investigate, whether the myristoylation and palmitoylation mutants of HIR2 cause dominant negative effects when stably transformed in *Arabidopsis* wild type plants. Dominant negative phenotypes were reported for proteins that form dimers or oligomers, when the functional site is mutated but the dimerization site is intact (Veitia, 2008).

This work could demonstrate that potential N-terminal lipid modifications within the SPFH-domain are important for the localization of HIR2 to the plasma membrane, although they are not the only determinants. HIR2 might possess additional lipid modifications than predicted. In addition to protein-lipid interactions, protein-protein interactions could potentially be involved in the association to the plasma membrane and in the cellular compartmentalization of HIR2.

4.1.9 Hypothesis for the function of HIR2

One aim of this thesis was to investigate the function of HIR2. It was proposed to act as a scaffold protein, linking PTI- and ETI signaling components in functional nanodomains (Qi & Katagiri, 2012). Evidence from this study pointed out that HIR2 possesses typical characteristics of a scaffold protein as it displays an immobile diffusion behavior at the plasma membrane as well as having multiple interaction partners (Figure 4-1). This work revealed that HIR2 is not specifically associated to PTI and ETI components but might also be involved in plant development.

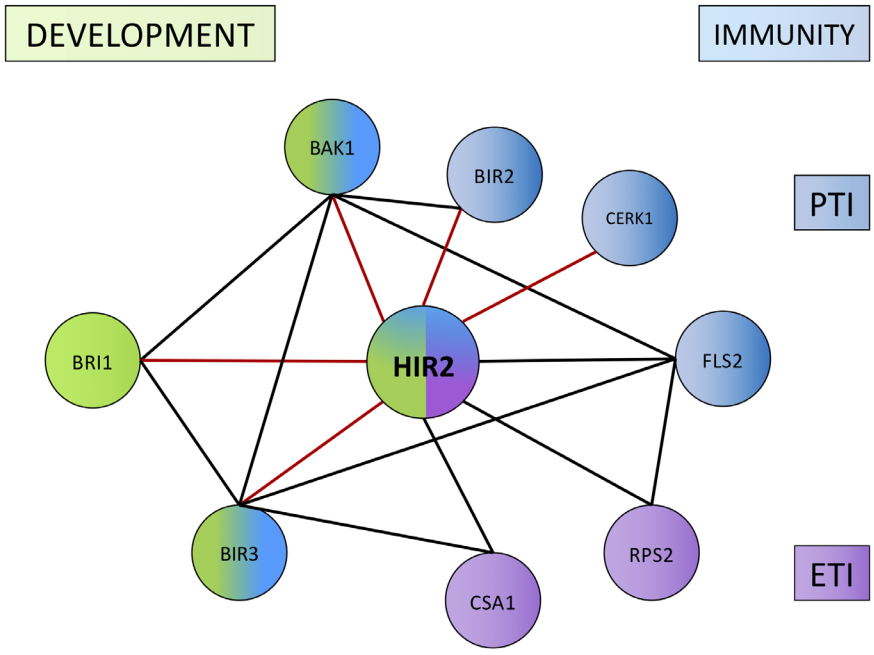

Figure 4-1*:* HIR2 interacts with proteins of multiple signaling pathways. Interactions of HIR2 with different proteins of developmental and immunity pathways are shown by connecting lines. Black lines indicate previously published protein-protein interactions, whereas red lines indicate novel interactions of HIR2 identified in this study. Immunity PTI components are shown in blue, ETI components in purple and BL-signaling proteins in green. Mixed colors indicate the participation of the respective proteins in plant immunity as well as in plant growth and development.

Besides the interactions, it is not clear whether HIR2 is involved in the respective signaling pathways as a signaling component or simply functions by binding to other membrane proteins. One major limitation in studying the function of HIR2 was the lack of a functional knock-out mutant. Due to the difficulty in obtaining a full null-mutant, it can be proposed that HIR2 is indispensable in *Arabidopsis* and loss of HIR2 might be lethal. Thus, HIR2 is hypothesized to function as an essential scaffold to provide spatially and temporally stable platforms for the assembly of multiprotein complexes at the plasma membrane.

4.2 Application of single and dual color sptPALM to compute the dynamic and cluster formation of plasma membrane proteins

4.2.1 mEos3.2 - a fluorophore that improves single color sptPALM

The super-resolution microscopy technique sptPALM features super-resolved information on the localization of single molecules and provides quantitative parameters to analyze single molecule dynamics on a nanoscale. It relies on photoconvertible or photoactivatable fluorescent proteins. So far, most of the published studies applying sptPALM in plant cells have performed measurements with the photoconvertible fluorophore mEos2 (Hosy et al., 2015; Gronnier et al., 2017; Platre et al., 2019; Bayle et al., 2021). Recently novel mEos variants, namely mEos3.2 and mEos4b, have been developed but not yet applied in plants in order to perform sptPALM (Zhang et al., 2016; De Zitter et al., 2019; Bayle et al., 2021). In contrast to mEos2, mEos3.2 and mEos4b are described to be truly monomeric fluorophores and to exhibit a better photostability, which are properties improving the imaging accuracy and notably facilitate obtaining longer trajectories of single molecules (Zhang et al., 2016; Bayle et al., 2021).

In the scope of this work, mEos3.2 was established for a plant expression system and for the first time, it was applied for sptPALM *in planta*. Initially, mEos3.2 has been engineered and optimized for the expression in mammalian cells, in which its biophysical properties, such as folding efficiently, and maturation time, might differ compared to plant cells (Shaner et al., 2005; Zhang et al., 2012). Here, plant-codon optimized mEos3.2 (kindly provided by Klaus Harter) was transiently expressed in *N. benthamiana* and analyzed as a probe in the nucleus as well as fusion protein at the plasma membrane. It was shown that mEos3.2 is functional in the green and the red emission state in both cellular compartments. Moreover, in VAEM, the fluorescence intensity of the red mEos3.2 state achieved a high signal-to-noise ratio, which was appropriate to allow precise localization of the single emitters. By adjusting the UV laser power, the photoconversion of mEos3.2 molecules was controllable and enabled imaging of an adequate number of emitters per frame. This allowed the spatial separation of single emitters and is a prerequisite for facilitating an appropriate tracking of the single molecules. By avoiding a high number of imaged emitters per frame, the localization precision increases and errors in the track reconstruction were reduced.

It has to be noted that measuring the diffusion of a fluorescence tagged protein in living plant cells holds technical difficulties. Particularly, numerous auto-fluorescent molecules in the cell wall and inside the cell (e.g., phenols, flavonoids, lignin, suberin, tannins, anthocyanins and chlorophyll) hamper imaging

(Donaldson, 2020; Bayle et al., 2021). Attention had to be paid to discriminate between the signal emitted from the fluorescence-labeled protein and the background signal from auto-fluorescent particles or dust on the cover slip. Moreover, it became apparent that the sptPALM experiments are prone to environmental factors such as temperature, light conditions, the health of the plants and stress during sample preparation (Bayle et al., 2021). Especially the daily temperature had a strong influence on the dynamics of the analyzed proteins. Elevated temperatures can directly alter the fluidity and the lipid composition of membranes, which might cause a remodeling of nanodomains (Niu & Xiang, 2018). Thus, experimental data, which were recorded on hot summer days usually exhibited a higher protein mobility and had to be excluded from the total analysis. Accordingly, it is crucial setting up controlled environmental and laboratory conditions to obtain sptPALM data sets.

Being aware of the discussed technical difficulties, repetitions of the experiments on different days displayed comparable values for the protein mobilities. The good reproducibility of the datasets reinforces the results obtained by the technique single color sptPALM with the newly established and improved fluorophore mEos3.2.

4.2.2 paGFP and paTagRFP – two fluorophores that enable dual color sptPALM in plant cells for the first time

The implementation of mEos3.2 contributed to an improvement of sptPALM *in planta* and this work proved that mEos3.2 works well for single color sptPALM. However, utilizing mEos3.2 for two color sptPALM is complicated since it occupies two different color channels. This largely precludes simultaneous imaging in combination with an additional genetic encoded fluorescing protein (Bayle et al., 2021). Dual color PALM experiments using an ancient version of EosFP have been performed in fixed mammalian cells (Shroff et al., 2007). However, the imaging had to be performed sequentially, causing large time differences in the collected data and did not displaying temporal relations of two various proteins. True dual color sptPALM experiments in living mammalian cells were performed by Subach et al. (2010), which was feasible with the development of the red photoactivatable fluorescent protein paTagRFP. It was used in combination with the spectrally distinct green photoactivatable fluorescent protein paGFP. The study enabled monitoring of the dynamics of two different tagged single molecules at the same time and showed that domains of co-localizing proteins were not compulsory present at the same time (Subach et al., 2010). Thus, dual color sptPALM is a powerful tool for studying spatiotemporal relations of two distinct proteins in living cells. However, its application is not yet established *in planta* (Bayle et al., 2021).

As part of this work, the two photoactivatable fluorophores paGFP and paTagRFP were established for dual color imaging in plant cells and dual color sptPALM was performed for the first time in living plant cells. PaGFP has been used in plant science studies before, but it has not been combined for multicolor imaging (Martinière et al., 2012; McKenna et al., 2019; Bayle et al., 2021). However, to develop dual color sptPALM, paGFP and paTagRFP were implemented equivalently in the system. The fluorophores were individually expressed as a fusion protein with an NLS signal and transiently expressed in *N. benthamiana*. The photoactivation of both fluorophores was clearly observable with a bright fluorescent signal in the imaged nuclei. Moreover, fusion proteins of BIR2-paGFP and BAK1-paTagRFP were generated and transiently expressed in *N. benthamiana.* Since the fusion proteins expressed under the control of the native promoters showed only a weak fluorescence signal, both proteins were subsequently expressed under the constitutively active 35S promoter. Overexpression of both proteins resulted in measurable protein levels in the case of BIR2-paGFP but led to severe cell death in BAK1-paTagRFP expressing leaf epidermal cells, thus largely precluding their visualization (He et al., 2007; Kemmerling et al., 2007; Domínguez-Ferreras et al., 2015). The cell death phenomenon made imaging challenging and made BAK1 an ineligible protein to establish the novel fluorophore. However, BAK1 is an important co-receptor for multiple signaling pathways (Li et al., 2002; Nam & Li, 2002; Chinchilla et al., 2009; Postel et al., 2010; Couto & Zipfel, 2016; Escocard de Azevedo Manhães et al., 2021). Simultaneously studying the spatiotemporal organization of BAK1 and its interaction partner is fundamental for the mechanistic understanding of signal transduction events in plant immune responses as well as in developmental processes. To reduce the overexpression-based cell death, the BAK1-paTagRFP fusion protein was expressed under the control of the weaker Ubiquitin1 promoter, which minimized the cell death and enabled proper imaging (Holtorf et al., 1995). The fusion proteins of Ubi1-BIR2-paGFP and Ubi1-BAK1-paTagRFP were co-expressed in *N. benthamiana* and simultaneous photoactivation of both fluorescent proteins was successfully achieved. Furthermore, VAEM imaging of paGFP and paTagRFP enabled displaying of single molecules in both color channels. The individual emitters were capable for tracking and the dynamics of the individual proteins were determinable. Currently, the software for data processing, which enables the overlay of individual VAEM images, is still under development by Sven zur Oven-Krockhaus. VAEM imaging of the fluorescent proteins in a single channel exhibited adequate fluorescent intensities. However, it was difficult to apply simultaneous photoactivation and excitation of both fluorophores to enable equal fluorescent intensities and a similar number of activated single molecules. One of the major challenges in this work was the expression of both proteins at the same time in the same cell with similar expression levels. Since the proteins were transiently co-expressed in *N.*

benthamiana leaves, there was always a biological bias that had to be taken into account. To circumvent those issues, the generation of stable *Arabidopsis* lines, co-expressing the fusion proteins, is favorable, which has already been started. The constant protein concentrations in the stable lines will contribute to facilitating imaging adjustments. Moreover, imaging of root cells will be possible, which excludes strong background signals caused by auto-fluorescent compartments in leaf cells, thus improving dual color sptPALM imaging quality (Donaldson, 2020; Bayle et al., 2021).

The establishment of dual color sptPALM enabled the simultaneous visualization of two distinct proteins in living plant cells for the first time. With this technique it will be possible to study spatiotemporal relations of two distinct proteins in real-time in living plant cells. This will give insights into the dynamical organization of proteins in the membrane in steady-state conditions and in response to external stimuli. Dual color sptPALM might provide information about stochiometric distributions of individual proteins in signaling complexes. Additionally, analyses of nanocluster formation and co-localization of different proteins within one domain can be accomplished.

Moreover, with the implementation of the fluorophores paGFP and paTagRFP single molecule FRET-FLIM (smFRET-FLIM) is feasible, which has not yet been performed in living plant cells (Guo et al., 2021). This would extend the understanding of protein dynamics in living plant cells. Additionally, smFRET-FLIM might be used in combination with sptPALM. This would provide quantitative parameters for dynamic interactions in real-time, and short-time interactions of proteins might be monitored, which is missing in biochemical and traditional cell biological approaches.

4.2.3 Alternative optical microscopy methods to analyze protein diffusion in plant cells

Apart from sptPALM, other optical microscopy techniques have been used to estimate protein diffusion in plant cells (Bayle et al., 2021). Fluorescence Recovery After Photobleaching (FRAP) quantifies the two-dimensional lateral diffusion of a fluorescent labeled protein (Deli et al., 2022). It is based on the irreversible photobleaching of a fluorescent probe in a spot within the tissue and is monitoring the recovery of fluorescence over time, which correlates with fluorescent labeled protein diffusing in the bleached spot (Wang et al., 2018). FRAP is not a single molecule imaging method and it is difficult to detect subpopulations of a protein with different diffusion behavior (Bayle et al., 2021). However, FRAP is a widely accessible approach. It can be performed on most confocal microscopes and conventional monomeric fluorophores can be used for labeling (Kang et al., 2012; Bayle et al., 2021). The molecular

diffusion, that can be measured with FRAP, is in a range of 0.2–50 µm²/s compared to sptPALM with a range of 0.001–1 µm²/s, indicating that the latter can capture proteins with much slower diffusion (Lippincott-Schwartz et al., 2003; Bayle et al., 2021). Platre et al. (2019) performed FRAP and sptPALM measurements to analyze ROP6 partitioning within the plasma membrane in response to auxin. The authors showed that FRAP and sptPALM cannot only be used as independent approaches to measure protein diffusion, it can also be used to complement the other.

Another possibility to measure protein diffusion is Fluorescence Correlation Spectroscopy (FCS). FCS measures molecular diffusion by analyzing fluctuations in the fluorescence emission of sample molecules, whereas the number of photons that can be collected depends on the diffusion time of the fluorescent molecule (Altan-Bonnet & Altan-Bonnet, 2009; Li et al., 2016b). Like FRAP, it has the advantage that it can be performed with conventional fluorescent proteins, but it requires low concentrations of the fluorophore, which limits the application in plant cells (Li et al., 2016b). FCS is eligible to measure molecules with high diffusion rates, which makes it rather unsuitable for analyzing the diffusion of most of the plasma membrane localized proteins, which usually exhibit a slow diffusion (Martinière et al., 2012; Hosy et al., 2015; Jaillais & Ott, 2019; Bayle et al., 2021).

4.2.4 Reconstructed cluster by Voronoi tessellation might not represent absolute nanodomain sizes

For the visualization of protein compartmentalization at the plasma membrane, clusters were computed based on the sptPALM data by using Voronoi tessellation in the SR-Tesseler software (Levet et al., 2015). Regarding the calculated cluster sizes in this study, it is important to mention that the dimensions obtained by the SR-Tesseler software do not doubtlessly display absolute values. The segmentation is based on local density parameters and a cluster was defined as an area with a density twice the average localization density (α= 2) (Levet et al., 2015). However, the factor can be set by choice and the average density depends on the number of localizations within the imaged cellular region, which is variable due to the stochastic conversation/activation of single emitters. Exemplary, (i) increasing the threshold, which defines a cluster region, would result in a decrease of the cluster size and (ii) increasing the number of localizations would result in smaller cluster as well. Consequently, the values of the cluster sizes quantified in this work should not be considered as representation of total sizes but rather used to analyze variations in the cluster formations of a proteins in response to ligand perception. Accordingly, this leads to two

hypothetical options to interpret alterations in the cluster sizes, where either the number of the respective proteins or their density is constant within a defined cluster. For the first option, an increase in the cluster size would indicate that the spacing between the proteins is increased. Based on the second option, an increase in the cluster size would indicate that more molecules accumulate in a cluster. Gronnier et al. (2017) referred smaller nanodomains to contain a lower number of molecules per cluster and thereby supporting the latter option.

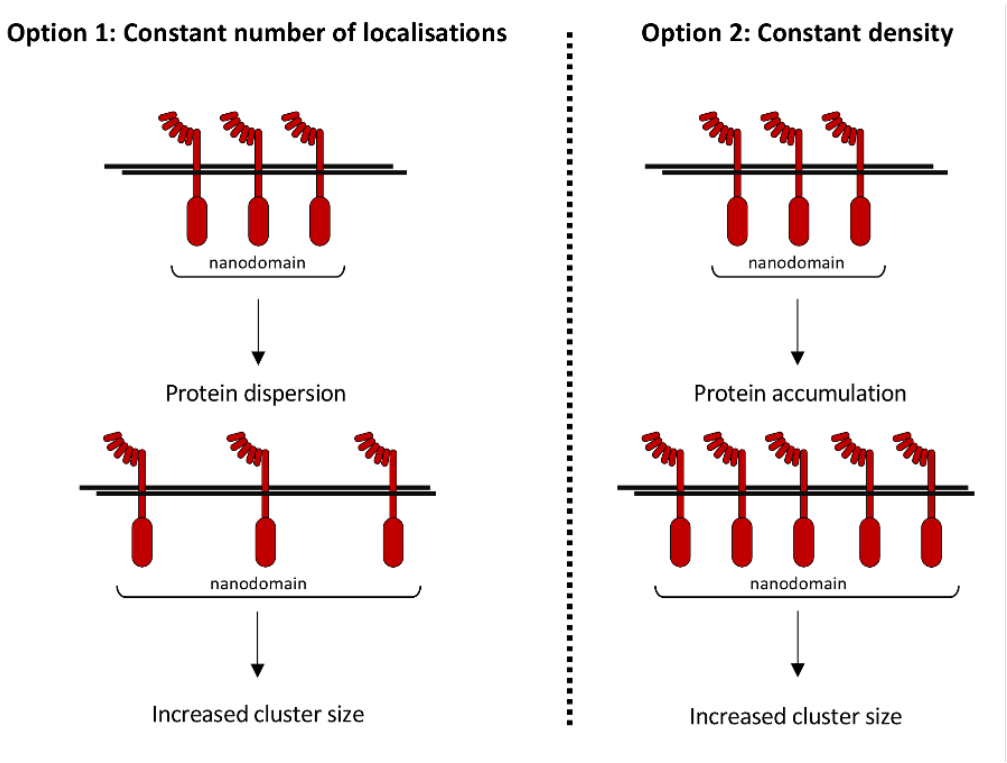

Figure 4-2: Options for interpretation of altered cluster sizes. Option 1: A constant number of localizations is given. An increased cluster size could be explained by dispersion of the proteins. Option 2: A constant density of the proteins is given. An increased cluster size could be explained by an accumulation of the proteins within one nanodomain.

In future, it is important to use defined fixed density parameters when characterizing sizes of nanodomains. It can be recommended to keep the definition of a density twice the average localization density (α= 2) in future experiments, so that reproducibility and comparability of the data can be guaranteed. Moreover, to reveal whether altering sizes in the computed nanodomains are due to changes in the protein quantity, the density or a combination of both, will be a complex challenge in future research.

4.3 Spatiotemporal organization of immunity related LRR-RLKs

The plasma membrane is highly structured and provides a selective environment for transmembrane and membrane-associated proteins (Jaillais & Ott, 2019). The fluid characteristic of biological membranes allows for lateral diffusion of proteins within the lipid bilayer, which is an important parameter for protein complex compartmentalization and the function of signaling processes (Jacobson et al., 2019; Jaillais & Ott, 2019; Bayle et al., 2021). Receptor kinases residing in the plasma membrane have been described to be rather immobile and a ligand-independent preorganization with their signaling components in nanodomains has been suggested (Martinière et al., 2012; Bücherl et al., 2013; Jaillais & Ott, 2019; Martinière & Zelazny, 2021). How nanodomains are formed and modulated in response to signaling activation is poorly understood (Jaillais & Ott, 2019). Therefore, it is of utmost interest to quantitatively study protein dynamics and protein nanodomain formation in response to external stimuli within membranes *in vivo*.

This study focused on the spatiotemporal organization of receptor kinases involved in the flg22-triggered signaling pathway. In the absence of the ligand flg22, BAK1 is associated with BIR2 and BIR3, which prevents its interaction with FLS2 (Halter et al., 2014; Imkampe et al., 2017). Upon flg22 perception, the interaction of BAK1 and the BIRs is released, allowing BAK1 to interact with FLS2 and subsequently initiate PTI signaling (Chinchilla et al., 2007; Halter et al., 2014; Imkampe et al., 2017). It is proposed that these receptors reside in preformed complexes and are organized by scaffold proteins (Bücherl et al., 2017; Hutten et al., 2017). This raised the question of whether FLS2, BAK1 and BIR proteins are localized together in preformed complexes or if there are pools of receptors and co-receptors that are rearranged after elicitation.

4.3.1 Nanoscale dynamics of FLS2 and BAK1 are differentially affected by flg22

The nanoscale dynamics of the LRR-RLKs FLS2, BAK1 and BIR3 within the plasma membrane were investigated in flg22-dependent manner by sptPALM. Measurements of the diffusion coefficient of FLS2 revealed a restricted and immobile dynamical behavior, which did not significantly alter in response to flg22 treatment. Similar results were obtained for BIR3. Interestingly, BAK1 showed a different nanoscale dynamic compared to FLS2 and BIR3. The median diffusion coefficient obtained for mock treated BAK1 molecules was around four times higher than the diffusion coefficient determined for FLS2. Moreover, BAK1 occurred in two diverse populations with distinguishable lateral mobility behaviors, whereas a

higher percentage of BAK1 molecules showed a faster diffusion. The highest diffusion coefficient measured in a cell was a coefficient of D= 0.03 $\mu m^2/s$, which is comparable with the values obtained for the mobile protein ROP6 in this study (Platre et al., 2019). Although no threshold was set to discriminate between mobile and immobile, the faster population of BAK1 can be phrased as mobile BAK1 regarding to the mobility of ROP6. Treatment with flg22 affected the lateral mobility of BAK1 in a way that the slower population increased while the faster population decreased.

This indicated that signaling activation and likely the complex formation with FLS2 slows down the diffusion of the co-receptor BAK1. Moreover, it is likely that the mobile BAK1 molecules are not in a complex with BIR3 since the vast majority of BIR3 molecules appeared to be immobile. However, it is elusive whether the interaction of BAK1 with BIR3 is permanent or whether the co-receptor undergoes a dynamical exchange. Thereby, BAK1 might switch from an immobile state, interacting with BIR3, into a mobile state, without interaction. Since the immobile population of BAK1 was increased after flg22 treatment, it might be that mobile BAK1 molecules are forming a complex with FLS2 and reducing its diffusion. Thus, it can be hypothesized that BAK1 is not permanently present in a preformed complex with FLS2, and the co-receptor dynamically rearranges in a ligand-dependent manner.

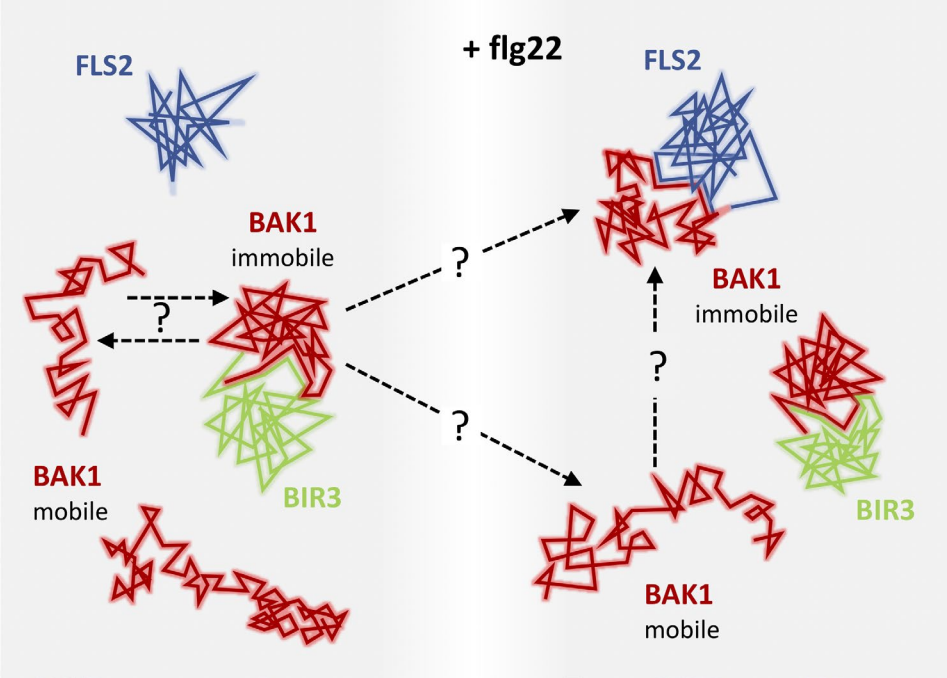

Figure 4-3: **Model of the nanoscale dynamics of FLS2, BAK1 and BIR3.** The receptors' dynamics are graphically illustrated by trajectories. If no ligand is present, a higher percentage of BAK1 molecules are mobile; FLS2 and BIR3 possess an immobile diffusion. The interaction with BAK1 might not be permanent, and thereby BAK1 might switch between an immobile and mobile diffusion. After flg22 treatment, the immobile fraction of BAK1 increases, possibly due to an interaction of the mobile BAK1 molecules with the immobile FLS2.

In future, simultaneous analyses of the spatiotemporal dynamics of BAK1 with BIR3, and BAK1 with FLS2 by dual color sptPALM will help elucidating timed association and interaction of the respective receptors during signaling activation. Furthermore, it will contribute to examining the spatiotemporal composition of nanodomains and will shed light on the question of preformed immune receptor complexes.

BAK1 is not only constitutively interacting with the BIR proteins, it also forms ligand-independently a complex with receptor kinases of developmental pathways such as BRI1 or PSKR1 (Bücherl et al., 2013; Halter et al., 2014; Ladwig et al., 2015; Hutten et al., 2017; Imkampe et al., 2017; Großeholz et al., 2020). Accordingly, it can be assumed that these interactions contribute to forming the immobile fraction of BAK1. Preliminary results from Klaus Harter's group described the nanoscale dynamic of ligand-binding receptors involved in developmental pathways. External stimulation with physiological concentrations of BL did not cause differences in the diffusion coefficient of the receptor BRI1, which was comparable with values obtained for FLS2 (Rausch, 2021, unpublished). Furthermore, PSK treatment did not affect the lateral diffusion of transiently expressed PSKR1 as well as it did not influence RLP44 mobility (Keck, 2021,

unpublished; Rohr, unpublished). As both, BRI1 and PSKR1 interact ligand-independently with BAK1, it would be of interest to analyze whether the mobility of BAK1 is influenced by BL and PSK as it was shown for flg22 (Nam & Li, 2002; Ladwig et al., 2015).

4.3.2 Divergent information on the nanoscale dynamics of FLS2 was reported in the literature

The lateral mobility of FLS2 and BAK1 has been investigated in various previous studies using different techniques. Results of McKenna et al. (2019) and Gronnier et al. (2022), who analyzed the diffusion behavior of FLS2, are in line with those of this work. McKenna et al. (2019) used single particle tracking of GFP tagged FLS2 in transgenic *Arabidopsis* hypocotyl cells, which displayed a diffusion coefficient of D= 0.005 $\mu m^2/s$ (McKenna et al., 2019). This is identical to the values obtained in this thesis. Gronnier et al. (2022) studied FLS2-GFP organization in transgenic *Arabidopsis* by kymograph analysis, in which the fluorescence signal along a given line is plotted for images of a time series and projects an *x-t* scan. Alike, they could show that the receptor localizes in well-defined static structures with a confined mobility behavior (Gronnier et al., 2022). The observation that the dynamics of FLS2 are unaffected in response to flg22 contradicts with previous studies, in which a decreased lateral mobility of FLS2 after ligand treatment was reported (Ali et al., 2007; Bücherl et al., 2017). At this point, it has to be mentioned that the data of Ali et al. (2007) were obtained by FRAP measurements of FLS2-YFP in protoplasts, which do not possess an intact cell wall (Ali et al., 2007). The diffusion rate of untreated FLS2 was described to be D= 0.34 $\mu m^2/s$, which correlates with a mobile and highly diffusive behavior as it was described by Hosy et al. (2015) for LTi6a and it is around two orders of magnitude higher than values obtained in this study. Therefore, the cell wall seems to be crucial for the nanoscale dynamics of plasma membrane localized proteins. Indeed, it has been reported that the presence of the cell wall has a major impact on the lateral mobility of proteins, and it is restricting their movements within the plasma membrane (Martinière et al., 2012; McKenna et al., 2019). Furthermore, a recently published work showed that the cell wall sensor FERONIA (FER) has an influence on the nanoscale organization of FLS2 and BAK1 (Gronnier et al., 2022). FLS2 was more mobile in *fer* mutant plants, whereas the opposite was observed for BAK1. The authors described BAK1-mCherry to form distinct clusters and to be more mobile than FLS2-GFP, which confirms the results of this thesis (Gronnier et al., 2022). Thus, the data of this work are largely in accordance with previously published results.

4.3.3 Ligand perception modulates the nanodomain formation of immunity-related LRR-RLKs

The segregation of proteins in nanodomains at the plasma membrane is critical for signaling pathways that regulate key physiological processes (Gronnier et al., 2018; Jaillais & Ott, 2019; Yu et al., 2020; Martinière & Zelazny, 2021). Many studies using biochemical approaches and fluorescence microscopy have shown that proteins are not homogeneously distributed in the plasma membrane (Brown & Rose, 1992; Mongrand et al., 2004; Borner et al., 2005; Morel et al., 2006; Kleine-Vehn et al., 2011; Jarsch et al., 2014; Bücherl et al., 2017; Hutten et al., 2017; Platre et al., 2019; Gronnier et al., 2022). The LRR-RLKs FLS2 and BRI1 are shown to be heterogeneously distributed in the plasma membrane and to localize in distinct nanodomains (Wang et al., 2015b; Bücherl et al., 2017; Hutten et al., 2017). While both PRRs share signaling components such as the co-receptor BAK1, BIR3 and the RLCK BIK1, it was hypothesized that the spatial separation of immune and developmental receptors in nanodomains provides signal specificity (Chinchilla et al., 2007; Lu et al., 2010; Lin et al., 2013; Bücherl et al., 2017) (Li et al., 2002; Imkampe et al., 2017; Großeholz et al., 2020).

In the scope of this thesis, the nanodomain formation of the receptor kinases FLS2, BAK1 and BIR3 and their modulation in a flg22-dependent matter were investigated by super resolution microscopy sptPALM and Voronoi tessellation. FLS2 and BAK1 showed a heterogeneous distribution, as it has been reported in previous studies (Bücherl et al., 2017; Hutten et al., 2017; McKenna et al., 2019). Also, BIR3 formed distinct clusters within the plasma membrane. In response to flg22 elicitation, a significant reduction in the cluster sizes of FLS2 and BIR3 was observed, whereas BAK1 clusters were significantly larger after flg22 treatment. The mock treated BAK1 clusters, with a mean diameter of around 320 nm, were 1.5 times larger than FLS2 clusters and smaller than reported by Hutten et al. (2017) of around 400 nm. Also, the mean cluster diameter of FLS2 with 219 nm was much smaller than the one reported by Bücherl et al. (2017), who described FLS2-GFP cluster with a diameter of around 387 nm in *N. benthamiana* and slightly smaller with around 356 nm for *A. thaliana* (Bücherl et al., 2017). The authors discussed that their measured sizes are most likely overestimated, because with the applied CLSM and VAEM it was not possible to resolve receptor clusters below the diffraction limit. Indeed, with the application of PALM and the imaging of the single proteins, smaller cluster sizes were computed than obtained by conventional fluorescence microscopy.

As discussed before in Chapter 4.2.4, the calculated cluster sized by Voronoi tessellation-based segmentation might not represent absolute values, but it is suitable to analyze variations in the cluster formations of a protein in response to ligand perception. While FLS2 and BIR3 nanodomains decreased in size after flg22 treatment, BAK1 nanodomains increased in their size. It is not clear whether the observed modulations within one nanodomain are due to (i) an alteration in the density of the receptors, (ii) a changing receptor number, or (iii) a mixture of both options. As numerous studies describe FLS2 to undergo endocytosis upon flg22 perception, it can be concluded that the number of FLS2 molecules decreases, and thereby supporting the second option (Robatzek et al., 2006; Mbengue et al., 2016; Cui et al., 2018). Accordingly, this would lead to the hypothesis of an accumulation of BAK1 molecules within certain nanodomains in response to flg22 perception. In the future, studying the stoichiometric composition of proteins within a nanodomain will contribute to a better understanding of the formation and dynamical modulations of receptor organization.

4.3.4 Hypothesis for the spatiotemporal organization of receptor kinases at the plasma membrane

Receptors kinases are heterogeneously distributed within the plasma membrane and possess a low lateral diffusion, which is unaffected by ligand perception. The exception is the co-receptor BAK1, which in addition to immobile molecules, also contains a fraction, which is mobile. After flg22 treatment, more BAK1 molecules showed an immobile diffusion behavior. Therefore, it is proposed that BAK1, which is interacting with other receptors such as the BIR3 or BRI1, exhibits a slow diffusion, while the faster molecules are currently not bound in a complex and available for recruitment, e.g., in a complex with FLS2.

Although the lateral mobility of most of the receptors is unaltered in response to ligand elicitation, it initiates modulations of their nanocluster environment. It is hypothesized that nanodomains decrease in size after ligand perception due to a decrease in the number of receptors, e.g., due to internalization. An increase in the size of nanodomains is possibly generated by an accumulation of the respective protein. Accordingly, flg22 perception probably reduces the number of FLS2 within one nanodomain, while it might initiate an accumulation of BAK1.

4.4 Conclusion

The two main objectives of this work were (i) the analysis of the spatiotemporal organization of immunity-related proteins in the plasma membrane by the super resolution microscopy technique sptPALM and (ii) studying the role of HIR2 as a putative scaffold protein in the nanodomain formation of those.

Since the limited resolution of conventional optical microscopy does not allow a detailed observation of protein assemblies within the plasma membrane, the development of the super resolution microscopy technique sptPALM was a breakthrough for analyzing the nanoscale dynamics and single proteins *in vivo* (Abbe, 1873; Betzig et al., 2006; Gronnier et al., 2018). With the application of the truly monomeric fluorescent protein mEos3.2, it was not only possible to image single receptors in the plasma membrane, but also to compute their dynamic properties and analyze their cluster formation *in vivo* (Zhang et al., 2016). In this way, this study has shown that the receptor kinases FLS2 and BIR3 possess a low lateral mobility within the plasma membrane and their diffusion behavior is not affected by ligand treatment. However, unlike most other receptors, the co-receptor BAK1 occurs in two distinguishable mobilities, whereas one fraction can be described as mobile and the other as immobile. In response to flg22 elicitation, the majority of BAK1 molecules became immobile. It can be hypothesized that BAK1 dynamically associates with different nanodomains and it is not permanently present in a preformed complex with FLS2. The differences in nanoscale dynamics of the PRR and the co-receptor might describe a regulatory mechanism to determine signaling specificity. Thus, this study expanded our knowledge about the spatiotemporal organization of receptor kinases involved in immunity signaling.

So far, it is not clear how the formation of nanodomains is determined and maintained. This research provided additional evidence that HIR2 forms a putative scaffold to stabilize interacting receptor kinases in functional nanodomains. The lack of a full *HIR2* knock-out mutant limited studying the involvement of HIR2 in the spatiotemporal organization of immune receptors, which will be required for future research.

The establishment of dual color sptPALM made it possible for the first time to visualize the nanoscale organization of two distinct proteins simultaneously and in real-time in a living plant cell. This cutting-edge technique holds great potential to significantly enhance the understanding of the plasma membrane architecture, as well as it will provide new insights into the spatiotemporal relation and modulation of two different proteins during signaling activation.

5 SUMMARY

The recognition of external and internal stimuli is mediated by plasma membrane-localized receptors, which are organized into nanodomains. So far, the formation and the maintenance of such preformed complexes is largely unknown, though it turns out that the spatiotemporal organization and the nanoscale dynamics of membrane proteins is a fundamental aspect of the function of signaling processes (Gronnier et al., 2018; Jaillais & Ott, 2019; Gronnier et al., 2022). The development of the super-resolution microscopy technique sptPALM enabled the visualization of single molecules in living cells and allowed obtaining quantitative analyses of the dynamics of single proteins within the plasma membrane. HIR2, which belongs to the protein family of SPFH-domain containing proteins, has been identified in interactome analysis of the small LRR-RLKs BIR2 and BIR3 and is hypothesized to be involved in the regulation of complex assembly of immune receptor kinases at the plasma membrane (Browman et al., 2007; Qi & Katagiri, 2012; Halter et al., 2014; Schulze, 2020). This thesis was divided into two parts, at which the first focused on the functional characterization of HIR2 as a putative scaffold protein and the second on the analysis of the nanoscale dynamics and nanocluster formation of receptor kinases at the plasma membrane by sptPALM.

The direct interaction of HIR2 with BIR2 and BIR3 was confirmed by multiple independent interaction experiments. Also, it was demonstrated that HIR2 directly interacts with the co-receptor BAK1, as well as with the PRRs FLS2 and CERK1. Besides the interactions, it remains to be elucitated how HIR2 is involved in PTI signaling. Additionally, HIR2 is suggested to be involved in developmental signaling pathways since it is associated with BRI1, and the *hir2-5* mutant exhibits a dwarf growth phenotype similar to weak *bri1* alleles. To study the nanoscale dynamics and cluster formation of plasma membrane localized proteins, single and dual color sptPALM were successfully established for their application *in planta* and the nanodomain formation was computed by Voronoi tessellation-based segmentation. The analysis revealed a heterogeneous distribution and cluster formation of all studied proteins within the plasma membrane. The receptor kinases FLS2 and BIR3 possessed low lateral mobility within the plasma membrane, which was unaffected by flg22 treatment. In contrast, BAK1 occurred in two different populations with distinguishable lateral mobility behaviors and flg22 treatment resulted in a slowdown of BAK1. Thus, it is hypothesized that BAK1 dynamically associates with different nanodomains and it is not permanently present in a preformed complex with FLS2. Moreover, the highly confined lateral mobility of HIR2 provided further evidence that it might act as a scaffold.

With this work, new insights were given (i) into the impact of HIR2 as a putative organizing factor for the assembly of spatially and temporally stable multiprotein complexes at the plasma membrane and (ii) into the spatiotemporal organization of immune receptor kinases and their modulation by ligand perception.

6 ZUSAMMENFASSUNG

Die Erkennung externen und internen Stimuli wird durch Rezeptoren vermittelt, welche in der Plasmamembran in Nanodomänen organsiert sind. Bisher ist weitgehend unbekannt, wie solche vorgeformte Komplexe gebildet und instandgehalten werden. Es zeigt sich jedoch, dass die räumlich-zeitliche Organisation und die Dynamik von Membranproteinen ein fundamentaler Aspekt für die Funktion von Signalprozessen ist (Gronnier et al., 2018; Jaillais & Ott, 2019; Gronnier et al., 2022). Durch die Entwicklung der Superresolution-Mikroskopie Technik sptPALM konnte die Visualisierung einzelner Moleküle in lebenden Zellen ermöglicht werden und erlaubt eine quantitative Analyse der Dynamik einzelner Proteine innerhalb der Plasmamembran. HIR2, welches zur Proteinfamilie der „SPFH-domain containing protein“ zählt, wurde in der Interaktomanalyse der kleinen LRR-RLKs BIR2 und BIR3 identifiziert und es wurde vermutet, dass HIR2 an der Regulation der Komplexbildung von Immunrezeptoren an der Plasmamembran beteiligt ist (Browman et al., 2007; Qi & Katagiri, 2012; Halter et al., 2014; Schulze, 2020). Diese Thesis wurde in zwei Teile gegliedert, wobei sich der Erste auf die funktionelle Charakterisierung von HIR2 als mutmaßliches Gerüstprotein konzentrierte und der Zweite auf die Analyse der Dynamik und Nanoclusterbildung von Rezeptorkinasen an der Plasmamembran durch sptPALM.

Die direkte Interaktion von HIR2 mit BIR2 und BIR3 wurde durch verschiedene, unabhängige Interaktionsexperimente bestätigt. Zusätzlich wurde gezeigt, dass HIR2 direkt mit dem Co-Rezeptor BAK1 sowie mit den PRRs FLS2 und CERK1 interagiert. Es ist jedoch nicht klar, inwiefern HIR2 in dem PTI-Signalweg involviert ist. Außerdem ist HIR2 möglicherweise auch in Entwicklungsprozessen beteiligt, was aufgrund der Assoziierung mit BRI1 und des Zwergenwachstums der *hir2-5* Mutante, welche phänotypisch schwachen *bri1* Allelen ähnelt, vermutet werden kann. Um die Dynamik und die Clusterbildung von einzelnen Proteinen an der Plasmamembran zu untersuchen, wurde ein- und zweifarbige sptPALM erfolgreich für die Anwendung in Pflanzen etabliert und die Bildung von Nanodomänen durch Voronoi-Tessellation untersucht. Dadurch konnte eine heterogene Verteilung und Clusterbildung aller untersuchten Proteine an der Plasmamembran gezeigt werden. Die Rezeptorkinasen FLS2 und BIR3 weisen dabei eine geringe laterale Mobilität innerhalb der Plasmamembran auf, welche durch die Behandlung mit flg22 nicht beeinträchtigt wurde. Im Gegensatz dazu trat BAK1 mit unterscheidbaren Diffusionsgeschwindigkeiten auf, und die Behandlung mit flg22 führte zu einer Verlangsamung von BAK1. Daraus ergibt sich die Hypothese, dass BAK1 dynamisch mit verschiedenen Nanodomänen assoziiert ist und nicht permanent in einem vorgeformten Komplex mit FLS2 vorliegt. Darüber hinaus lieferte die stark eingeschränkte laterale Mobilität von HIR2 weitere Hinweise, dass es als Gerüstprotein fungieren könnte.

Mit dieser Arbeit wurden neue Einblicke (i) in den Einfluss von HIR2 als mutmaßlich organisierender Faktor für den Aufbau räumlich und zeitlich stabiler Multiproteinkomplexe an der Plasmamembran und (ii) in die räumlich-zeitliche Organisation von Immun-Rezeptorkinasen und deren Veränderung nach Liganden-Wahrnehmung gewonnen.

7 REFERENCES

Abbe, E. (1873). Beiträge zur Theorie des Mikroskops und der mikroskopischen Wahrnehmung. *Archiv für Mikroskopische Anatomie*, *9*(1), 413-468. https://doi.org/10.1007/BF02956173

Albert, I., Hua, C., Nürnberger, T., Pruitt, R. N., & Zhang, L. (2019). Surface Sensor Systems in Plant Immunity. *Plant Physiology*, *182*(4), 1582-1596. https://doi.org/10.1104/pp.19.01299

Ali, G. S., Prasad, K. V. S. K., Day, I., & Reddy, A. S. N. (2007). Ligand-Dependent Reduction in the Membrane Mobility of FLAGELLIN SENSITIVE2, an Arabidopsis Receptor-Like Kinase. *Plant and Cell Physiology*, *48*(11), 1601-1611. https://doi.org/10.1093/pcp/pcm132

Altan-Bonnet, N., & Altan-Bonnet, G. (2009). Fluorescence correlation spectroscopy in living cells: a practical approach. *Current protocols in cell biology*, *45*(1), 4.24.21-24.24.14. https://doi.org/10.1002/0471143030.cb0424s45

Ambrose, E. J. (1956). A Surface Contact Microscope for the study of Cell Movements. *Nature*, *178*(4543), 1194-1194. https://doi.org/10.1038/1781194a0

Axelrod, D., Burghardt, T., & Thompson N. (1984). Total Internal Reflection Fluorescence. *Annual Review of Biophysics and Bioengineering*, *13*(1), 247-268. https://doi.org/10.1146/annurev.bb.13.060184.001335

Axtell, M. J., & Staskawicz, B. J. (2003). Initiation of RPS2-specified disease resistance in Arabidopsis is coupled to the AvrRpt2-directed elimination of RIN4. *Cell*, *112*(3), 369-377. https://doi.org/10.1016/s0092-8674(03)00036-9

Bariola, P., Retelska, D., Stasiak, A., Kammerer, R., Fleming, A., Hijri, M., Frank, S., & Farmer, E. (2004). Remorins form a novel family of coiled coil-forming oligomeric and filamentous proteins associated with apical, vascular and embryonic tissues in plants. *Plant Molecular Biology*, *55*(4), 579-594. https://doi.org/10.1007/s11103-004-1520-4

Bartel, D. P. (2004). MicroRNAs: Genomics, Biogenesis, Mechanism, and Function. *Cell*, *116*(2), 281-297. https://doi.org/10.1016/S0092-8674(04)00045-5

Bates, M., Blosser, T. R., & Zhuang, X. (2005). Short-Range Spectroscopic Ruler Based on a Single-Molecule Optical Switch. *Physical Review Letters*, *94*(10), 108101. https://doi.org/10.1103/PhysRevLett.94.108101

Batistič, O. (2012). Genomics and Localization of the Arabidopsis DHHC-Cysteine-Rich Domain S-Acyltransferase Protein Family *Plant Physiology*, *160*(3), 1597-1612. https://doi.org/10.1104/pp.112.203968

Bayle, V., Fiche, J.-B., Burny, C., Platre, M. P., Nollmann, M., Martinière, A., & Jaillais, Y. (2021). Single-particle tracking photoactivated localization microscopy of membrane proteins in living plant tissues. *Nature Protocols*, *16*(3), 1600-1628. https://doi.org/10.1038/s41596-020-00471-4

Belkhadir, Y., & Chory, J. (2006). Brassinosteroid Signaling: A Paradigm for Steroid Hormone Signaling from the Cell Surface. *Science*, *314*(5804), 1410-1411. https://doi.org/10.1126/science.1134040

Belkhadir, Y., Jaillais, Y., Epple, P., Balsemão-Pires, E., Dangl, J. L., & Chory, J. (2012). Brassinosteroids modulate the efficiency of plant immune responses to microbe-associated molecular patterns. *Proceedings of the National Academy of Sciences*, *109*(1), 297-302. https://doi.org/10.1073/pnas.1112840108

Belkhadir, Y., Yang, L., Hetzel, J., Dangl, J. L., & Chory, J. (2014). The growth-defense pivot: crisis management in plants mediated by LRR-RK surface receptors. *Trends in Biochemical Sciences*, *39*(10), 447-456. https://doi.org/10.1016/j.tibs.2014.06.006

Bent, A. F., Kunkel, B. N., Dahlbeck, D., Brown, K. L., Schmidt, R., Giraudat, J., Leung, J., & Staskawicz, B. J. (1994). RPS2 of Arabidopsis thaliana: a leucine-rich repeat class of plant disease resistance genes. *Science*, *265*(5180), 1856-1860. https://doi.org/10.1126/science.8091210

Betzig, E., Patterson, G. H., Sougrat, R., Lindwasser, O. W., Olenych, S., Bonifacino, J. S., Davidson, M. W., Lippincott-Schwartz, J., & Hess, H. F. (2006). Imaging Intracellular Fluorescent Proteins at Nanometer Resolution. *Science*, *313*(5793), 1642-1645. https://doi.org/10.1126/science.1127344

Bigeard, J., Colcombet, J., & Hirt, H. (2015). Signaling Mechanisms in Pattern-Triggered Immunity (PTI). *Molecular Plant*, *8*(4), 521-539. https://doi.org/10.1016/j.molp.2014.12.022

Binder, A., Lambert, J., Morbitzer, R., Popp, C., Ott, T., Lahaye, T., & Parniske, M. (2014). A Modular Plasmid Assembly Kit for Multigene Expression, Gene Silencing and Silencing Rescue in Plants. *PLOS ONE*, *9*(2), e88218. https://doi.org/10.1371/journal.pone.0088218

Blaum, B. S., Mazzotta, S., Nöldeke, E. R., Halter, T., Madlung, J., Kemmerling, B., & Stehle, T. (2014). Structure of the pseudokinase domain of BIR2, a regulator of BAK1-mediated immune signaling in Arabidopsis. *Journal of Structural Biology*, *186*(1), 112-121. https://doi.org/10.1016/j.jsb.2014.02.005

Böhm, H., Albert, I., Fan, L., Reinhard, A., & Nürnberger, T. (2014). Immune receptor complexes at the plant cell surface. *Current Opinion in Plant Biology*, *20*, 47-54. https://doi.org/10.1016/j.pbi.2014.04.007

Boller, T., & Felix, G. (2009). A Renaissance of Elicitors: Perception of Microbe-Associated Molecular Patterns and Danger Signals by Pattern-Recognition Receptors. *Annual Review of Plant Biology*, *60*(1), 379-406. https://doi.org/10.1146/annurev.arplant.57.032905.105346

Bologna, G., Yvon, C., Duvaud, S., & Veuthey, A. L. (2004). N-Terminal myristoylation predictions by ensembles of neural networks. *Proteomics*, *4*(6), 1626-1632. https://doi.org/10.1002/pmic.200300783

Borner, G. H. H., Sherrier, D. J., Weimar, T., Michaelson, L. V., Hawkins, N. D., MacAskill, A., Napier, J. A., Beale, M. H., Lilley, K. S., & Dupree, P. (2005). Analysis of Detergent-Resistant Membranes in Arabidopsis. Evidence for Plasma Membrane Lipid Rafts. *Plant Physiology*, *137*(1), 104-116. https://doi.org/10.1104/pp.104.053041

Brandt, B., & Hothorn, M. (2016). SERK co-receptor kinases. *Current Biology*, *26*(6), R225-226. https://doi.org/10.1016/j.cub.2015.12.014

Browman, D. T., Hoegg, M. B., & Robbins, S. M. (2007). The SPFH domain-containing proteins: more than lipid raft markers. *Trends in Cell Biology*, *17*(8), 394-402. https://doi.org/10.1016/j.tcb.2007.06.005

Brown, D. A., & Rose, J. K. (1992). Sorting of GPI-anchored proteins to glycolipid-enriched membrane subdomains during transport to the apical cell surface. *Cell*, *68*(3), 533-544. https://doi.org/10.1016/0092-8674(92)90189-J

Bücherl, C. A., Jarsch, I. K., Schudoma, C., Segonzac, C., Mbengue, M., Robatzek, S., MacLean, D., Ott, T., & Zipfel, C. (2017). Plant immune and growth receptors share common signalling components but localise to distinct plasma membrane nanodomains. *eLife*, *6*, e25114. https://doi.org/10.7554/eLife.25114

Bücherl, C. A., van Esse, G. W., Kruis, A., Luchtenberg, J., Westphal, A. H., Aker, J., van Hoek, A., Albrecht, C., Borst, J. W., & de Vries, S. C. (2013). Visualization of BRI1 and BAK1(SERK3) Membrane Receptor Heterooligomers during Brassinosteroid Signaling *Plant Physiology*, *162*(4), 1911-1925. https://doi.org/10.1104/pp.113.220152

Burr, C. A., Leslie, M. E., Orlowski, S. K., Chen, I., Wright, C. E., Daniels, M. J., & Liljegren, S. J. (2011). CAST AWAY, a Membrane-Associated Receptor-Like Kinase, Inhibits Organ Abscission in Arabidopsis *Plant Physiology*, *156*(4), 1837-1850. https://doi.org/10.1104/pp.111.175224

Cao, Y., He, Q., Qi, Z., Zhang, Y., Lu, L., Xue, J., Li, J., & Li, R. (2020). Dynamics and Endocytosis of Flot1 in Arabidopsis Require CPI1 Function. *International Journal of Molecular Sciences*, *21*(5). https://doi.org/10.3390/ijms21051552

Cao, Y., Liang, Y., Tanaka, K., Nguyen, C. T., Jedrzejczak, R. P., Joachimiak, A., & Stacey, G. (2014). The kinase LYK5 is a major chitin receptor in Arabidopsis and forms a chitin-induced complex with related kinase CERK1. *eLife*, *3*, e03766. https://doi.org/10.7554/eLife.03766

Chinchilla, D., Shan, L., He, P., de Vries, S., & Kemmerling, B. (2009). One for all: the receptor-associated kinase BAK1. *Trends in Plant Science*, *14*(10), 535-541. https://doi.org/10.1016/j.tplants.2009.08.002

Chinchilla, D., Zipfel, C., Robatzek, S., Kemmerling, B., Nürnberger, T., Jones, J. D. G., Felix, G., & Boller, T. (2007). A flagellin-induced complex of the receptor FLS2 and BAK1 initiates plant defence. *Nature*, *448*(7152), 497-500. https://doi.org/10.1038/nature05999

Choe, S., Dilkes, B. P., Fujioka, S., Takatsuto, S., Sakurai, A., & Feldmann, K. A. (1998). The DWF4 Gene of Arabidopsis Encodes a Cytochrome P450 That Mediates Multiple 22α-Hydroxylation Steps in Brassinosteroid Biosynthesis. *The Plant cell*, *10*(2), 231-243. https://doi.org/10.1105/tpc.10.2.231

Choi, H. W., Kim, Y. J., & Hwang, B. K. (2011). The hypersensitive induced reaction and leucine-rich repeat proteins regulate plant cell death associated with disease and plant immunity. *Molecular Plant-Microbe Interactions*, *24*(1), 68-78. https://doi.org/10.1094/mpmi-02-10-0030

Couto, D., & Zipfel, C. (2016). Regulation of pattern recognition receptor signalling in plants. *Nature Reviews Immunology*, *16*(9), 537-552. https://doi.org/10.1038/nri.2016.77

Cui, Y., Li, X., Yu, M., Li, R., Fan, L., Zhu, Y., & Lin, J. (2018). Sterols regulate endocytic pathways during flg22-induced defense responses in Arabidopsis. *Development*, *145*(19). https://doi.org/10.1242/dev.165688

Daněk, M., Valentová, O., & Martinec, J. (2016). Flotillins, Erlins, and HIRs: From Animal Base Camp to Plant New Horizons. *Critical Reviews in Plant Sciences*, *35*(4), 191-214. https://doi.org/10.1080/07352689.2016.1249690

De Sousa Abreu, R., Penalva, L. O., Marcotte, E. M., & Vogel, C. (2009). Global signatures of protein and mRNA expression levels. *Molecular BioSystems*, *5*(12), 1512-1526. https://doi.org/10.1039/b908315d

De Zitter, E., Thédié, D., Mönkemöller, V., Hugelier, S., Beaudouin, J., Adam, V., Byrdin, M., Van Meervelt, L., Dedecker, P., & Bourgeois, D. (2019). Mechanistic investigation of mEos4b reveals a strategy to reduce track interruptions in sptPALM. *Nature Methods*, *16*(8), 707-710. https://doi.org/10.1038/s41592-019-0462-3

DeFalco, T. A., & Zipfel, C. (2021). Molecular mechanisms of early plant pattern-triggered immune signaling. *Molecular Cell*, *81*(17), 3449-3467. https://doi.org/10.1016/j.molcel.2021.07.029

Deli, A., Tympa, L.-E., & Moschou, P. N. (2022). Analyses of Protein Turnover at the Cell Plate by Fluorescence Recovery After Photobleaching During Cytokinesis. In M.-C. Caillaud (Ed.), *Plant Cell Division: Methods and Protocols* (pp. 233-243). Springer US. https://doi.org/10.1007/978-1-0716-1744-1_14

Di Rubbo, S., Irani, N. G., Kim, S. Y., Xu, Z. Y., Gadeyne, A., Dejonghe, W., Vanhoutte, I., Persiau, G., Eeckhout, D., Simon, S., Song, K., Kleine-Vehn, J., Friml, J., De Jaeger, G., Van Damme, D., Hwang, I., & Russinova, E. (2013). The clathrin adaptor complex AP-2 mediates endocytosis of brassinosteroid insensitive1 in Arabidopsis. *The Plant cell*, *25*(8), 2986-2997. https://doi.org/10.1105/tpc.113.114058

Domínguez-Ferreras, A., Kiss-Papp, M., Jehle, A. K., Felix, G., & Chinchilla, D. (2015). An Overdose of the Arabidopsis Coreceptor BRASSINOSTEROID INSENSITIVE1-ASSOCIATED RECEPTOR KINASE1 or Its Ectodomain Causes Autoimmunity in a SUPPRESSOR OF BIR1-1-Dependent Manner. *Plant Physiology*, *168*(3), 1106-1121. https://doi.org/10.1104/pp.15.00537

Donaldson, L. (2020). Autofluorescence in Plants. *Molecules*, *25*(10), 2393. https://doi.org/10.3390/molecules25102393

Durisic, N., Laparra-Cuervo, L., Sandoval-Álvarez, A., Borbely, J. S., & Lakadamyali, M. (2014). Single-molecule evaluation of fluorescent protein photoactivation efficiency using an in vivo nanotemplate. *Nature Methods*, *11*(2), 156-162. https://doi.org/10.1038/nmeth.2784

Edwards, K., Johnstone, C., & Thompson, C. (1991). A simple and rapid method for the preparation of plant genomic DNA for PCR analysis. *Nucleic Acids Research*, *19*(6), 1349. https://doi.org/10.1093/nar/19.6.1349

Escocard de Azevedo Manhães, A. M., Ortiz-Morea, F. A., He, P., & Shan, L. (2021). Plant plasma membrane-resident receptors: Surveillance for infections and coordination for growth and development. *Journal of Integrative Plant Biology*, *63*(1), 79-101. https://doi.org/10.1111/jipb.13051

Felix, G., Duran, J. D., Volko, S., & Boller, T. (1999). Plants have a sensitive perception system for the most conserved domain of bacterial flagellin. *The Plant Journal*, *18*(3), 265-276. https://doi.org/10.1046/j.1365-313x.1999.00265.x

Franck, C. M., Westermann, J., & Boisson-Dernier, A. (2018). Plant Malectin-Like Receptor Kinases: From Cell Wall Integrity to Immunity and Beyond. *Annual Review of Plant Biology*, *69*(1), 301-328. https://doi.org/10.1146/annurev-arplant-042817-040557

Gao, M., Wang, X., Wang, D., Xu, F., Ding, X., Zhang, Z., Bi, D., Cheng, Y. T., Chen, S., Li, X., & Zhang, Y. (2009). Regulation of Cell Death and Innate Immunity by Two Receptor-like Kinases in Arabidopsis. *Cell Host & Microbe*, *6*(1), 34-44. https://doi.org/10.1016/j.chom.2009.05.019

Gao, X., Ruan, X., Sun, Y., Wang, X., & Feng, B. (2019). BAKing up to Survive a Battle: Functional Dynamics of BAK1 in Plant Programmed Cell Death. *Frontiers in plant science*, *9*, 1913-1913. https://doi.org/10.3389/fpls.2018.01913

Garbett, D., & Bretscher, A. (2014). The surprising dynamics of scaffolding proteins. *Molecular biology of the cell*, *25*(16), 2315-2319. https://doi.org/10.1091/mbc.E14-04-0878

Garnelo Gómez, B., Holzwart, E., Shi, C., Lozano-Durán, R., & Wolf, S. (2021). Phosphorylation-dependent routing of RLP44 towards brassinosteroid or phytosulfokine signalling. *Journal of cell science*, *134*(20). https://doi.org/10.1242/jcs.259134

Gehl, B., & Sweetlove, L. J. (2014). Mitochondrial Band-7 family proteins: scaffolds for respiratory chain assembly? *Frontiers in plant science*, *5*, 141-141. https://doi.org/10.3389/fpls.2014.00141

Glöckner, N., Oven-Krockhaus, S. z., Rohr, L., Wackenhut, F., Burmeister, M., Wanke, F., Holzwart, E., Meixner, A. J., Wolf, S., & Harter, K. (2020). Three-fluorophore FRET enables the analysis of ternary protein association in living plant cells. *bioRxiv*, 722124. https://doi.org/10.1101/722124

Gómez-Gómez, L., & Boller, T. (2000). FLS2: An LRR Receptor–like Kinase Involved in the Perception of the Bacterial Elicitor Flagellin in Arabidopsis. *Molecular Cell*, *5*(6), 1003-1011. https://doi.org/10.1016/S1097-2765(00)80265-8

Gong, B.-Q., Guo, J., Zhang, N., Yao, X., Wang, H.-B., & Li, J.-F. (2019). Cross-Microbial Protection via Priming a Conserved Immune Co-Receptor through Juxtamembrane Phosphorylation in Plants. *Cell Host & Microbe*, *26*(6), 810-822.e817. https://doi.org/10.1016/j.chom.2019.10.010

Gou, X., Yin, H., He, K., Du, J., Yi, J., Xu, S., Lin, H., Clouse, S. D., & Li, J. (2012). Genetic Evidence for an Indispensable Role of Somatic Embryogenesis Receptor Kinases in Brassinosteroid Signaling. *PLOS Genetics*, *8*(1), e1002452. https://doi.org/10.1371/journal.pgen.1002452

Gouguet, P., Gronnier, J., Legrand, A., Perraki, A., Jolivet, M.-D., Deroubaix, A.-F., German-Retana, S., Boudsocq, M., Habenstein, B., Mongrand, S., & Germain, V. (2020). Connecting the dots: from

nanodomains to physiological functions of REMORINs. *Plant Physiology*, *185*(3), 632-649. https://doi.org/10.1093/plphys/kiaa063

Grefen, C. (2007). Split-Ubiquitin System for Identifying Protein-Protein Interactions in Membrane and Full-Length Proteins. *Current Protocols in Neuroscience*, *41*(1), 5.27.21-25.27.41. https://doi.org/10.1002/0471142301.ns0527s41

Grefen, C., Donald, N., Hashimoto, K., Kudla, J., Schumacher, K., & Blatt, M. R. (2010). A ubiquitin-10 promoter-based vector set for fluorescent protein tagging facilitates temporal stability and native protein distribution in transient and stable expression studies. *The Plant Journal*, *64*(2), 355-365. https://doi.org/10.1111/j.1365-313X.2010.04322.x

Grefen, C., Obrdlik, P., & Harter, K. (2009). The Determination of Protein-protein Interactions by the Mating-based Split-ubiquitin system (mbSUS). In T. Pfannschmidt (Ed.), *Plant Signal Transduction: Methods and Protocols* (pp. 217-233). Humana Press. https://doi.org/10.1007/978-1-59745-289-2_14

Gronnier, J., Crowet, J.-M., Habenstein, B., Nasir, M. N., Bayle, V., Hosy, E., Platre, M. P., Gouguet, P., Raffaele, S., Martinez, D., Grelard, A., Loquet, A., Simon-Plas, F., Gerbeau-Pissot, P., Der, C., Bayer, E. M., Jaillais, Y., Deleu, M., Germain, V., Lins, L., & Mongrand, S. (2017). Structural basis for plant plasma membrane protein dynamics and organization into functional nanodomains. *eLife*, *6*, e26404. https://doi.org/10.7554/eLife.26404

Gronnier, J., Franck, C. M., Stegmann, M., DeFalco, T. A., Abarca, A., Von Arx, M., Dünser, K., Lin, W., Yang, Z., Kleine-Vehn, J., Ringli, C., & Zipfel, C. (2022). Regulation of immune receptor kinase plasma membrane nanoscale organization by a plant peptide hormone and its receptors. *eLife*, *11*, e74162. https://doi.org/10.7554/eLife.74162

Gronnier, J., Gerbeau-Pissot, P., Germain, V., Mongrand, S., & Simon-Plas, F. (2018). Divide and Rule: Plant Plasma Membrane Organization. *Trends in Plant Science*, *23*(10), 899-917. https://doi.org/10.1016/j.tplants.2018.07.007

Großeholz, R., Feldman-Salit, A., Wanke, F., Schulze, S., Glöckner, N., Kemmerling, B., Harter, K., & Kummer, U. (2020). Specifying the role of BAK1-interacting receptor-like kinase 3 in brassinosteroid signaling. *Journal of Integrative Plant Biology*, *62*(4), 456-469. https://doi.org/10.1111/jipb.12803

Gui, J., Zheng, S., Liu, C., Shen, J., Li, J., & Li, L. (2016). OsREM4.1 Interacts with OsSERK1 to Coordinate the Interlinking between Abscisic Acid and Brassinosteroid Signaling in Rice. *Developmental Cell*, *38*(2), 201-213. https://doi.org/10.1016/j.devcel.2016.06.011

Guo, A.-Y., Zhang, Y.-M., Wang, L., Bai, D., Xu, Y.-P., & Wu, W.-Q. (2021). Single-Molecule Imaging in Living Plant Cells: A Methodological Review. *International Journal of Molecular Sciences*, *22*(10), 5071. https://doi.org/10.3390/ijms22105071

Gust, A. A., Pruitt, R., & Nürnberger, T. (2017). Sensing Danger: Key to Activating Plant Immunity. *Trends in Plant Science*, *22*(9), 779-791. https://doi.org/10.1016/j.tplants.2017.07.005

Habuchi, S., Ando, R., Dedecker, P., Verheijen, W., Mizuno, H., Miyawaki, A., & Hofkens, J. (2005). Reversible single-molecule photoswitching in the GFP-like fluorescent protein Dronpa. *Proceedings of the National Academy of Sciences*, *102*(27), 9511-9516. https://doi.org/10.1073/pnas.0500489102

Halter, T., Imkampe, J., Mazzotta, S., Wierzba, M., Postel, S., Bücherl, C., Kiefer, C., Stahl, M., Chinchilla, D., Wang, X., Nürnberger, T., Zipfel, C., Clouse, S., Borst, J. W., Boeren, S., de Vries, S. C., Tax, F., & Kemmerling, B. (2014). The leucine-rich repeat receptor kinase BIR2 is a negative regulator of BAK1 in plant immunity. *Current Biology*, *24*(2), 134-143. https://doi.org/10.1016/j.cub.2013.11.047

Haney, C. H., Riely, B. K., Tricoli, D. M., Cook, D. R., Ehrhardt, D. W., & Long, S. R. (2011). Symbiotic Rhizobia Bacteria Trigger a Change in Localization and Dynamics of the Medicago truncatula Receptor Kinase LYK3. *The Plant cell*, *23*(7), 2774-2787. https://doi.org/10.1105/tpc.111.086389

Hartmann, J., Stührwohldt, N., Dahlke, R. I., & Sauter, M. (2013). Phytosulfokine control of growth occurs in the epidermis, is likely to be non-cell autonomous and is dependent on brassinosteroids. *The Plant Journal*, *73*(4), 579-590. https://doi.org/10.1111/tpj.12056

Haruta, M., Sabat, G., Stecker, K., Minkoff, B. B., & Sussman, M. R. (2014). A Peptide Hormone and Its Receptor Protein Kinase Regulate Plant Cell Expansion. *Science*, *343*(6169), 408-411. https://doi.org/10.1126/science.1244454

He, K., Gou, X., Yuan, T., Lin, H., Asami, T., Yoshida, S., Russell, S. D., & Li, J. (2007). BAK1 and BKK1 regulate brassinosteroid-dependent growth and brassinosteroid-independent cell-death pathways. *Current Biology*, *17*(13), 1109-1115. https://doi.org/10.1016/j.cub.2007.05.036

He, Y., Zhou, J., Shan, L., & Meng, X. (2018). Plant cell surface receptor-mediated signaling - a common theme amid diversity. *Journal of cell science*, *131*(2), jcs209353. https://doi.org/10.1242/jcs.209353

Hegenauer, V., Fürst, U., Kaiser, B., Smoker, M., Zipfel, C., Felix, G., Stahl, M., & Albert, M. (2016). Detection of the plant parasite Cuscuta reflexa by a tomato cell surface receptor. *Science*, *353*(6298), 478-481. https://doi.org/10.1126/science.aaf3919

Hemsley, P. A. (2015). The importance of lipid modified proteins in plants. *New Phytologist*, *205*(2), 476-489. https://doi.org/10.1111/nph.13085

Hemsley, P. A., Weimar, T., Lilley, K. S., Dupree, P., & Grierson, C. S. (2013). A proteomic approach identifies many novel palmitoylated proteins in Arabidopsis. *New Phytologist*, *197*(3), 805-814. https://doi.org/10.1111/nph.12077

Henriques, R., Griffiths, C., Hesper Rego, E., & Mhlanga, M. M. (2011). PALM and STORM: Unlocking live-cell super-resolution. *Biopolymers*, *95*(5), 322-331. https://doi.org/10.1002/bip.21586

Herbert, S., Soares, H., Zimmer, C., & Henriques, R. (2012). Single-Molecule Localization Super-Resolution Microscopy: Deeper and Faster. *Microscopy and Microanalysis*, *18*(6), 1419-1429. https://doi.org/10.1017/S1431927612013347

Holtorf, S., Apel, K., & Bohlmann, H. (1995). Comparison of different constitutive and inducible promoters for the overexpression of transgenes in Arabidopsis thaliana. *Plant Molecular Biology*, *29*(4), 637-646. https://doi.org/10.1007/bf00041155

Holzwart, E., Huerta, A. I., Glöckner, N., Garnelo Gómez, B., Wanke, F., Augustin, S., Askani, J. C., Schürholz, A.-K., Harter, K., & Wolf, S. (2018). BRI1 controls vascular cell fate in the *Arabidopsis* root through RLP44 and phytosulfokine signaling. *Proceedings of the National Academy of Sciences*, *115*(46), 11838-11843. https://doi.org/10.1073/pnas.1814434115

Holzwart, E., Wanke, F., Glöckner, N., Höfte, H., Harter, K., & Wolf, S. (2019). A Mutant Allele Uncouples the Brassinosteroid-Dependent and Independent Functions of BRASSINOSTEROID INSENSITIVE 11. *Plant Physiology*, *182*(1), 669-678. https://doi.org/10.1104/pp.19.00448

Hosy, E., Martinière, A., Choquet, D., Maurel, C., & Luu, D.-T. (2015). Super-Resolved and Dynamic Imaging of Membrane Proteins in Plant Cells Reveal Contrasting Kinetic Profiles and Multiple Confinement Mechanisms. *Molecular Plant*, *8*(2), 339-342. https://doi.org/10.1016/j.molp.2014.10.006

Huang, D., Sun, Y., Ma, Z., Ke, M., Cui, Y., Chen, Z., Chen, C., Ji, C., Tran, T. M., Yang, L., Lam, S. M., Han, Y., Shu, G., Friml, J., Miao, Y., Jiang, L., & Chen, X. (2019). Salicylic acid-mediated plasmodesmal closure via Remorin-dependent lipid organization. *Proceedings of the National Academy of Sciences*, *116*(42), 21274-21284. https://doi.org/10.1073/pnas.1911892116

Huffaker, A., Pearce, G., & Ryan, C. A. (2006). An endogenous peptide signal in Arabidopsis activates components of the innate immune response. *Proceedings of the National Academy of Sciences*, *103*(26), 10098-10103. https://doi.org/10.1073/pnas.0603727103

Hutten, S. J., Hamers, D. S., Aan den Toorn, M., van Esse, W., Nolles, A., Bücherl, C. A., de Vries, S. C., Hohlbein, J., & Borst, J. W. (2017). Visualization of BRI1 and SERK3/BAK1 Nanoclusters in Arabidopsis Roots. *PLOS ONE*, *12*(1), e0169905. https://doi.org/10.1371/journal.pone.0169905

Imkampe, J., Halter, T., Huang, S., Schulze, S., Mazzotta, S., Schmidt, N., Manstretta, R., Postel, S., Wierzba, M., Yang, Y., van Dongen, W., Stahl, M., Zipfel, C., Goshe, M. B., Clouse, S., de Vries, S. C., Tax, F., Wang, X., & Kemmerling, B. (2017). The Arabidopsis Leucine-Rich Repeat Receptor Kinase BIR3 Negatively Regulates BAK1 Receptor Complex Formation and Stabilizes BAK1. *The Plant cell*, *29*(9), 2285-2303. https://doi.org/10.1105/tpc.17.00376

Irani, N. G., Di Rubbo, S., Mylle, E., Van den Begin, J., Schneider-Pizoń, J., Hniliková, J., Šíša, M., Buyst, D., Vilarrasa-Blasi, J., Szatmári, A. M., Van Damme, D., Mishev, K., Codreanu, M. C., Kohout, L., Strnad, M., Caño-Delgado, A. I., Friml, J., Madder, A., & Russinova, E. (2012). Fluorescent castasterone reveals BRI1 signaling from the plasma membrane. *Nature Chemical Biology*, *8*(6), 583-589. https://doi.org/10.1038/nchembio.958

Jacobson, K., Liu, P., & Lagerholm, B. C. (2019). The Lateral Organization and Mobility of Plasma Membrane Components. *Cell*, *177*(4), 806-819. https://doi.org/10.1016/j.cell.2019.04.018

Jaillais, Y., & Ott, T. (2019). The Nanoscale Organization of the Plasma Membrane and Its Importance in Signaling: A Proteolipid Perspective. *Plant Physiology*, *182*(4), 1682-1696. https://doi.org/10.1104/pp.19.01349

Jarsch, I. K., Konrad, S. S., Stratil, T. F., Urbanus, S. L., Szymanski, W., Braun, P., Braun, K. H., & Ott, T. (2014). Plasma Membranes Are Subcompartmentalized into a Plethora of Coexisting and Diverse Microdomains in Arabidopsis and Nicotiana benthamiana. *The Plant cell*, *26*(4), 1698-1711. https://doi.org/10.1105/tpc.114.124446

Jones, J. D., Vance, R. E., & Dangl, J. L. (2016). Intracellular innate immune surveillance devices in plants and animals. *Science*, *354*(6316). https://doi.org/10.1126/science.aaf6395

Jung, H. W., & Hwang, B. K. (2007). The leucine-rich repeat (LRR) protein, CaLRR1, interacts with the hypersensitive induced reaction (HIR) protein, CaHIR1, and suppresses cell death induced by the CaHIR1 protein. *Molecular Plant Pathology*, *8*(4), 503-514. https://doi.org/10.1111/j.1364-3703.2007.00410.x

Jung, H. W., Lim, C. W., Lee, S. C., Choi, H. W., Hwang, C. H., & Hwang, B. K. (2008). Distinct roles of the pepper hypersensitive induced reaction protein gene CaHIR1 in disease and osmotic stress, as determined by comparative transcriptome and proteome analyses. *Planta*, *227*(2), 409-425. https://doi.org/10.1007/s00425-007-0628-6

Junková, P., Daněk, M., Kocourková, D., Brouzdová, J., Kroumanová, K., Zelazny, E., Janda, M., Hynek, R., Martinec, J., & Valentová, O. (2018). Mapping of Plasma Membrane Proteins Interacting With Arabidopsis thaliana Flotillin 2. *Frontiers in plant science*, *9*, 991. https://doi.org/10.3389/fpls.2018.00991

Kang, M., Day, C. A., Kenworthy, A. K., & DiBenedetto, E. (2012). Simplified Equation to Extract Diffusion Coefficients from Confocal FRAP Data. *Traffic*, *13*(12), 1589-1600. https://doi.org/10.1111/tra.12008

Keck, J. (2021, unpublished). *Effects of cytoskeleton integrity and hormone treatment on the dynamics of the PHYTOSULFOKINE RECEPTOR 1 in the plasma membrane* [Master Thesis, University of Tübingen].

Kemmerling, B., Schwedt, A., Rodriguez, P., Mazzotta, S., Frank, M., Qamar, S. A., Mengiste, T., Betsuyaku, S., Parker, J. E., Müssig, C., Thomma, B. P. H. J., Albrecht, C., de Vries, S. C., Hirt, H., & Nürnberger, T. (2007). The BRI1-Associated Kinase 1, BAK1, Has a Brassinolide-Independent Role in Plant Cell-Death Control. *Current Biology*, *17*(13), 1116-1122. https://doi.org/https://doi.org/10.1016/j.cub.2007.05.046

Khater, I. M., Nabi, I. R., & Hamarneh, G. (2020). A Review of Super-Resolution Single-Molecule Localization Microscopy Cluster Analysis and Quantification Methods. *Patterns*, *1*(3), 100038. https://doi.org/10.1016/j.patter.2020.100038

Kierszniowska, S., Seiwert, B., & Schulze, W. X. (2009). Definition of Arabidopsis Sterol-rich Membrane Microdomains by Differential Treatment with Methyl-β-cyclodextrin and Quantitative Proteomics*S. *Molecular & Cellular Proteomics*, *8*(4), 612-623. https://doi.org/10.1074/mcp.M800346-MCP200

Kleine-Vehn, J., Wabnik, K., Martinière, A., Łangowski, Ł., Willig, K., Naramoto, S., Leitner, J., Tanaka, H., Jakobs, S., Robert, S., Luschnig, C., Govaerts, W., Hell, S. W., Runions, J., & Friml, J. (2011).

Recycling, clustering, and endocytosis jointly maintain PIN auxin carrier polarity at the plasma membrane. *Molecular systems biology*, *7*, 540-540. https://doi.org/10.1038/msb.2011.72

Komis, G., Šamajová, O., Ovečka, M., & Šamaj, J. (2015). Super-resolution Microscopy in Plant Cell Imaging. *Trends in Plant Science*, *20*(12), 834-843. https://doi.org/10.1016/j.tplants.2015.08.013

Konopka, C. A., & Bednarek, S. Y. (2008). Variable-angle epifluorescence microscopy: a new way to look at protein dynamics in the plant cell cortex. *The Plant Journal*, *53*(1), 186-196. https://doi.org/10.1111/j.1365-313X.2007.03306.x

Konrad, S. S., Popp, C., Stratil, T. F., Jarsch, I. K., Thallmair, V., Folgmann, J., Marín, M., & Ott, T. (2014). S-acylation anchors remorin proteins to the plasma membrane but does not primarily determine their localization in membrane microdomains. *New Phytologist*, *203*(3), 758-769. https://doi.org/10.1111/nph.12867

Kwon, M., & Choe, S. (2005). Brassinosteroid biosynthesis anddwarf mutants. *Journal of Plant Biology*, *48*(1), 1. https://doi.org/10.1007/BF03030559

Labun, K., Montague, T. G., Krause, M., Torres Cleuren, Y. N., Tjeldnes, H., & Valen, E. (2019). CHOPCHOP v3: expanding the CRISPR web toolbox beyond genome editing. *Nucleic Acids Research*, *47*(W1), W171-w174. https://doi.org/10.1093/nar/gkz365

Ladwig, F., Dahlke, R. I., Stührwohldt, N., Hartmann, J., Harter, K., & Sauter, M. (2015). Phytosulfokine Regulates Growth in Arabidopsis through a Response Module at the Plasma Membrane That Includes CYCLIC NUCLEOTIDE-GATED CHANNEL17, H+-ATPase, and BAK1. *The Plant cell*, *27*(6), 1718-1729. https://doi.org/10.1105/tpc.15.00306

Laloi, M., Perret, A.-M., Chatre, L., Melser, S., Cantrel, C., Vaultier, M.-N. l., Zachowski, A., Bathany, K., Schmitter, J.-M., Vallet, M., Lessire, R., Hartmann, M.-A. e., & Moreau, P. (2006). Insights into the Role of Specific Lipids in the Formation and Delivery of Lipid Microdomains to the Plasma Membrane of Plant Cells. *Plant Physiology*, *143*(1), 461-472. https://doi.org/10.1104/pp.106.091496

Langhans, M., & Meckel, T. (2014). Single-molecule detection and tracking in plants. *Protoplasma*, *251*(2), 277-291. https://doi.org/10.1007/s00709-013-0601-0

Langhorst, M. F., Reuter, A., & Stuermer, C. A. O. (2005). Scaffolding microdomains and beyond: the function of reggie/flotillin proteins. *Cellular and Molecular Life Sciences*, *62*(19), 2228-2240. https://doi.org/10.1007/s00018-005-5166-4

Lefebvre, B., Furt, F., Hartmann, M.-A. e., Michaelson, L. V., Carde, J.-P., Sargueil-Boiron, F. o., Rossignol, M., Napier, J. A., Cullimore, J., Bessoule, J.-J., & Mongrand, S. b. (2007). Characterization of Lipid Rafts from Medicago truncatula Root Plasma Membranes: A Proteomic Study Reveals the Presence of a Raft-Associated Redox System. *Plant Physiology*, *144*(1), 402-418. https://doi.org/10.1104/pp.106.094102

Levet, F., Hosy, E., Kechkar, A., Butler, C., Beghin, A., Choquet, D., & Sibarita, J.-B. (2015). SR-Tesseler: a method to segment and quantify localization-based super-resolution microscopy data. *Nature Methods*, *12*(11), 1065-1071. https://doi.org/10.1038/nmeth.3579

Li, C., Wu, H.-M., & Cheung, A. Y. (2016a). FERONIA and Her Pals: Functions and Mechanisms *Plant Physiology*, *171*(4), 2379-2392. https://doi.org/10.1104/pp.16.00667

Li, J., & Chory, J. (1997). A Putative Leucine-Rich Repeat Receptor Kinase Involved in Brassinosteroid Signal Transduction. *Cell*, *90*(5), 929-938. https://doi.org/10.1016/S0092-8674(00)80357-8

Li, J., Wen, J., Lease, K. A., Doke, J. T., Tax, F. E., & Walker, J. C. (2002). BAK1, an Arabidopsis LRR Receptor-like Protein Kinase, Interacts with BRI1 and Modulates Brassinosteroid Signaling. *Cell*, *110*(2), 213-222. https://doi.org/10.1016/S0092-8674(02)00812-7

Li, R., Liu, P., Wan, Y., Chen, T., Wang, Q., Mettbach, U., Baluska, F., Samaj, J., Fang, X., Lucas, W. J., & Lin, J. (2012). A membrane microdomain-associated protein, Arabidopsis Flot1, is involved in a clathrin-independent endocytic pathway and is required for seedling development. *The Plant cell*, *24*(5), 2105-2122. https://doi.org/10.1105/tpc.112.095695

Li, S., Zhao, J., Zhai, Y., Yuan, Q., Zhang, H., Wu, X., Lu, Y., Peng, J., Sun, Z., Lin, L., Zheng, H., Chen, J., & Yan, F. (2019). The hypersensitive induced reaction 3 (HIR3) gene contributes to plant basal resistance via an EDS1 and salicylic acid-dependent pathway. *The Plant Journal*, *98*(5), 783-797. https://doi.org/10.1111/tpj.14271

Li, X., Wang, X., Yang, Y., Li, R., He, Q., Fang, X., Luu, D.-T., Maurel, C., & Lin, J. (2011). Single-Molecule Analysis of PIP2;1 Dynamics and Partitioning Reveals Multiple Modes of Arabidopsis Plasma Membrane Aquaporin Regulation *The Plant cell*, *23*(10), 3780-3797. https://doi.org/10.1105/tpc.111.091454

Li, X., Xing, J., Qiu, Z., He, Q., & Lin, J. (2016b). Quantification of Membrane Protein Dynamics and Interactions in Plant Cells by Fluorescence Correlation Spectroscopy. *Molecular Plant*, *9*(9), 1229-1239. https://doi.org/10.1016/j.molp.2016.06.017

Liang, P., Stratil, T. F., Popp, C., Marín, M., Folgmann, J., Mysore, K. S., Wen, J., & Ott, T. (2018). Symbiotic root infections in Medicago truncatula require remorin-mediated receptor stabilization in membrane nanodomains. *Proceedings of the National Academy of Sciences*, *115*(20), 5289-5294. https://doi.org/10.1073/pnas.1721868115

Lin, W., Lu, D., Gao, X., Jiang, S., Ma, X., Wang, Z., Mengiste, T., He, P., & Shan, L. (2013). Inverse modulation of plant immune and brassinosteroid signaling pathways by the receptor-like cytoplasmic kinase BIK1. *Proceedings of the National Academy of Sciences*, *110*(29), 12114-12119. https://doi.org/10.1073/pnas.1302154110

Lippincott-Schwartz, J., Altan-Bonnet, N., & Patterson, G. H. (2003). Photobleaching and photoactivation: following protein dynamics in living cells. *Nature Cell Biology*, *Supplement to volume 5*, S7-14. https://doi.org/10.1038/ncb1032

Liu, D., Kumar, R., Claus, L. A. N., Johnson, A. J., Siao, W., Vanhoutte, I., Wang, P., Bender, K. W., Yperman, K., Martins, S., Zhao, X., Vert, G., Van Damme, D., Friml, J., & Russinova, E. (2020). Endocytosis of BRASSINOSTEROID INSENSITIVE1 Is Partly Driven by a Canonical Tyr-Based Motif. *The Plant cell*, *32*(11), 3598-3612. https://doi.org/10.1105/tpc.20.00384

Liu, H., Ding, Y., Zhou, Y., Jin, W., Xie, K., & Chen, L.-L. (2017). CRISPR-P 2.0: An Improved CRISPR-Cas9 Tool for Genome Editing in Plants. *Molecular Plant*, *10*(3), 530-532. https://doi.org/10.1016/j.molp.2017.01.003

Loake, G., & Grant, M. (2007). Salicylic acid in plant defence--the players and protagonists. *Current Opinion in Plant Biology*, *10*(5), 466-472. https://doi.org/10.1016/j.pbi.2007.08.008

Lu, D., Wu, S., Gao, X., Zhang, Y., Shan, L., & He, P. (2010). A receptor-like cytoplasmic kinase, BIK1, associates with a flagellin receptor complex to initiate plant innate immunity. *Proceedings of the National Academy of Sciences*, *107*(1), 496-501. https://doi.org/10.1073/pnas.0909705107

Lv, M., Li, M., Chen, W., Wang, Y., Sun, C., Yin, H., He, K., & Li, J. (2018). Thermal-Enhanced bri1-301 Instability Reveals a Plasma Membrane Protein Quality Control System in Plants. *Frontiers in plant science*, *9*. https://doi.org/10.3389/fpls.2018.01620

Lv, X., Jing, Y., Xiao, J., Zhang, Y., Zhu, Y., Julian, R., & Lin, J. (2017). Membrane microdomains and the cytoskeleton constrain AtHIR1 dynamics and facilitate the formation of an AtHIR1-associated immune complex. *The Plant Journal*, *90*(1), 3-16. https://doi.org/10.1111/tpj.13480

Ma, X., Xu, G., He, P., & Shan, L. (2016). SERKing Coreceptors for Receptors. *Trends in Plant Science*, *21*(12), 1017-1033. https://doi.org/10.1016/j.tplants.2016.08.014

Mackay, J. P., Sunde, M., Lowry, J. A., Crossley, M., & Matthews, J. M. (2007). Protein interactions: is seeing believing? *Trends in Biochemical Sciences*, *32*(12), 530-531. https://doi.org/10.1016/j.tibs.2007.09.006

Mackey, D., Belkhadir, Y., Alonso, J. M., Ecker, J. R., & Dangl, J. L. (2003). Arabidopsis RIN4 is a target of the type III virulence effector AvrRpt2 and modulates RPS2-mediated resistance. *Cell*, *112*(3), 379-389. https://doi.org/10.1016/s0092-8674(03)00040-0

Majeran, W., Le Caer, J.-P., Ponnala, L., Meinnel, T., & Giglione, C. (2018). Targeted Profiling of Arabidopsis thaliana Subproteomes Illuminates Co- and Posttranslationally N-Terminal Myristoylated Proteins. *The Plant cell*, *30*(3), 543-562. https://doi.org/10.1105/tpc.17.00523

Manley, S., Gillette, J. M., Patterson, G. H., Shroff, H., Hess, H. F., Betzig, E., & Lippincott-Schwartz, J. (2008). High-density mapping of single-molecule trajectories with photoactivated localization microscopy. *Nature Methods*, *5*(2), 155-157. https://doi.org/10.1038/nmeth.1176

Martinez, D., Legrand, A., Gronnier, J., Decossas, M., Gouguet, P., Lambert, O., Berbon, M., Verron, L., Grélard, A., Germain, V., Loquet, A., Mongrand, S., & Habenstein, B. (2019). Coiled-coil oligomerization controls localization of the plasma membrane REMORINs. *Journal of Structural Biology*, *206*(1), 12-19. https://doi.org/10.1016/j.jsb.2018.02.003

Martinière, A., Fiche, J. B., Smokvarska, M., Mari, S., Alcon, C., Dumont, X., Hematy, K., Jaillais, Y., Nollmann, M., & Maurel, C. (2019). Osmotic Stress Activates Two Reactive Oxygen Species Pathways with Distinct Effects on Protein Nanodomains and Diffusion. *Plant Physiology*, *179*(4), 1581-1593. https://doi.org/10.1104/pp.18.01065

Martinière, A., Lavagi, I., Nageswaran, G., Rolfe, D. J., Maneta-Peyret, L., Luu, D.-T., Botchway, S. W., Webb, S. E. D., Mongrand, S., Maurel, C., Martin-Fernandez, M. L., Kleine-Vehn, J., Friml, J., Moreau, P., & Runions, J. (2012). Cell wall constrains lateral diffusion of plant plasma-membrane proteins. *Proceedings of the National Academy of Sciences*, *109*(31), 12805-12810. https://doi.org/10.1073/pnas.1202040109

Martinière, A., & Zelazny, E. (2021). Membrane nanodomains and transport functions in plant. *Plant Physiology*, *187*(4), 1839-1855. https://doi.org/10.1093/plphys/kiab312

Mbengue, M., Bourdais, G., Gervasi, F., Beck, M., Zhou, J., Spallek, T., Bartels, S., Boller, T., Ueda, T., Kuhn, H., & Robatzek, S. (2016). Clathrin-dependent endocytosis is required for immunity mediated by pattern recognition receptor kinases. *Proceedings of the National Academy of Sciences*, *113*(39), 11034-11039. https://doi.org/10.1073/pnas.1606004113

McKenna, J. F., Rolfe, D. J., Webb, S. E. D., Tolmie, A. F., Botchway, S. W., Martin-Fernandez, M. L., Hawes, C., & Runions, J. (2019). The cell wall regulates dynamics and size of plasma-membrane nanodomains in *Arabidopsis*. *Proceedings of the National Academy of Sciences*, *116*(26), 12857-12862. https://doi.org/10.1073/pnas.1819077116

Miya, A., Albert, P., Shinya, T., Desaki, Y., Ichimura, K., Shirasu, K., Narusaka, Y., Kawakami, N., Kaku, H., & Shibuya, N. (2007). CERK1, a LysM receptor kinase, is essential for chitin elicitor signaling in *Arabidopsis*. *Proceedings of the National Academy of Sciences*, *104*(49), 19613-19618. https://doi.org/10.1073/pnas.0705147104

Mongrand, S., Morel, J., Laroche, J., Claverol, S., Carde, J.-P., Hartmann, M.-A., Bonneu, M., Simon-Plas, F., Lessire, R., & Bessoule, J.-J. (2004). Lipid Rafts in Higher Plant Cells: PURIFICATION AND CHARACTERIZATION OF TRITON X-100-INSOLUBLE MICRODOMAINS FROM TOBACCO PLASMA MEMBRANE *Journal of Biological Chemistry*, *279*(35), 36277-36286. https://doi.org/10.1074/jbc.M403440200

Morel, J., Claverol, S., Mongrand, S., Furt, F., Fromentin, J., Bessoule, J.-J., Blein, J.-P., & Simon-Plas, F. (2006). Proteomics of Plant Detergent-resistant Membranes *Molecular & Cellular Proteomics*, *5*(8), 1396-1411. https://doi.org/10.1074/mcp.M600044-MCP200

Morrow, I. C., Rea, S., Martin, S., Prior, I. A., Prohaska, R., Hancock, J. F., James, D. E., & Parton, R. G. (2002). Flotillin-1/reggie-2 traffics to surface raft domains via a novel golgi-independent pathway. Identification of a novel membrane targeting domain and a role for palmitoylation. *Journal of Biological Chemistry*, *277*(50), 48834-48841. https://doi.org/10.1074/jbc.M209082200

Mueller, K., Bittel, P., Chinchilla, D., Jehle, A. K., Albert, M., Boller, T., & Felix, G. (2012). Chimeric FLS2 receptors reveal the basis for differential flagellin perception in Arabidopsis and tomato. *The Plant cell*, *24*(5), 2213-2224. https://doi.org/10.1105/tpc.112.096073

Nadimpalli, R., Yalpani, N., Johal, G. S., & Simmons, C. R. (2000). Prohibitins, stomatins, and plant disease response genes compose a protein superfamily that controls cell proliferation, ion channel regulation, and death. *Journal of Biological Chemistry*, *275*(38), 29579-29586. https://doi.org/10.1074/jbc.M002339200

Nam, K. H., & Li, J. (2002). BRI1/BAK1, a Receptor Kinase Pair Mediating Brassinosteroid Signaling. *Cell*, *110*(2), 203-212. https://doi.org/10.1016/S0092-8674(02)00814-0

Neumann-Giesen, C., Falkenbach, B., Beicht, P., Claasen, S., Lüers, G., Stuermer, C. A., Herzog, V., & Tikkanen, R. (2004). Membrane and raft association of reggie-1/flotillin-2: role of myristoylation, palmitoylation and oligomerization and induction of filopodia by overexpression. *Biochemical Journal*, *378*(Pt 2), 509-518. https://doi.org/10.1042/bj20031100

Ngou, B. P. M., Ahn, H.-K., Ding, P., & Jones, J. D. G. (2021). Mutual potentiation of plant immunity by cell-surface and intracellular receptors. *Nature*, *592*(7852), 110-115. https://doi.org/10.1038/s41586-021-03315-7

Ning, W., Jiang, P., Guo, Y., Wang, C., Tan, X., Zhang, W., Peng, D., & Xue, Y. (2020). GPS-Palm: a deep learning-based graphic presentation system for the prediction of S-palmitoylation sites in proteins. *Briefings in Bioinformatics*, *22*(2), 1836-1847. https://doi.org/10.1093/bib/bbaa038

Niu, Y., & Xiang, Y. (2018). An Overview of Biomembrane Functions in Plant Responses to High-Temperature Stress. *Frontiers in plant science*, *9*. https://doi.org/10.3389/fpls.2018.00915

Ordon, J., Gantner, J., Kemna, J., Schwalgun, L., Reschke, M., Streubel, J., Boch, J., & Stuttmann, J. (2017). Generation of chromosomal deletions in dicotyledonous plants employing a user-friendly genome editing toolkit. *The Plant Journal*, *89*(1), 155-168. https://doi.org/10.1111/tpj.13319

Ott, T. (2017). Membrane nanodomains and microdomains in plant–microbe interactions. *Current Opinion in Plant Biology*, *40*, 82-88. https://doi.org/10.1016/j.pbi.2017.08.008

Patterson, G. H., & Lippincott-Schwartz, J. (2002). A photoactivatable GFP for selective photolabeling of proteins and cells. *Science*, *297*(5588), 1873-1877. https://doi.org/10.1126/science.1074952

Perraki, A., Gronnier, J., Gouguet, P., Boudsocq, M., Deroubaix, A.-F., Simon, V., German-Retana, S., Legrand, A., Habenstein, B., Zipfel, C., Bayer, E., Mongrand, S., & Germain, V. (2018). REM1.3's phospho-status defines its plasma membrane nanodomain organization and activity in restricting PVX cell-to-cell movement. *PLOS Pathogens*, *14*(11), e1007378. https://doi.org/10.1371/journal.ppat.1007378

Pieterse, C. M. J., Leon-Reyes, A., Van der Ent, S., & Van Wees, S. C. M. (2009). Networking by small-molecule hormones in plant immunity. *Nature Chemical Biology*, *5*(5), 308-316. https://doi.org/10.1038/nchembio.164

Platre, M. P., Bayle, V., Armengot, L., Bareille, J., Marquès-Bueno, M. d. M., Creff, A., Maneta-Peyret, L., Fiche, J.-B., Nollmann, M., Miège, C., Moreau, P., Martinière, A., & Jaillais, Y. (2019). Developmental control of plant Rho GTPase nano-organization by the lipid phosphatidylserine. *Science*, *364*(6435), 57-62. https://doi.org/10.1126/science.aav9959

Postel, S., Küfner, I., Beuter, C., Mazzotta, S., Schwedt, A., Borlotti, A., Halter, T., Kemmerling, B., & Nürnberger, T. (2010). The multifunctional leucine-rich repeat receptor kinase BAK1 is implicated in Arabidopsis development and immunity. *European Journal of Cell Biology*, *89*(2), 169-174. https://doi.org/10.1016/j.ejcb.2009.11.001

Pruitt, R. N., Locci, F., Wanke, F., Zhang, L., Saile, S. C., Joe, A., Karelina, D., Hua, C., Fröhlich, K., Wan, W.-L., Hu, M., Rao, S., Stolze, S. C., Harzen, A., Gust, A. A., Harter, K., Joosten, M. H. A. J., Thomma, B. P. H. J., Zhou, J.-M., Dangl, J. L., Weigel, D., Nakagami, H., Oecking, C., Kasmi, F. E., Parker, J. E., & Nürnberger, T. (2021). The EDS1–PAD4–ADR1 node mediates Arabidopsis pattern-triggered immunity. *Nature*, *598*(7881), 495-499. https://doi.org/10.1038/s41586-021-03829-0

Qi, Y., & Katagiri, F. (2009). Purification of low-abundance Arabidopsis plasma-membrane protein complexes and identification of candidate components. *The Plant Journal*, *57*(5), 932-944. https://doi.org/10.1111/j.1365-313X.2008.03736.x

Qi, Y., & Katagiri, F. (2012). Membrane microdomain may be a platform for immune signaling. *Plant Signaling & Behavior*, *7*(4), 454-456. https://doi.org/10.4161/psb.19398

Qi, Y., Tsuda, K., Nguyen, L. V., Wang, X., Lin, J., Murphy, A. S., Glazebrook, J., Thordal-Christensen, H., & Katagiri, F. (2011). Physical Association of Arabidopsis Hypersensitive Induced Reaction Proteins (HIRs) with the Immune Receptor RPS2. *Journal of Biological Chemistry*, *286*(36), 31297-31307. https://doi.org/10.1074/jbc.M110.211615

Raffaele, S., Mongrand, S., Gamas, P., Niebel, A., & Ott, T. (2007). Genome-wide annotation of remorins, a plant-specific protein family: evolutionary and functional perspectives. *Plant Physiology*, *145*(3), 593-600. https://doi.org/10.1104/pp.107.108639

Ranf, S., Eschen-Lippold, L., Fröhlich, K., Westphal, L., Scheel, D., & Lee, J. (2014). Microbe-associated molecular pattern-induced calcium signaling requires the receptor-like cytoplasmic kinases, PBL1 and BIK1. *BMC plant biology*, *14*(1), 374. https://doi.org/10.1186/s12870-014-0374-4

Rausch, L. (2021, unpublished). *Spatiotemporal studies of functional components in the fast brassinosteroid response pathway of Arabidopsis thaliana* [Master Thesis, University of Tübingen].

Rivera-Milla, E., Stuermer, C. A. O., & Málaga-Trillo, E. (2006). Ancient origin of reggie (flotillin), reggie-like, and other lipid-raft proteins: convergent evolution of the SPFH domain. *Cellular and Molecular Life Sciences*, *63*(3), 343-357. https://doi.org/10.1007/s00018-005-5434-3

Robatzek, S., Chinchilla, D., & Boller, T. (2006). Ligand-induced endocytosis of the pattern recognition receptor FLS2 in Arabidopsis. *Genes & development*, *20*(5), 537-542. https://doi.org/10.1101/gad.366506

Rohr, L. (unpublished). In. University of Tübingen.

Roux, M., Schwessinger, B., Albrecht, C., Chinchilla, D., Jones, A., Holton, N., Malinovsky, F. G., Tör, M., de Vries, S., & Zipfel, C. (2011). The Arabidopsis Leucine-Rich Repeat Receptor–Like Kinases BAK1/SERK3 and BKK1/SERK4 Are Required for Innate Immunity to Hemibiotrophic and Biotrophic Pathogens. *The Plant cell*, *23*(6), 2440-2455. https://doi.org/10.1105/tpc.111.084301

Rust, M. J., Bates, M., & Zhuang, X. (2006). Sub-diffraction-limit imaging by stochastic optical reconstruction microscopy (STORM). *Nature Methods*, *3*(10), 793-796. https://doi.org/10.1038/nmeth929

Santiago, J., Henzler, C., & Hothorn, M. (2013). Molecular Mechanism for Plant Steroid Receptor Activation by Somatic Embryogenesis Co-Receptor Kinases. *Science*, *341*(6148), 889-892. https://doi.org/10.1126/science.1242468

Schlöffel, M. A., Salzer, A., Wan, W.-L., van Wijk, R., Del Corvo, R., Šemanjski, M., Symeonidi, E., Slaby, P., Kilian, J., Maček, B., Munnik, T., & Gust, A. A. (2020). The BIR2/BIR3-Associated Phospholipase Dγ1 Negatively Regulates Plant Immunity. *Plant Physiology*, *183*(1), 371-384. https://doi.org/10.1104/pp.19.01292

Schulze, B., Mentzel, T., Jehle, A. K., Mueller, K., Beeler, S., Boller, T., Felix, G., & Chinchilla, D. (2010). Rapid heteromerization and phosphorylation of ligand-activated plant transmembrane receptors and their associated kinase BAK1. *Journal of Biological Chemistry*, *285*(13), 9444-9451. https://doi.org/10.1074/jbc.M109.096842

Schulze, S. (2020). *The BIR3 interactome revealed the NLR CSA1 as a component necessary for BIR- and BAK1-mediated cell death* [University of Tübingen].

Schulze, S., Yu, L., Ehinger, A., Kolb, D., Saile, S. C., Stahl, M., Franz-Wachtel, M., Li, L., Kasmi, F. E., Cevik, V., & Kemmerling, B. (2021). The TIR-NBS-LRR protein CSA1 is required for autoimmune cell death in Arabidopsis pattern recognition co-receptor *bak1* and *bir3* mutants. *bioRxiv*, 2021.2004.2011.438637. https://doi.org/10.1101/2021.04.11.438637

Schwab, R., Ossowski, S., Riester, M., Warthmann, N., & Weigel, D. (2006). Highly specific gene silencing by artificial microRNAs in Arabidopsis. *The Plant cell*, *18*(5), 1121-1133. https://doi.org/10.1105/tpc.105.039834

Shaner, N. C., Steinbach, P. A., & Tsien, R. Y. (2005). A guide to choosing fluorescent proteins. *Nature Methods*, *2*(12), 905-909. https://doi.org/10.1038/nmeth819

Shiu, S.-H., & Bleecker, A. B. (2001). Receptor-like kinases from *Arabidopsis* form a monophyletic gene family related to animal receptor kinases. *Proceedings of the National Academy of Sciences*, *98*(19), 10763-10768. https://doi.org/10.1073/pnas.181141598

Shroff, H., Galbraith, C. G., Galbraith, J. A., White, H., Gillette, J., Olenych, S., Davidson, M. W., & Betzig, E. (2007). Dual-color superresolution imaging of genetically expressed probes within individual adhesion complexes. *Proceedings of the National Academy of Sciences*, *104*(51), 20308-20313. https://doi.org/10.1073/pnas.0710517105

Simons, K., & Van Meer, G. (1988). Lipid sorting in epithelial cells. *Biochemistry*, *27*(17), 6197-6202. https://doi.org/10.1021/bi00417a001

Singer, S. J., & Nicolson, G. L. (1972). The Fluid Mosaic Model of the Structure of Cell Membranes. *Science*, *175*(4023), 720-731. https://doi.org/10.1126/science.175.4023.720

Solis, Gonzalo P., Hoegg, M., Munderloh, C., Schrock, Y., Malaga-Trillo, E., Rivera-Milla, E., & Stuermer, Claudia A. O. (2007). Reggie/flotillin proteins are organized into stable tetramers in membrane microdomains. *Biochemical Journal*, *403*(2), 313-322. https://doi.org/10.1042/bj20061686

Stael, S., Bayer, R. G., Mehlmer, N., & Teige, M. (2011). Protein N-acylation overrides differing targeting signals. *FEBS Letters*, *585*(3), 517-522. https://doi.org/10.1016/j.febslet.2011.01.001

Stegmann, M., Monaghan, J., Smakowska-Luzan, E., Rovenich, H., Lehner, A., Holton, N., Belkhadir, Y., & Zipfel, C. (2017). The receptor kinase FER is a RALF-regulated scaffold controlling plant immune signaling. *Science*, *355*(6322), 287-289. https://doi.org/doi:10.1126/science.aal2541

Stemmer, M., Thumberger, T., del Sol Keyer, M., Wittbrodt, J., & Mateo, J. L. (2015). CCTop: An Intuitive, Flexible and Reliable CRISPR/Cas9 Target Prediction Tool. *PLOS ONE*, *10*(4), e0124633. https://doi.org/10.1371/journal.pone.0124633

Stuttmann, J., Barthel, K., Martin, P., Ordon, J., Erickson, J. L., Herr, R., Ferik, F., Kretschmer, C., Berner, T., Keilwagen, J., Marillonnet, S., & Bonas, U. (2021). Highly efficient multiplex editing: one-shot generation of 8× Nicotiana benthamiana and 12× Arabidopsis mutants. *The Plant Journal*, *106*(1), 8-22. https://doi.org/10.1111/tpj.15197

Su, Z., Dhusia, K., & Wu, Y. (2020). Understand the Functions of Scaffold Proteins in Cell Signaling by a Mesoscopic Simulation Method. *Biophysical Journal*, *119*(10), 2116-2126. https://doi.org/10.1016/j.bpj.2020.10.002

Subach, F. V., Patterson, G. H., Manley, S., Gillette, J. M., Lippincott-Schwartz, J., & Verkhusha, V. V. (2009). Photoactivatable mCherry for high-resolution two-color fluorescence microscopy. *Nature Methods*, *6*(2), 153-159. https://doi.org/10.1038/nmeth.1298

Subach, F. V., Patterson, G. H., Renz, M., Lippincott-Schwartz, J., & Verkhusha, V. V. (2010). Bright monomeric photoactivatable red fluorescent protein for two-color super-resolution sptPALM of live cells. *Journal of American Chemical Society*, *132*(18), 6481-6491. https://doi.org/10.1021/ja100906g

Sun, C., Yan, K., Han, J.-T., Tao, L., Lv, M.-H., Shi, T., He, Y.-X., Wierzba, M., Tax, F. E., & Li, J. (2017). Scanning for New BRI1 Mutations via TILLING Analysis. *Plant Physiology*, *174*(3), 1881-1896. https://doi.org/10.1104/pp.17.00118

Sun, Y., Li, L., Macho, A. P., Han, Z., Hu, Z., Zipfel, C., Zhou, J.-M., & Chai, J. (2013). Structural Basis for flg22-Induced Activation of the *Arabidopsis* FLS2-BAK1 Immune Complex. *Science*, *342*(6158), 624-628. https://doi.org/doi:10.1126/science.1243825

Tang, D., Wang, G., & Zhou, J. M. (2017). Receptor Kinases in Plant-Pathogen Interactions: More Than Pattern Recognition. *The Plant cell*, *29*(4), 618-637. https://doi.org/10.1105/tpc.16.00891

Tang, W., Kim, T.-W., Oses-Prieto, J. A., Sun, Y., Deng, Z., Zhu, S., Wang, R., Burlingame, A. L., & Wang, Z.-Y. (2008). BSKs Mediate Signal Transduction from the Receptor Kinase BRI1 in Arabidopsis. *Science*, *321*(5888), 557-560. http://www.jstor.org/stable/20054597

Tanner, W., Malinsky, J., & Opekarová, M. (2011). In Plant and Animal Cells, Detergent-Resistant Membranes Do Not Define Functional Membrane Rafts. *The Plant cell*, *23*(4), 1191-1193. https://doi.org/10.1105/tpc.111.086249

Thomma, B. P. H. J., Nürnberger, T., & Joosten, M. H. A. J. (2011). Of PAMPs and Effectors: The Blurred PTI-ETI Dichotomy. *The Plant cell*, *23*(1), 4-15. https://doi.org/10.1105/tpc.110.082602

Turnbull, D., & Hemsley, P. A. (2017). Fats and function: protein lipid modifications in plant cell signalling. *Current Opinion in Plant Biology*, *40*, 63-70. https://doi.org/10.1016/j.pbi.2017.07.007

Veitia, R. A. (2008). Exploring the Molecular Etiology of Dominant-Negative Mutations. *The Plant cell*, *19*(12), 3843-3851. https://doi.org/10.1105/tpc.107.055053

Vogel, C., & Marcotte, E. M. (2012). Insights into the regulation of protein abundance from proteomic and transcriptomic analyses. *Nature Reviews Genetics*, *13*(4), 227-232. https://doi.org/10.1038/nrg3185

Voinnet, O., Rivas, S., Mestre, P., & Baulcombe, D. (2003). Retracted: An enhanced transient expression system in plants based on suppression of gene silencing by the p19 protein of tomato bushy stunt virus. *The Plant Journal*, *33*(5), 949-956. https://doi.org/10.1046/j.1365-313X.2003.01676.x

Wang, J., Jiang, J., Wang, J., Chen, L., Fan, S.-L., Wu, J.-W., Wang, X., & Wang, Z.-X. (2014). Structural insights into the negative regulation of BRI1 signaling by BRI1-interacting protein BKI1. *Cell Research*, *24*(11), 1328-1341. https://doi.org/10.1038/cr.2014.132

Wang, J., Li, H., Han, Z., Zhang, H., Wang, T., Lin, G., Chang, J., Yang, W., & Chai, J. (2015a). Allosteric receptor activation by the plant peptide hormone phytosulfokine. *Nature*, *525*(7568), 265-268. https://doi.org/10.1038/nature14858

Wang, L., Li, H., Lv, X., Chen, T., Li, R., Xue, Y., Jiang, J., Jin, B., Baluška, F., Šamaj, J., Wang, X., & Lin, J. (2015b). Spatiotemporal Dynamics of the BRI1 Receptor and its Regulation by Membrane Microdomains in Living Arabidopsis Cells. *Molecular Plant*, *8*(9), 1334-1349. https://doi.org/10.1016/j.molp.2015.04.005

Wang, L., Xue, Y., Xing, J., Song, K., & Lin, J. (2018). Exploring the Spatiotemporal Organization of Membrane Proteins in Living Plant Cells. *Annual Review of Plant Biology*, *69*, 525-551. https://doi.org/10.1146/annurev-arplant-042817-040233

Wang, X., & Chory, J. (2006). Brassinosteroids Regulate Dissociation of BKI1, a Negative Regulator of BRI1 Signaling, from the Plasma Membrane. *Science*, *313*(5790), 1118-1122. https://doi.org/10.1126/science.1127593

Wang, X., Goshe, M. B., Soderblom, E. J., Phinney, B. S., Kuchar, J. A., Li, J., Asami, T., Yoshida, S., Huber, S. C., & Clouse, S. D. (2005). Identification and Functional Analysis of in Vivo Phosphorylation Sites of the Arabidopsis BRASSINOSTEROID-INSENSITIVE1 Receptor Kinase. *The Plant cell*, *17*(6), 1685-1703. https://doi.org/10.1105/tpc.105.031393

Wolf, S. (2020). Deviating from the Beaten Track: New Twists in Brassinosteroid Receptor Function. *International Journal of Molecular Sciences*, *21*(5), 1561. https://doi.org/10.3390/ijms21051561

Wolf, S., van der Does, D., Ladwig, F., Sticht, C., Kolbeck, A., Schürholz, A.-K., Augustin, S., Keinath, N., Rausch, T., Greiner, S., Schumacher, K., Harter, K., Zipfel, C., & Höfte, H. (2014). A receptor-like protein mediates the response to pectin modification by activating brassinosteroid signaling.

Proceedings of the National Academy of Sciences, *111*(42), 15261-15266. https://doi.org/10.1073/pnas.1322979111

Wu, Y., Gao, Y., Zhan, Y., Kui, H., Liu, H., Yan, L., Kemmerling, B., Zhou, J.-M., He, K., & Li, J. (2020). Loss of the common immune coreceptor BAK1 leads to NLR-dependent cell death. *Proceedings of the National Academy of Sciences*, *117*(43), 27044-27053. https://doi.org/10.1073/pnas.1915339117

Xiao, Y., Stegmann, M., Han, Z., DeFalco, T. A., Parys, K., Xu, L., Belkhadir, Y., Zipfel, C., & Chai, J. (2019). Mechanisms of RALF peptide perception by a heterotypic receptor complex. *Nature*, *572*(7768), 270-274. https://doi.org/10.1038/s41586-019-1409-7

Xue, D.-X., Li, C.-L., Xie, Z.-P., & Staehelin, C. (2019). LYK4 is a component of a tripartite chitin receptor complex in Arabidopsis thaliana. *Journal of experimental botany*, *70*(19), 5507-5516. https://doi.org/10.1093/jxb/erz313

Xue, Y., Chen, H., Jin, C., Sun, Z., & Yao, X. (2006). NBA-Palm: prediction of palmitoylation site implemented in Naïve Bayes algorithm. *BMC Bioinformatics*, *7*(1), 458. https://doi.org/10.1186/1471-2105-7-458

Yamaguchi, Y., Huffaker, A., Bryan, A. C., Tax, F. E., & Ryan, C. A. (2010). PEPR2 is a second receptor for the Pep1 and Pep2 peptides and contributes to defense responses in Arabidopsis. *The Plant cell*, *22*(2), 508-522. https://doi.org/10.1105/tpc.109.068874

Yamaguchi, Y., Pearce, G., & Ryan, C. A. (2006). The cell surface leucine-rich repeat receptor for AtPep1, an endogenous peptide elicitor in Arabidopsis, is functional in transgenic tobacco cells. *Proceedings of the National Academy of Sciences*, *103*(26), 10104-10109. https://doi.org/10.1073/pnas.0603729103

Yu, M., Cui, Y., Zhang, X., Li, R., & Lin, J. (2020). Organization and dynamics of functional plant membrane microdomains. *Cellular and Molecular Life Sciences*, *77*(2), 275-287. https://doi.org/10.1007/s00018-019-03270-7

Yu, M., Liu, H., Dong, Z., Xiao, J., Su, B., Fan, L., Komis, G., Šamaj, J., Lin, J., & Li, R. (2017a). The dynamics and endocytosis of Flot1 protein in response to flg22 in Arabidopsis. *Journal of Plant Physiology*, *215*, 73-84. https://doi.org/10.1016/j.jplph.2017.05.010

Yu, X., Feng, B., He, P., & Shan, L. (2017b). From Chaos to Harmony: Responses and Signaling upon Microbial Pattern Recognition. *Annual Review of Phytopathology*, *55*(1), 109-137. https://doi.org/10.1146/annurev-phyto-080516-035649

Yuan, M., Jiang, Z., Bi, G., Nomura, K., Liu, M., Wang, Y., Cai, B., Zhou, J.-M., He, S. Y., & Xin, X.-F. (2021). Pattern-recognition receptors are required for NLR-mediated plant immunity. *Nature*, *592*(7852), 105-109. https://doi.org/10.1038/s41586-021-03316-6

Zhang, M., Chang, H., Zhang, Y., Yu, J., Wu, L., Ji, W., Chen, J., Liu, B., Lu, J., Liu, Y., Zhang, J., Xu, P., & Xu, T. (2012). Rational design of true monomeric and bright photoactivatable fluorescent proteins. *Nature Methods*, *9*(7), 727-729. https://doi.org/10.1038/nmeth.2021

Zhang, X., Yang, Z., Wu, D., & Yu, F. (2020). RALF–FERONIA Signaling: Linking Plant Immune Response with Cell Growth. *Plant Communications*, *1*(4), 100084. https://doi.org/10.1016/j.xplc.2020.100084

Zhang, X., Zhang, M., Li, D., He, W., Peng, J., Betzig, E., & Xu, P. (2016). Highly photostable, reversibly photoswitchable fluorescent protein with high contrast ratio for live-cell superresolution microscopy. *Proceedings of the National Academy of Sciences*, *113*(37), 10364-10369. https://doi.org/10.1073/pnas.1611038113

Zhou, L., Cheung, M.-Y., Li, M.-W., Fu, Y., Sun, Z., Sun, S.-M., & Lam, H.-M. (2010). Rice hypersensitive induced reaction protein 1 (OsHIR1) associates with plasma membrane and triggers hypersensitive cell death. *BMC plant biology*, *10*, 290-290. https://doi.org/10.1186/1471-2229-10-290

Zhou, L., Cheung, M.-Y., Zhang, Q., Lei, C.-L., Zhang, S.-H., Sun, S. S.-M., & Lam, H.-M. (2009). A novel simple extracellular leucine-rich repeat (eLRR) domain protein from rice (OsLRR1) enters the endosomal pathway and interacts with the hypersensitive-induced reaction protein 1 (OsHIR1). *Plant, Cell & Environment*, *32*(12), 1804-1820. https://doi.org/10.1111/j.1365-3040.2009.02039.x

Zhou, X.-H., Gao, S., & Hui, S. L. (1997). Methods for Comparing the Means of Two Independent Log-Normal Samples. *Biometrics*, *53*(3), 1129-1135. https://doi.org/10.2307/2533570

Zhu, J.-Y., Sae-Seaw, J., & Wang, Z.-Y. (2013). Brassinosteroid signalling. *Development*, *140*(8), 1615-1620. https://doi.org/10.1242/dev.060590

zur Oven-Krockhaus, S. (2021). *A modular, comprehensive microscopy platform for modern live cell imaging* [University of Tübingen].

APPENDIX

I. Supplemental Figures

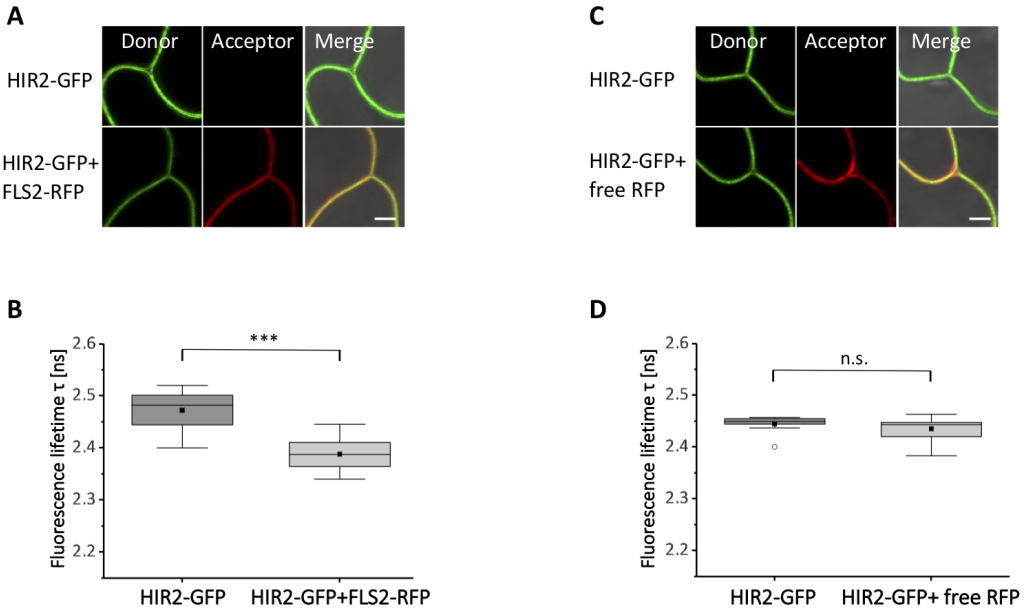

Supplemental figure 1: HIR2 is in close proximity with FLS2. FRET-FLIM measurements were performed in *N. benthamiana* leaves transiently expressing 35S-HIR2-GFP as donor alone and co-expressing with 35S-FLS2-RFP or Ubi10-RFP (free RFP) as acceptor. [**A, C**] CLSM images of a representative part of the plasma membrane. The scale bar represents 5 µm and applies to all images. [**B, D**] The average GFP fluorescence lifetime τ [ns] was obtained by bi-exponential curve fitting in a defined region of interest covering the plasma membrane and shown in the Boxplot. The center line indicates the median and the square indicates the mean. The bounds of the box show the 25th and the 75th percentiles, the whiskers indicate a range within 1.5 × IQR, outliers are displayed by open circles. Significant differences were analyzed with Kruskal-Wallis test followed by a Steel-Dwass post hoc correction and indicated by asterisks ($p<0.001$ ***; n.s. not significant). [B] Donor HIR2-GFP: $n= 20$; Acceptor FLS2-RFP: $n= 27$. Experiments were performed on three independent days. [D] Donor HIR2-GFP: $n= 10$; Acceptor free RFP: $n= 15$. Experiments were performed on two independent days.

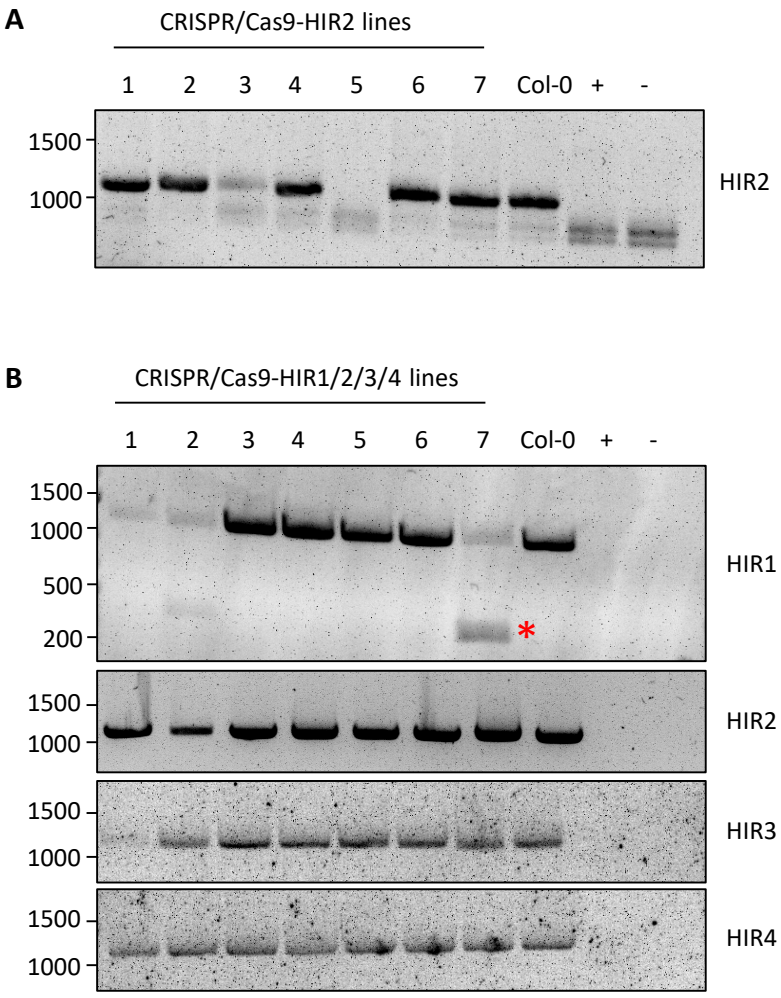

Supplemental figure 2: Identification of potential CRISPR/Cas9 deletions in *HIR* genes. [**A**] Amplification of *HIR2* in CRISPR/Cas9-HIR2 plants. The full-length of *HIR2* was amplified by PCR (Primer: HIR2-cds_F and HIR2-cds_R). Samples of Line 1, 3, 5 and 7 were send to sequencing, but no deletion in *HIR2* were identified. [**B**] Amplification of the full length of all four *HIRs* in CRISPR/Cas9-HIR1/2/3/4 plants. Plant 7 had a deletion of around 800 bp, amplicon indicated by red star. Amplification of Col-0 genomic DNA was used as positive control, (+) vector used for transformation (-) water control. [**C**] Sequencing alignment of shortened amplicon of CRISPR/Cas9-HIR1/2/3/4 plant 7 by HIR1-cds_R primer.

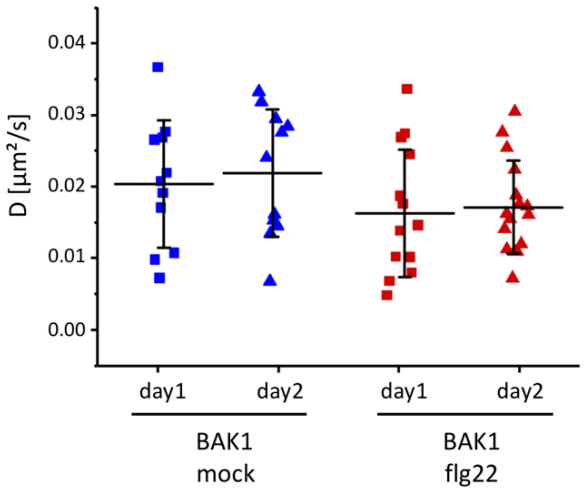

Supplemental figure 3: Comparative analysis of the diffusion coefficient of the duplicate data set of BAK1. The data points of the diffusion coefficient (D) of two individual measuring days of BAK1 mock treatment and BAK1 flg22 treatment were compared to indicate the replicability of the data spread.

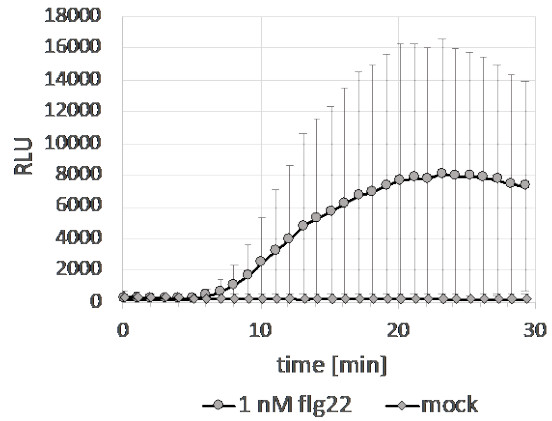

Supplemental figure 4: ROS assay to proof the functionality of flg22 peptide used in sptPALM experiments. ROS production was measured by a luminol-based approach and represented by relative light units. The reaction was triggered by 1 nM flg22 peptide. Peptide treated leaf pieces showed ROS production, whereas mock treated samples did not. Results are means (n=4 ± SD).

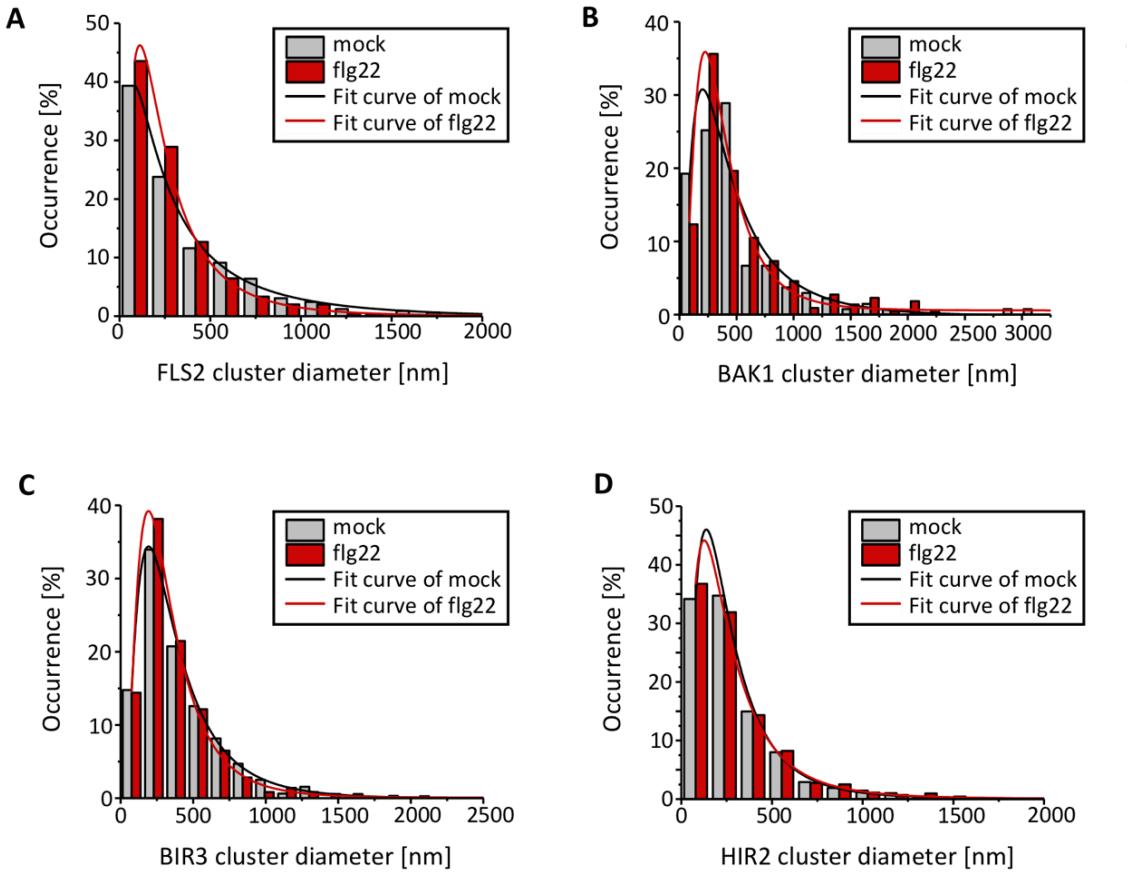

Supplemental figure 5: Frequency distribution of the respective protein cluster diameters. The cluster diameters were calculated based on the cluster area obtained by the SR-Tesseler software and their relative occurrence graphed in the histogram. The bins were set according to the number of respective values. A log-normal curve was fitted to the respective dataset. Histograms showing the occurrence of [**A**] FLS2-mEos3.2, [**B**] BAK1-mEos3.2, [**C**] BIR3-mEos3.2 and [**D**] HIR2-mEos3.2 cluster diameter of mock and flg22 treated samples.

II. List of Abbreviation

35S	Promoter of cauliflower mosaic virus
A. thaliana	*Arabidopsis thaliana*
BAK1	BRI1-ASSOCIATED KINASE
BIK1	BOTRYTIS-INDUCED KINASE 1
BIR	BAK1-INTERACTING RECEPTOR KINASE
BKI1	BRI1 KINASE INHIBITOR 1
BL	Brassinolide
BR	Brassinosteroid
BRI1	BRASSINOSTEROID INSENSITIVE 1
BSK1	BR SIGNALING KINASE 1
CERK1	CHITIN ELICITOR RECEPTOR 1
CLC2	CLATHRIN LIGHT CHAIN 2
CLSM	Confocal Laser Scanning Microscopy
CLSM	Confocal laser scanning microscopy
Co-IP	Co-immunoprecipitation
Col-0	Columbia-0
CSA1	CONSTITUTIVE SHADE-AVOIDANCE 1
CST	CAST AWAY
D	Diffusion coefficient
DAMP	Damage-Associated Molecular Pattern
DRM	Detergent Resistant Membranes

E. coli	*Escherichia coli*
EDS1	ENHANCED DISEASE SUSCEPTIBILITY 1
EFR	ELONGATION FACTOR-TU RECEPTOR
elf18	Epitope of Elongation Factor-Tu
ET	Ethylene
ETI	Effector-Triggered Immunity
FCS	Fluorescence Correlation Spectroscopy
FER	FERONIA
Flg22	22-amino acid minimal epitope of flagellin
FLIM	Fluorescence Lifetime Imaging Microscopy
FLOT	FLOTILLIN
FLS2	FLAGELLIN SENSING 2
FP	Fluorescing Protein
FRAP	Fluorescence Recovery After Photobleaching
FRET	Fluorescence Resonance Energy Transfer
GFP	Green Fluorescing Protein
HIR	HYPERSENSITIVE INDUCED REACTION
JA	Jasmonic Acid
LC/ESI-MS/MS	Liquid Chromatography Electrospray Ionization Tandem Mass Spectrometric
Leu	Leucine
LLG1	LORELEI-LIKE GPI-ANCHORED PROTEIN 1
LRR	Leucine-Rich Repeat
LTI6a	LOW TEMPERATURE INDUCIBLE 6a

LYK	LYSIN MOTIF KINASE
LysM	Lysin motif
mβCD	Methyl-β-cyclodextrin
MAMPs	Microbe-associated Molecular Pattern
MAPK	MITOGEN-ACTIVATED PROTEIN KINASE
mbSUS	Mating-based split-ubiquitin system
MSD	Mean Square Displacement
N. benthamiana	*Nicotiana benthamiana*
NA	Numerical Aperture
NLR	Nucleotide-binding domain Leucine Rich-Repeat Receptors
pa	Photoactivatable
PAD4	PHYTOALEXIN DEFICIENT 4
PALM	Photoactivated Localization Microscopy
PAMP	Pathogen-Associated Molecular Pattern
PI4P	Phosphatidylinositol 4-phosphate
PIP2;1	PLASMA MEMBRANE INTRINSIC PROTEIN 2;1
PRR	Pattern Recognition Receptors
PSF	Point-Spread Function
PSK	Phytosulfokine
PSKR	PSK RECEPTOR
Pst D3000	*Pseudomonas syringae* pv. *tomato* DC3000
PTI	Pattern-Triggered Immunity
RALF	RAPID ALKALIZATION FACTOR

REM	REMORIN
REM-CA	REMORIN C-terminal Anchor
RFP	Red Fluorescing Protein
RIN4	RPM1 INTERACTING PROTEIN 4
RLCK	Receptor-Like Cytoplasmatic Kinases
RLK	Receptor-Like Kinases
RLP	Receptor-Like Protein
ROP6	Rho GTPase RHO OF PLANTS 6
ROS	Reactive Oxygen Species
RPS2	RESISTENCE TO P. SYRINGAE 2
SA	Salicylic Acid
SERK	SOMATIC EMBRYOGENESIS RECEPTOR KINASE
SMLM	Single-Molecule Localization Microscopy
SPFH	Stomatin/Prohibitin/Flotillin/HflK/C
spt	single particle tracking
STORM	Stochastic Optical Reconstruction Microscopy
TIRF	Total Internal Reflection Fluorescence Microscopy
Trp	Tryptophan
Ubi1	Ubiquitin1 promoter
Ura	Uracil
VAEM	Variable-Angle Epifluorescence Microscopy

III. List of Figures

IV. List of Tables

ACKNOWLEDGEMENT

First, I would like to express my special thanks to Prof. Klaus Harter for his suggestions, discussions and support throughout this project.

Also, I would like to express my sincere thanks to Prof. Thorsten Nürnberger, who kindly agreed to be the second reviewer of my thesis.

I would like to thank my supervisor Dr. Birgit Kemmerling for giving me the opportunity to advance my research in her group and for providing this interesting project.

I am grateful to Sven zur Oven-Krockhaus. Zok, thanks for your help, the effort you made for my project and for your patience.

Moreover, I would also like to extend my deepest gratitude to Friederike Wanke. Thank you for all your advices, for your encouragements and the good coffee when I needed it.

Very special thanks go to my group members Sarina Schulze and Eleonora Ferrari. Thank you for your support, for exchanging and discussing new ideas and thank you for the backing you have given me.

Finally, I would like to acknowledge my colleagues and friends from the Plant Biochemistry and Plant Physiology Department for the good times we spend together in the lab and on conferences, for the stimulating scientific discussions as well as for the happy distractions to rest my mind outside of my research.